

Spring 2016

A Direct Simple Shear Device for the Dynamic Characterization of Partially Saturated Soils

Khoa Ngoc Le

University of New Hampshire, Durham

Follow this and additional works at: <https://scholars.unh.edu/thesis>

Recommended Citation

Le, Khoa Ngoc, "A Direct Simple Shear Device for the Dynamic Characterization of Partially Saturated Soils" (2016). *Master's Theses and Capstones*. 1082.

<https://scholars.unh.edu/thesis/1082>

This Thesis is brought to you for free and open access by the Student Scholarship at University of New Hampshire Scholars' Repository. It has been accepted for inclusion in Master's Theses and Capstones by an authorized administrator of University of New Hampshire Scholars' Repository. For more information, please contact nicole.hentz@unh.edu.

A DIRECT SIMPLE SHEAR DEVICE FOR THE DYNAMIC
CHARACTERIZATION OF PARTIALLY SATURATED SOILS

BY

KHOA N. LE

Bachelor of Science, University of New Hampshire, 2014

THESIS

Submitted to the University of New Hampshire
in Partial Fulfillment of
the Requirements for the Degree of

Master of Science

in

Civil Engineering

May, 2016

This thesis has been examined and approved in partial fulfillment of the requirements for the degree of Master of Science in Civil Engineering by:

Thesis Director, Dr. Majid Ghayoomi, Assistant Professor, Civil and Environmental Engineering

Dr. Jean Benoît, Professor, Civil and Environmental Engineering

Dr. Eshan Dave, Assistant Professor, Civil and Environmental Engineering

On April 8, 2016

Original approval signatures are on file with the University of New Hampshire Graduate School.

ACKNOWLEDGEMENTS

I would like to give my upmost appreciation to my advisor, Dr. Majid Ghayoomi, for providing the opportunity, guidance, and patience for this project. I would also like to acknowledge James Abare, Kevan Carpenter, Scott Campbell, and David Kinney for their assistance with the electrical, mechanical, and technical knowledge and contributions to the project. I would also like to acknowledge the faculty and professors at the University of New Hampshire who have provided me with the foundation of knowledge that I am privileged to have accumulated over the years. Furthermore, I would like to acknowledge the partial funding from the National Science Foundation (CMMI grant No. 1333810).

Additionally, I would also like to thank my friends for their uplifting attitude, and Anthony Hamstank for making me strive for success in order to fulfill a promise. Lastly, I would like to thank my phenomenal parents and family for providing me the much needed support, encouragement, and affection to complete this challenging endeavor.

TABLE OF CONTENTS

| | |
|---|-----|
| ACKNOWLEDGEMENTS | iii |
| TABLE OF CONTENTS | iv |
| LIST OF TABLES | xi |
| LIST OF SYMBOLS | xii |
| ABSTRACT | xv |
| CHAPTER 1 | 1 |
| 1.1 Motivation..... | 1 |
| 1.2 Objective/ Scope of Project | 2 |
| 1.3 Outline..... | 2 |
| CHAPTER 2 | 5 |
| 2.1 Dynamic Properties of Soils | 5 |
| 2.1.1 Introduction..... | 5 |
| 2.1.2 Basic Definitions..... | 6 |
| 2.1.3 Dynamic Behavior of Soils..... | 7 |
| 2.1.4 Small-Strain Shear Modulus, G_{\max} | 9 |
| 2.1.5 Cyclic Degradation & the Modulus Reduction Curve..... | 10 |
| 2.1.6 Damping Ratio | 12 |
| 2.2 Partially Saturated (Unsaturated) Soils | 15 |
| 2.2.1 Introduction to Unsaturated Soils | 15 |

| | |
|--|----|
| 2.2.2 Unsaturated Zone | 15 |
| 2.2.3 Soil Water Retention Curves | 17 |
| 2.2.4 Effective Stress in Unsaturated Soils..... | 19 |
| 2.2.5 Axis Translation Technique..... | 20 |
| 2.3.1 Previous investigations on Dynamic Soil Properties..... | 21 |
| 2.3.2 Previous investigations on Seismic Compression | 25 |
| 2.3.3 Current Investigation on Dynamic Properties of Unsaturated Soils | 28 |
| CHAPTER 3 | 29 |
| 3.1 Introduction to Direct Simple Shear Machines..... | 29 |
| 3.2 Variation of DSS Machines | 30 |
| 3.2.1 Effects of Sample Confinement (SGI, NGI, and Cambridge) | 30 |
| 3.2.2 Effects of Specimen Sample Size | 31 |
| 3.3 UNH DSS System..... | 34 |
| 3.4 Modification for Partially Saturated Soils | 37 |
| CHAPTER 4 | 40 |
| 4.1 Testing Material Properties..... | 40 |
| 4.2 Sample Preparation | 41 |
| 4.3 Vertical Consolidation | 43 |
| 4.4 Sample Saturation and desaturation to the target matric suction..... | 43 |
| 4.5 Applying cyclic loads (Direct Simple Shear Testing) | 48 |

| | |
|---|----|
| 4.6 System Mechanical Compliance Corrections | 50 |
| 4.6.1 Top Table Movement..... | 50 |
| 4.6.2 Friction Response Correction | 51 |
| 4.7 Testing Program | 52 |
| CHAPTER 5 | 54 |
| 5.1 Data Analysis | 54 |
| 5.2 Modification of the G_{sec} values | 58 |
| 5.3 Modification of Damping Ratio Values..... | 62 |
| 5.4 Determination of the G_{max} and ζ_{max} values..... | 62 |
| 5.4.1 Determining the Small Strain Shear Modulus, G_{max} | 63 |
| 5.4.2 Determining the Large Strain Damping Ratio, ζ_{max} | 63 |
| CHAPTER 6 | 65 |
| 6.1 Seismic Compression Results..... | 65 |
| 6.1.1 Pore Fluid Response | 65 |
| 6.1.2 Axial/ Volumetric Strain Response | 67 |
| 6.2 Results of the Dynamic Properties..... | 68 |
| 6.2.1 Results from Sample Series A | 69 |
| 6.2.2 Results from Sample Series B | 73 |
| 6.3 Shear Modulus Reduction and Damping Curves..... | 75 |
| CHAPTER 7 | 78 |

| | |
|--|-----|
| 7.1 Summary | 78 |
| 7.2 Conclusions..... | 79 |
| 7.3 Potential Research/Modifications for the Future | 79 |
| REFERENCES | 82 |
| APPENDIX..... | 86 |
| Appendix A: List of Sensors and Instrumentation..... | 87 |
| Appendix B: Dimensions of the Modified Platen..... | 90 |
| Appendix C: DSS Control System – Block Diagram | 93 |
| Appendix D: Sample Preparation Procedure | 95 |
| Appendix E: Various Procedures (from Vertical Consolidation to Cyclic Testing) | 104 |
| Appendix F: MATLAB Code for post-processing analysis | 110 |

LIST OF FIGURES

| | |
|---|----|
| Figure 1: Stress Conditions of a Soil Element (after Dunstan, 1998)..... | 6 |
| Figure 2: Typical Shear Stress-Strain Response of Soil (after Hardin and Drnevich, 1970) | 8 |
| Figure 3: Modulus Reduction Curve (after Kramer, 1996) | 11 |
| Figure 4: Relationship between Shear Modulus & Damping w/ respect to Shear Strain | 14 |
| Figure 5: Typical Soil Profiles (after Lu and Likos, 2004)..... | 15 |
| Figure 6: Various phases in a soil element. (after Suprunenko, 2015) | 16 |
| Figure 7: Illustration of the Unsaturated Soil Zones (after Lu and Likos, 2006) | 17 |
| Figure 8: Regimes of the Soil Water Retention Curve (after Lu et al., 2007) | 18 |
| Figure 9: Configuration for a partially saturated soil cell chamber (after Lu and Likos, 2004)... | 21 |
| Figure 10: Effect of Saturation on Gmax a) (after Kumar and Madhusudhan, 2012) b) (after Ghayoomi and McCartney, 2011)..... | 22 |
| Figure 11: Effect of Matric Suction on Gmax a) (after Khosravi and McCartney, 2011) b) (after Hoyos et al., 2015)..... | 23 |
| Figure 12: Recorded Shear Modulus Values of Partially Saturated Samples (after Ghayoomi et al., 2015) | 23 |
| Figure 13: Results of the Normalized Shear Modulus and Damping Ratios (after Jafarzedah and Sadeghi, 2012) | 24 |
| Figure 14: Shear Moduli and Damping Ratios (after Biglari, 2011) | 25 |
| Figure 15: Effects of Relative Density and Saturation on Seismic Compression (after Whang et al., 2004) | 26 |
| Figure 16: Lack of Effect of Saturation on Seismic Compression (after Duku et al., 2008)..... | 26 |

| | |
|---|----|
| Figure 17: Effect of Saturation and Shear Strain on Volumetric Strain (after Sawada et al., 2006) | 27 |
| | 27 |
| Figure 18: Effect of Saturation on Settlement (after Ghayoomi and McCartney, 2013)..... | 28 |
| Figure 19: Conceptual Example of a Seismic Shear Wave System..... | 30 |
| Figure 20: Cross-Sectional Views of Various DSS Apparatuses (after Dunstan, 1998)..... | 31 |
| Figure 21: Digitally Controlled –Simple Shear Apparatus at UCLA (after Duku, 2007) | 33 |
| Figure 22: Current Configuration of the UNH - DSS..... | 35 |
| Figure 23: Current damper configuration for horizontal movement (top view)..... | 36 |
| Figure 24: DSS Schematic Architecture: Full System..... | 37 |
| Figure 25: Modified Base Platen w/ embedded HAEV ceramic disk | 38 |
| Figure 26: Soil Cell with Piping Schematic..... | 39 |
| Figure 27: Grain Size Distribution of F75 Ottawa Sand (after Suprunenko, 2015) | 40 |
| Figure 28: Bottom platen of cell with assembled vacuum mold | 42 |
| Figure 29: Soil Sample Chamber installed in the DSS system..... | 42 |
| Figure 30: GeoTac software for the DigiFlow Pump | 45 |
| Figure 31: Soil Water Retention Curve of F75 Ottawa Sand | 46 |
| Figure 32: Comparison of SWRC before and after consolidation..... | 47 |
| Figure 33: Degree of Saturation before and after consolidation..... | 47 |
| Figure 34: van Genuchten curve vs HAEV threshold | 48 |
| Figure 35: User Interface of UNH-DSS Data Acquisition System and Control..... | 49 |
| Figure 36: Correlation between the top and bottom table movement..... | 50 |
| Figure 37: Top and Bottom LVDT sensors for distance corrections..... | 51 |
| Figure 38: Correlation between Frictional Resistance and Net Horizontal Movement..... | 52 |

| | |
|--|----|
| Figure 39: DAQ signals of various sensors after a cyclic test | 54 |
| Figure 40: Recorded Horizontal Motion Feedback | 55 |
| Figure 41: Recorded Horizontal Stress Feedback..... | 56 |
| Figure 42: Soil Response of a partially saturated soil..... | 57 |
| Figure 43: Soil Response with Reference Lines for the Dynamic Property calculations | 57 |
| Figure 44: Shear Modulus Reduction Curve of F75 Ottawa Sand (after, Oztoprak and Bolton 2013) | 60 |
| Figure 45: Pore Water Pressure Response over Cyclical Testing..... | 66 |
| Figure 46: Changes in Pore Water Pressure Response during Loading | 67 |
| Figure 47: Multistage Seismic Compression Results | 68 |
| Figure 48: Modified Shear Modulus Values vs Degree of Saturation..... | 69 |
| Figure 49: Modified Shear Modulus vs Matric Suction | 70 |
| Figure 50: Normalized Shear Modulus w/ respect to Dry Shear Modulus, A-series | 71 |
| Figure 51: Modified Damping Ratio vs Degree of Saturation..... | 72 |
| Figure 52: Modified Damping Ratio vs Matric Suction | 72 |
| Figure 53: Shear Modulus vs Shear Strain | 73 |
| Figure 54: Damping Ratio vs Shear Strain | 74 |
| Figure 55: G/G_{max} vs Shear Strain..... | 76 |
| Figure 56: ζ/ζ_{max} vs Strain..... | 77 |

LIST OF TABLES

| | |
|--|----|
| Table 1: Dimensions of various DSS Sample Specimens | 32 |
| Table 2: Various properties of F75 - Ottawa Sand | 41 |
| Table 3: van Genuchten Parameters of F75 Ottawa Sand | 46 |
| Table 4: Summary of Test Parameters | 53 |

LIST OF SYMBOLS

σ_v – total vertical stress

σ_h – total horizontal stress

K_0 – coefficient of lateral earth pressure at rest

φ –angle of internal soil friction

σ'_v – vertical effective stress.

σ'_h – horizontal effective stress

τ_c – cyclic shear stress

A – soil elements cross sectional area

Δ – horizontal displacement

H – soil elements initial height

γ –shear strain of the specimen

G –shear modulus

G_{sec} –secant shear modulus

G_{tan} –tangent shear modulus

$\bar{\sigma}'_m$ - mean effective confining pressure

K_2 – influence factor for the determination of G based off of relative density and shear strain

e –void ratio

P_a, P_{atm} – Atmospheric Pressure

OCR – overconsolidation ratio

D_R – Relative Density

G_{max} – small strain shear modulus

$K_{2,\text{max}}$ – empirical value based on relative density to calculate small strain shear modulus

ρ – density of the material

v_s – shear wave velocity

γ_{tv} – volumetric cyclic threshold shear strain

γ_r – reference shear strain

a – curvature parameter

C_u – Coefficient of Uniformity

C_c – Coefficient of Curvature

γ_e – elastic threshold shear strain

ζ – soil damping ratio

ζ_{\min} – small strain damping ratio

ζ_{\max} – large shear strain damping ratio

N – number of cycles in dynamic loading

ζ_{Masing} – damping based on Masing behavior

b – scaling coefficient for Masing behavior

h_c – height of capillary zone

c – coefficient based on soil angularity and shape

D_{10} – diameter of soil passing 10% in soil gradation curve

ψ_t – total suction

ψ_m – matric suction

ψ_o – osmotic suction

$(u_a - u_w)$ – matric suction

$(u_a - u_w)_b$ – soil air entry pressure

θ – volumetric water content

θ_r – residual volumetric water contents

θ_s – saturated volumetric water contents

S – degree of saturation

S_R – residual degree of saturation

S_e – effective degree of saturation

u_a – pore air pressure

u_w – pore water pressure

α – van Genuchten fitting parameter

n – van Genuchten fitting parameter

χ – soil parameter that is related to water degree of saturation

τ_f – shear stress at failure

c – soil cohesion

$(\sigma - u_a)$ – net normal stress

φ^b – friction angle in matric suction stress space

G_s – specific gravity of soil particles

e_{\min} – maximum void ratio

e_{\max} – maximum void ratio

$\rho_{d\min}$ – minimum unit density

$\rho_{d\max}$ – maximum unit density

ε_a – axial strain of the specimen

ρ_w – density of water

γ – unit weight of the soil.

ABSTRACT

A DIRECT SIMPLE SHEAR DEVICE FOR THE DYNAMIC CHARACTERIZATION OF PARTIALLY SATURATED SOILS

by

KHOA N. LE

University of New Hampshire, May, 2016

The importance of unsaturated soil mechanics has become of interest in recent decades to the geotechnical community. Previous investigations have led to the conclusion that inter-particle interactions present in unsaturated soils can contribute additional strength to the soil structure. Recent renovations made to a custom built Direct Simple Shear Apparatus at the University of New Hampshire has allowed researchers to study the dynamic properties of partially saturated soils. The renovations included a new control system, hydraulic components, and data acquisition system to allow the system to become functional from its previous working state. Modifications made to the soil chamber and the installation of a flow pump allows users to use the axis translation technique to control the degree of saturation in the soil specimens. An investigation conducted on a clean sand subjected to medium shear strains were tested at different degrees of saturation from a completely dry to a saturated state. The investigation confirmed the importance of matric suction on both the seismic compression and dynamic properties, as well as the validation of the system to record these properties. Results indicated that higher shear modulus values and lower damping ratios were observed for specimens subjected to larger matric suction values. Further investigations will be needed to address some of the challenges encountered in the system.

CHAPTER 1

INTRODUCTION

1.1 Motivation

As the world uses more seismic resistant structures, the fundamental concepts of soil dynamics are often applied for design and construction. Soil dynamics becomes an important aspect when considering the seismic response analysis of a soil mass and structure system. When modeling site conditions, certain material variables like the shear modulus, G , and the damping ratio, ζ , are needed in order to accurately predict the behavior of the system when subjected to dynamic loads.

Furthermore, the emergence of the behavior of partially saturated soils has been examined over the past decade due to advancements in technology and testing methodology. The effects of inter-particle forces available in unsaturated soils have been found to contribute significantly to the strength and stiffness of soil system. Previous investigations have utilized acoustical methods (e.g. bender elements) and conventional laboratory methods (i.e. triaxial, resonant column, and direct shear tests) to study the effects of matric suction on the dynamic properties (i.e. shear moduli and damping ratios) of unsaturated soils. However, different testing methods can induce different response mechanisms and results in different soil characteristics.

Dynamic shear modulus and damping can be measured in the laboratory through direct or indirect application of cyclic shear stress to the soil specimen. The Dynamic Direct Simple Shear (DSS) apparatus is a well-established equipment that has been successfully implemented to directly apply shear to the soil specimen. The apparatus is capable of providing in-situ conditions (ie. confining pressures and saturation levels) to a soil sample and applying a horizontal cyclic motion to the soil. The displacement and loads are recorded by sensors and the dynamic properties

can then be determined by analyzing the recorded data. Adapting DSS testing for unsaturated soil conditions would enable us to better understand the changes in dynamic material properties under different moisture conditions.

1.2 Objective/ Scope of Project

The main objectives of this thesis is to outline and explain the renovations made to the Direct Simple Shear (DSS) apparatus at the University of New Hampshire. These renovations allowed the apparatus to become operational since its last known previous working state in 1998. In addition, modifications were made to soil sample cell and system to allow suction control (axis translation technique) to control the degree of saturation of the samples. Post processing techniques were developed to analyze the raw data recorded by the newly installed data acquisition system.

An investigation on a clean F -75 Ottawa Sand was conducted to study the dynamic properties with respect to different degrees of saturation and varying cyclic shear strains. Additionally, the investigation provides insight on the viability of the system to record dynamic properties for a range of degree of saturation (suction).

1.3 Outline

This thesis is divided into several sections to allow the reader to understand every aspect of thesis investigation from the background information on soil dynamics to the methodology used for testing. The current chapter provides the motivation behind the thesis and the reason for testing, objectives and scope, and outline of the thesis.

Chapter 2 reviews the basics of soil mechanics and dynamics. The methods used to determine dynamic properties of soils are presented and empirical formulas for the small strain and strain-dependent shear modulus and damping are shown. The mechanisms and concepts

associated with partially saturated soils are briefly introduced. Previous investigations regarding dynamics of partially saturated soils are presented and discussed.

The importance of direct simple shear systems and the different variations of the machine utilized by different institutions are discussed in Chapter 3. An in-depth description of the Direct Simple Shear System at the University of New Hampshire (UNH –DSS) and the modifications that were made to enable testing partially saturated soils are presented. Schematics of the system layout and details of water flow are shown. Additionally, the mechanisms involving the horizontal control system is presented. System compliance issues are discussed and examined.

Chapter 4 presents the geotechnical properties of F75 Ottawa Sand used for this investigation and the soil water retention curves. The procedure of preparing a soil sample for the UNH – DSS and testing procedures are presented. The system software user interfaces for the data acquisition system and flow pump are shown. The testing program outlining the state variables (i.e. confining pressures, relative density, matric suctions, and applied shear strains) and naming sequences used to test and identify soil specimens are explained.

Chapter 5 exhibits a set of example raw signals outputted from one of the tests. The data reduction methods and analysis techniques converting signals to motions and then into dynamic properties is discussed. The modification methods used to compare the dynamic properties between different samples and to account for system compliance issues are explained.

Chapter 6 presents the analyzed results of the investigation. These results include the seismic compression behavior (pore fluid response and axial/volumetric strain), dynamic properties (shear modulus and damping), and normalized dynamic properties (G/G_{max} and D/D_{max}). The discussion of these results against the conclusions from previous investigations and the viability of the system is made.

A summary on the renovations made and on the results of the investigation is presented in Chapter 7. Suggestions and potential modifications to the UNH – DSS to address the challenges encountered from this investigation for future research are also provided.

The appendix section of this thesis includes the various sensors and equipment specification and known model numbers that are used for the current system setup. Dimensions and modifications made to a part of the soil sample chamber to accommodate partially saturated soils are shown. A block diagram of the Proportional – Integral – Derivative (PID) horizontal control system showing the interactions between the sensors – controller – hydraulic equipment is included. A step by step procedure on the creation and running a test (from vertical consolidation to cyclic testing) is also provided. The MATLAB code for post processing is also provided.

CHAPTER 2

BACKGROUND

2.1 Dynamic Properties of Soils

2.1.1 Introduction

The importance of soil dynamics has become more prominent in recent decades due to advances in both technology and stricter regulations in building codes. Soils can be subjected to dynamic loads from a wide variety of sources. These sources could be in the form of railroad/traffic vibrations, ocean waves, Soil – Foundation - Structure Interactions (SFSI) (SFSI via wind loads, dynamic machine foundations, etc.), and earthquakes.

In order to investigate any of these problems, specific information about site dynamics is needed. For example, site response analysis is often conducted by geotechnical engineers to evaluate seismic motion propagation in a site and to estimate the design motion at the soil surface. In order to properly conduct this analysis, dynamic properties such as the shear modulus and damping ratio are needed. In an earthquake, a seismic motion originated from the bedrock will propagate upwards through the overlying strata. The seismic wave is then distorted through the soil and will result in different responses (in terms of displacement, velocities, and accelerations) at the surface.

Historically, there have been numerous methods that investigators have used to model a soil system. One of the most fundamental ways to model the movement of soil when subjected to dynamic loads is using a representative soil element. Then, this element is dynamically loaded and its response is evaluated. However, this approach incorporates a fair amount of assumptions and

approximation with regards to the boundary conditions. The element level response would be used to characterize the dynamic properties of soil system in larger scales.

2.1.2 Basic Definitions

In order to conduct any geotechnical seismic analysis, certain soils properties are needed. A typical soil element under field conditions is presented in Figure 1. When a soil element is at rest, a vertical effective confining stress, σ'_v is exerted on the top and bottom of the soil element and a horizontal effective confining stress, σ'_h is exerted around the sides. The vertical pressure is often provided by the weight of the overlying soil and any additional surcharge load at the soil surface while the effective stress is obtained by subtracting water pore pressure from the vertical stress. It should be noted that the horizontal effective stress is usually taken as a portion of the vertical effective stress by multiplying the at-rest lateral earth coefficient, K_0 .

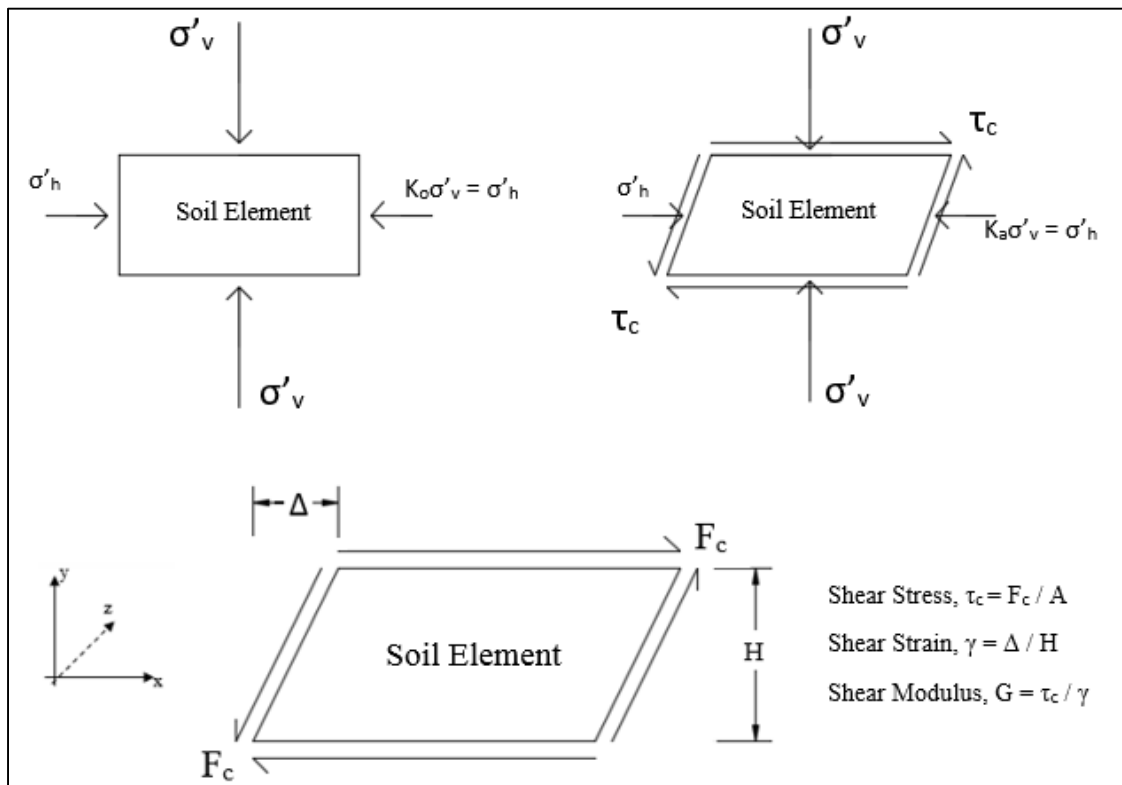


Figure 1: Stress Conditions of a Soil Element (after Dunstan, 1998)

The mean effective confining stress, $\bar{\sigma}'_m$ describes the stress surrounding the soil element. In most cases, the pressure on the sides are considered to be identical (in the x and z directions), the stress would then be in the following form,

$$\bar{\sigma}'_m = \frac{1}{3}(\sigma'_v + [2K_0\sigma'_v]) \quad (1)$$

In an earthquake, shear waves originated from the underlying bedrock will propagate up through the overlying soil strata and will result in a cyclic shearing force, F_c applied to the soil system and consequently on any soil element (Figure 1). The cyclic shearing stress, τ_c is calculated as the shear force divided by the cross-sectional area of the soil element, A (in the xz-plane). When the shear stress is applied to the sample, a resulting horizontal displacement, Δ will also be imparted onto the element (in the x-direction). The shear strain, γ_c is then defined as the horizontal displacement over the original height, H (in the y-direction) of the element.

2.1.3 Dynamic Behavior of Soils

The secant shear modulus, G , is one such material variable that describes the stiffness of the soil. This parameter in cyclic shear test is the ratio between the cyclic shear stress, τ_c to cyclic shear strain, γ_c .

$$G = \frac{\tau_c}{\gamma_c} \quad (2)$$

Empirical relations have been established and confirmed through the work of various researchers (e.g. Equation 3) to estimate this parameter.

(Seed and Idriss, 1970)
$$G = 1000K_2(\bar{\sigma}'_m)^{0.5} \quad (3)$$

In this equation, $\bar{\sigma}'_m$ represents the mean effective stress confining the soil element (in psf) at a particular depth and K_2 is an influence factor that is a function of the void ratio and the subjected strain amplitude.

Cyclically loaded soils often exhibit a non-linear shear stress-strain response. Depending on the shear stress or strain imparted on the particular soil, the response of the soil can be shown as a hysteresis loop in Figure 2.

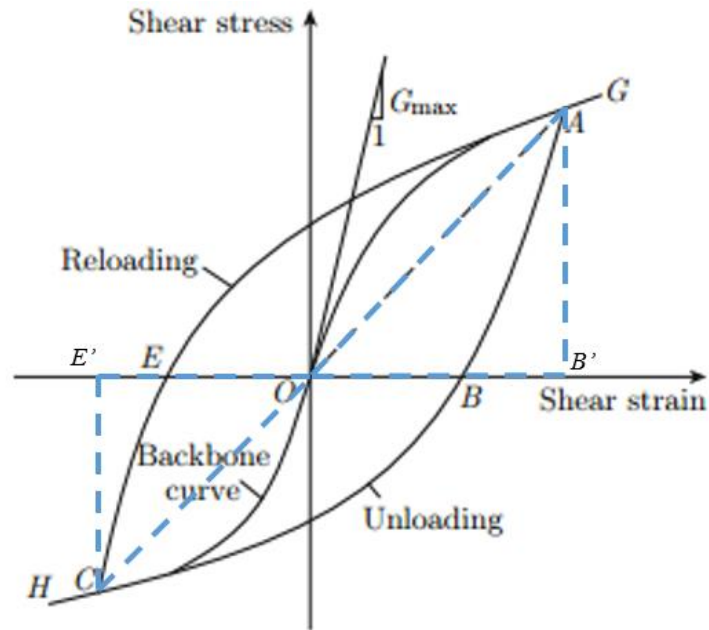


Figure 2: Typical Shear Stress-Strain Response of Soil (after Hardin and Drnevich, 1970)

The at-rest condition of the soil begins at the origin, O and is loaded to point A. It is then unloaded following the hysteresis curve ABC and then reloaded on the curve CEG. The backbone curve of the hysteresis loop, HOG describes the behavior of the soil when subjected to initial loading at different strains. The hysteresis behavior of soil can be attributed to the dissipation of energy in the soil element and between individual soil particles. It can be observed that the shear modulus is steepest at small shear strains, thus resulting in a stiffer soil. The line tangent to the hysteresis loop at small strain is often referred to as the small strain shear modulus or maximum shear modulus, G_{max} . The shear strain range for this modulus is usually less than $1 \cdot 10^{-4} \%$ (Kramer, 1996). On the contrary, as the shear strain increases, the slope of the backbone curve tends to decrease, thus indicating a softer soil.

When calculating the shear modulus, the calculations can be done through two separate approaches from the shear stress-strain curve. One way is to calculate the shear modulus from the origin to the point of interest; this value yields the G_{sec} (secant shear modulus) value. Alternatively, the modulus can also be taken as the tangential slope of the curved response; this value is referenced as the G_{tan} (tangent shear modulus). This value is continuously changing over the response of the soil.

2.1.4 Small-Strain Shear Modulus, G_{max}

The general form of the maximum shear modulus value is typically written in the following form,

$$G_{\text{max}} = A * F(e) * \left(\frac{\sigma'_m}{P_a}\right)^n \quad (4)$$

where, A and n are empirical fitting parameters, $F(e)$ is function based on the void ratio of the soil, σ'_m is the mean effective confining stress on a particular soil element, and P_a is the atmospheric pressure.

Empirical relationships that have been established by various investigators (Hardin and Drnevich 1970, Seed et al. 1971) on the small strain shear modulus with common laboratory parameters have the following forms;

$$(Hardin \text{ and } Drnevich, 1970) \quad G_{\text{max}} = 14760 * \frac{(2.973-e)^2}{1+e} * OCR^a * (\sigma'_m)^{\frac{1}{2}} \quad (5)$$

$$(Seed \text{ and } Idriss, 1970) \quad G_{\text{max}} = 1000K_{2,\text{max}}(\bar{\sigma}'_m)^{0.5} \quad (6)$$

where, e is the void ratio, OCR is the overconsolidation ratio (and represents the stress history of the soil), σ'_m is the mean effective confining stress, a is a fitting parameter, and $K_{2,\text{max}}$ is a function of the relative density, D_R of the soil. Variations of $K_{2,\text{max}}$ obtained from experimental data are provided by Seed and Idriss, (1970) shown in Equation 7:

$$K_{2,\text{max}} = 0.6D_R + 16 \quad (7)$$

The shear wave's wave velocity is directly correlated with the small strain shear modulus, shown in the ensuing equation and often measured in the laboratory using acoustical method (e.g. bender elements).

$$G_{max} = \rho v_s^2 \quad (8)$$

In this equation, the maximum shear modulus is a function of the total density of the soil medium, ρ , and the shear wave velocity, v_s . The shear wave velocity is determined by measuring the time it takes for the shear wave to travel a set distance. This is often accomplished by using an acoustical method that utilizes shear wave transducers/ bender elements (Hall and Richart, 1963).

An alternative laboratory method that is often used is the resonant column test. This test involves creating a column of soil and subjecting the soil to a small torsional shear with a range of frequencies. The natural frequency of a soil column excited with different frequencies will be related to the soils' shear wave velocity. Then, the soil small-strain shear modulus is estimated (Hall and Richart 1963, Hardin and Richart 1963). It should also be noted that empirical relations between standard in-situ tests (Standard Penetration Test, Cone Penetration Test, Dilatometer, and Pressuremeter) and the maximum shear modulus have also been established over the past decades (Ohta and Goto 1976, Baldi et al. 1986, Bellotti et al. 1986, Rix and Stokoe 1991).

2.1.5 Cyclic Degradation & the Modulus Reduction Curve

In a comprehensive study by Hsu and Vucetic (2004) the degradation of the shear modulus occurs when the imparted shear strain to the soil is larger than a certain value. This value is often termed as the volumetric cyclic threshold shear strain, γ_{tv} and varies for different types of soils. Typical values for clean sands (SP) are around (0.01% - 0.02%), while for sands with incorporated fines and clayey soils yield larger values (0.4% - 0.49%). These values tend to increase as the

relative densities and amount of fines (and plasticities for clays) increase. The threshold value distinguishes when the soil experiences permanent deformation and changes in volume.

The modulus reduction curve presents a normalized approach in determining the effects of state variables on the behavior of soils over a wide range of strain levels, shown in Figure 4.

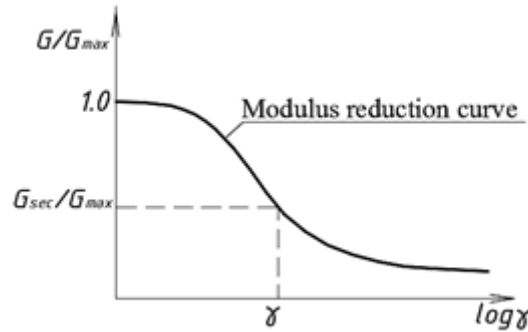


Figure 3: Modulus Reduction Curve (after Kramer, 1996)

Previous investigators (Hardin and Drnevich 1972, Darendeli 2001, Menq 2003, Oztoprak and Bolton 2013) have produced empirical relations for this curve. These relations are presented in Equations 9, 10, and 13.

(Hardin and Drnevich, 1972)
$$\frac{G}{G_{max}} = \frac{1}{1 + \frac{\gamma}{\gamma_r}} \quad (9)$$

In this equation γ_r is the reference shear strain at which G_{max} is determined and γ is the shear strain corresponding with the shear modulus. Modifications are presented in the following equations.

(Darendeli, 2001)
$$\frac{G}{G_{max}} = \frac{1}{1 + (\frac{\gamma}{\gamma_r})^a} \quad (10)$$

(Menq, 2003)
$$\gamma_r = 0.12 \cdot C_u^{-0.6} \cdot \left(\frac{\bar{\sigma}'_m}{P_a}\right)^{0.5 \cdot C_u^{-0.15}} \quad (11)$$

$$a = 0.86 + 0.1 \cdot \log\left(\frac{\bar{\sigma}'_m}{P_a}\right) \quad (12)$$

In these equations, γ_r is the reference shear strain, a is a curvature parameter, C_u is the soils coefficient of uniformity, P_a is the atmospheric pressure, and $\bar{\sigma}'_m$ is the effective mean confining pressure. Recently, a more detailed form is introduced as:

(Oztoprak and Bolton, 2013)

$$\frac{G}{G_{max}} = \frac{1}{[1 + (\frac{\gamma - \gamma_e}{\gamma_r})^a]} \quad (13)$$

In this equation G_{max} is the max shear modulus, γ_r is the reference shear strain, a is a curvature fitting parameter that describes the rate of degradation, and γ_e is the elastic threshold strain (volumetric threshold strain). It should be noted that Oztoprak and Bolton's equation used a regression model that compiled data from dozens of investigations (using test data from different tests and soils) to accurately form an equation that has both an upper and lower bound by altering the parameters, γ_r and γ_e .

$$\gamma_r (\%) = 0.01U_c^{-0.3} \left(\frac{p'}{P_{atm}} \right) + 0.08eD_r \quad (14)$$

$$\gamma_e = 0.0002 + 0.012\gamma_r \quad (15)$$

$$a = C_u^{-0.075} \quad (16)$$

where C_u is the coefficient of uniformity, P_{atm} is atmospheric pressure, p' is the mean effective stress, e is void ratio, and D_r is the relative density.

2.1.6 Damping Ratio

Another material variable that is important when determining the response of the system is the damping ratio, ζ . This parameter represents the amount of energy that is dissipated by the soil when subjected to dynamic loading. The damping ratio is often calculated from the area within the hysteresis loop (shown in Figure 2).

$$\zeta = \frac{1}{2\pi} * \frac{\text{Area of Hysteresis Loop}}{\text{Area of Triangle OAB}' + \text{Area of Triangle OCE}'} \quad (17)$$

The damping ratio and the shear modulus are often reciprocals of the other parameter. Often as the shear modulus degrades with larger imparted shear strains, the damping ratio will increase. Conversely, as the shear modulus increases, a smaller damping ratio will be observed. Thus, a soil element exhibiting G_{max} , at the same time will also have a minimum damping ratio, ζ_{min} . An empirical relation for this value was developed by Menq (2003).

$$\zeta_{min} = 0.55 * C_u^{0.1} * D_{50}^{-0.3} * \left(\frac{\bar{\sigma}'_m}{P_{atm}}\right)^{-0.08} \quad (18)$$

The equation for the minimum damping ratio, ζ_{min} , is a function of various parameters including: the soils' coefficient of uniformity, C_u , the medium grain size (in mm) determined from the soil gradation curve, D_{50} , mean effective confining pressure, $\bar{\sigma}'_m$, and atmospheric pressure, P_{atm} . Alternatively, the maximum damping ratio, ζ_{max} is exhibited by the soil when the soil is subjected to large strains. Seed and Idriss (1970) provided the basis for this value in the following equation,

$$\zeta_{max}(\%) = x - 1.5(\log_{10} N) \quad (19)$$

where, x is a value that ranges from 28 (for clean saturated sands) to 33 (for clean dry sands) and N is the number of cycles. The relationship between the degradation of the normalized shear modulus and the increasing trend of the damping ratio is provided in the following equations.

$$(Hardin \text{ and } Drnevich, 1972) \quad \zeta = \zeta_{max} \left(1 - \frac{G}{G_{max}}\right) \quad (20)$$

$$(Menq, 2003) \quad \zeta = b \left(\frac{G}{G_{max}}\right)^{0.1} * \zeta_{masing} + \zeta_{min} \quad (21)$$

The damping ratio, ζ is a function of the normalized shear modulus, ζ_{masing} , which is a modified form of damping based on “Masing behavior”, b is a scaling coefficient (based on the cycle number) for the ζ_{masing} response, and ζ_{min} , the damping ratio at small strains. “Masing behavior” relates the soils' monotonic loading response (via the backbone curve) with the cyclic unloading and reloading response (Masing 1926, Darendeli 2001). In both functions, the damping ratio increases as the shear strain increases as shown in Figure 4.

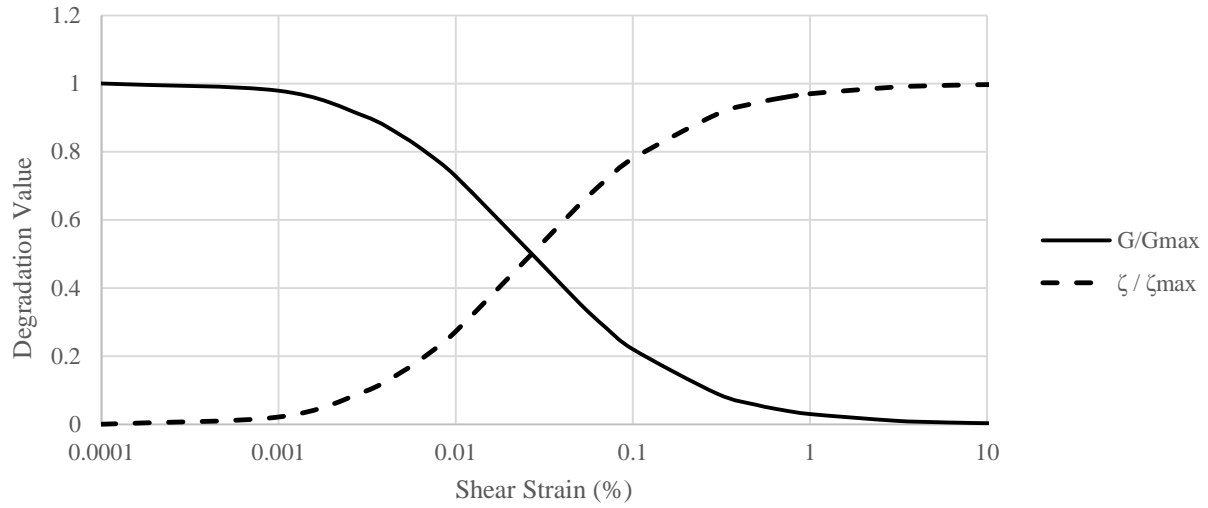


Figure 4: Relationship between Normalized Shear Modulus and Damping w/ respect to Shear Strain

In this figure, the degradation value of the shear modulus and the increase in damping values was created using the relationship established in Equations 13 and 20, respectively. The assumptions for the Oztoprak and Bolton equation parameters are as follows; $C_u = 1.83$, $e = 0.6605$, $p' = 28.57$ kPa, $p_{atm} = 101.3$ kPa, and $D_R = 0.45$.

2.2 Partially Saturated (Unsaturated) Soils

2.2.1 Introduction to Unsaturated Soils

Unsaturated zone in a soil layer is the zone above the water table where often most foundations, embankments, and dams are built. This zone is also known as the “phreatic” or “vadose” zone. Flow- (hydraulic), stress-, and deformation-related behavior can be greatly influenced by the properties of the unsaturated soil which these structures are built upon.

Partially saturated soils are considered a relatively new field of study in the geotechnical profession. The extent of the unsaturated zone is often a function of numerous variables including the depth of the water table, soil grain size, evaporation, rainwater, snowmelt infiltration, and other climatic and local factors (vegetation growth, etc.). A typical soil profile is shown in Figure 5.

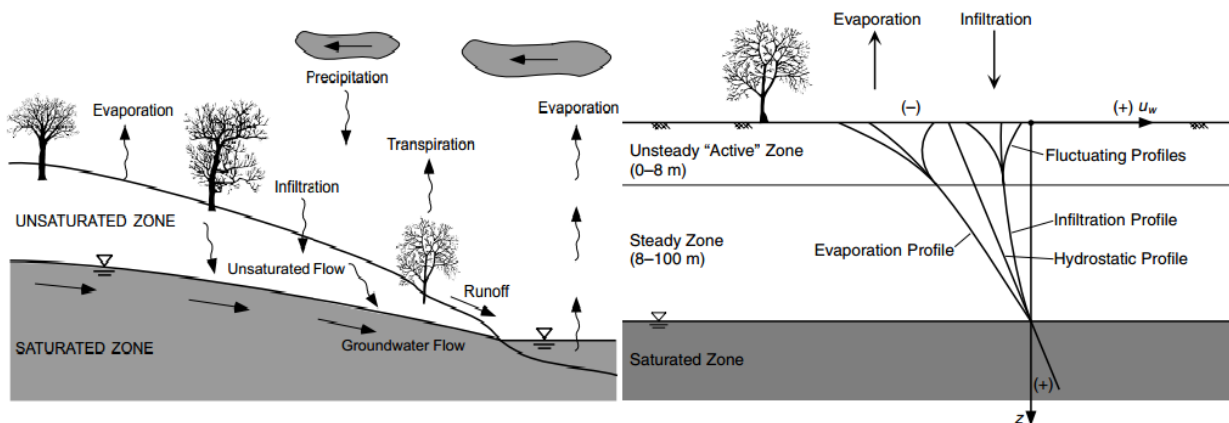


Figure 5: Typical Soil Profiles (after Lu and Likos, 2004)

2.2.2 Unsaturated Zone

Classical soil mechanics often cover a two phase system of soil considering the soil as either completely dry or fully saturated. In partially saturated soils, the soil system consists of three phases comprised in a soil-water-air interface at equilibrium (e.g. Figure 6).

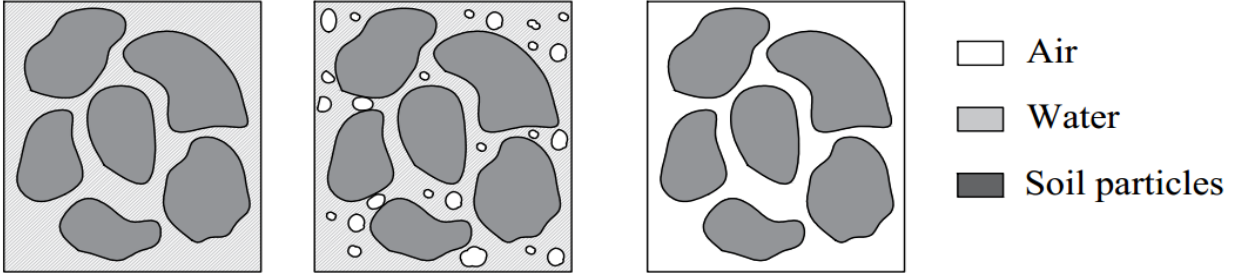


Figure 6: Various phases in a soil element. Fully Saturated (Right), Unsaturated (Center), Dry (Left) (after Suprunenko, 2015)

The unsaturated zone encompasses three different regions in itself. Located right above the water table is the *capillary fringe* region. The pores in between the soil particles are completely saturated with water. The water uptake through the soil structure is contributed to the negative pore water pressure in the system. The height of the capillary zone is often a function of the effective pore size diameter of the soil and can be represented by Equation 22 (Holtz et al. 2011).

$$h_c = \frac{C}{e * D_{10}} \quad (22)$$

where, h_c is the height of the capillary zone, e is the void ratio, D_{10} is the diameter of the soil from the soil grain distribution chart, and C is an empirical coefficient based on the angularity and shape of the individual soil grains.

The soil starts to become unsaturated once the (matric) suction becomes larger than the air entry value. This region of soil is known as the *funicular* zone. Next is the *residual* or *pendular* zone that is located closest to the ground surface. The soil interface has a layer of water covering the surface and inside of the disconnected pores between the individual particles. It should be noted that at this state, more water can be extracted from the soil only by additional heat (ie. oven dried, desert regions, etc.).

Total suction, ψ_t , is comprised of two different mechanisms displayed in the following equation.

$$\psi_t = \psi_m + \psi_o \quad (23)$$

These mechanisms include matric suction effects, ψ_m and osmotic effects, ψ_o . Matric suction consists of capillary and physiochemical forces such as Van der Waals and electrical double layer attractions and repulsion. While osmotic effects are due to dissolved solutes which can affect the chemical potential of water through hydration and solvation (Lu and Likos, 2004). The approximation of the measured matric suction is typically taken as the negative pore water pressure that is present in the soil matrix.

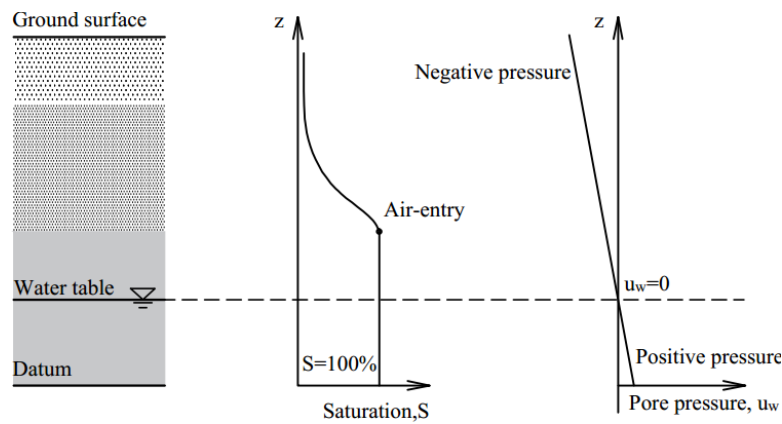


Figure 7: Illustration of the Unsaturated Soil Zones (after Lu and Likos, 2006)

2.2.3 Soil Water Retention Curves

The soil-water retention curve (SWRC) is often used to show the characteristics of the volumetric water content against the applied matric soil suction. The SWRC is highly dependent on the soil type, the particle size, void ratio, and confinement pressure. The curve consists of different regimes shown in the ensuing figure.

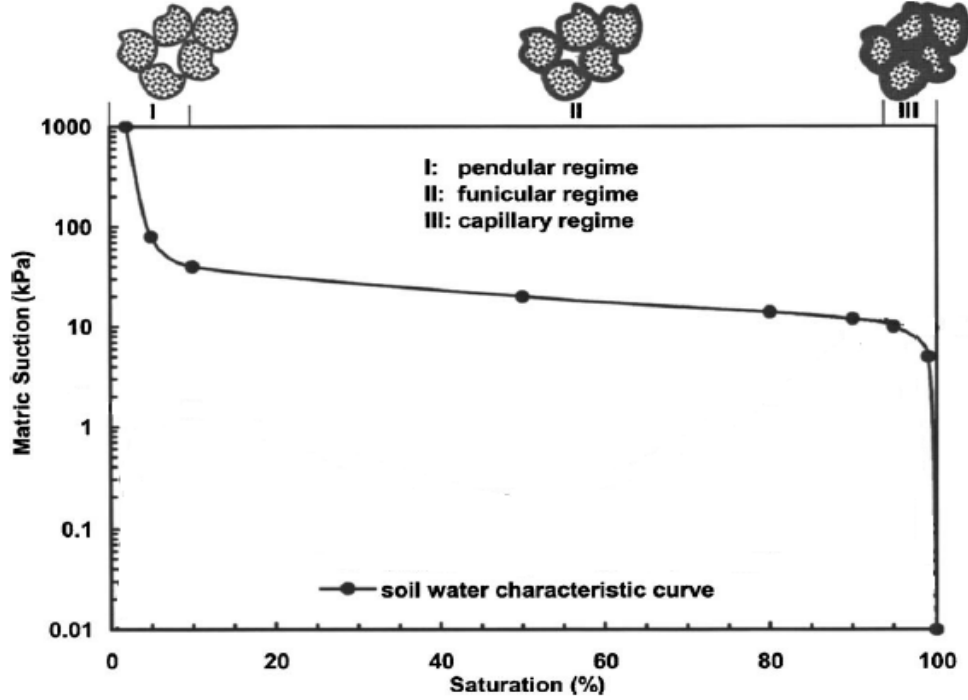


Figure 8: Regimes of the Soil Water Retention Curve (after Lu et al., 2007)

In the first regime, the rightmost, the soil is completely saturated and the upper part of the regime is the air entry value $(u_a - u_w)_b$. In the second regime, the soil matrix experiences matric suction mostly through capillary action and the surface tension by the menisci formed from the interactions between soil particles, water, and air. The third and final regime describes the soil at the residual state; water exists in the soil element by thinly coating the surface of the soil particles. It should be noted that the volumetric water content could vary for an identical soil sample subjected to the same matric suction depending on whether the soil is being saturated (wetting) or desaturated (drying). A hydraulic model of the water retained by the soil element at different matric suctions was developed by van Genuchten (1980). The closed form solution is provided in the subsequent equation.

$$\frac{s - s_r}{1 - s_r} = S_e = \left\{ \frac{1}{1 + [\alpha(u_a - u_w)]^n} \right\}^{1 - \frac{1}{n}} \quad (24)$$

In this equation the parameter, S_e is the effective degree of saturation of the soil, S is the current degree of saturation, S_r is the residual degree of saturation, α and n are van Genuchten

fitting parameters that are empirically determined by running a soil water retention curve analysis, $u_a - u_w$ is the applied matric suction.

2.2.4 Effective Stress in Unsaturated Soils

Terzaghi (1943) introduced the concept of the effective stress in soils, σ' , to be determined by the equation below. This relation was found to be considerably accurate for fully saturated soils and is still used in current geotechnical practice.

$$\sigma' = \sigma - u_w \quad (25)$$

Bishop (1959) expanded on the effective strength equation, with the idea of an additional term to the equation to represent the “matric suction” caused by the air-water interface and effective stress parameter, χ .

$$\sigma' = (\sigma - u_a) + \chi (u_a - u_w) \quad (26)$$

$$\chi = f(S) \quad (27)$$

where, $\sigma - u_a$ represents the net normal stress, χ is the effective stress parameter, and $u_a - u_w$ is the matric suction stress, and S is the degree of saturation. The effective stress parameter is a material variable and ranges between $0 \leq \chi \leq 1$; a soil is considered completely dry when this value is 0 and completely saturated when this value is 1. Lu and Likos (2010) proposed the redevelopment of Bishop's equation to determine the effective stress of the soil when subjected to a matric suction using the van Genuchten (1980) model and incorporating the concept of suction stress using the following form,

$$\sigma' = \sigma - u_a + \frac{u_a - u_w}{(1 + [\alpha(u_a - u_w)]^n)^{1 - \frac{1}{n}}} \quad (28)$$

By incorporating the modelling of the matric suction into the effective stress equation, it is readily apparent that the matric suction can contribute “additional” strength to the soil element.

When combining the effective stress equation with the standard Mohr-Coulomb failure criterion for the shear strength of soils Fredlund and Morgenstern (1977) proposed a two state variable approach. The formulation for the ultimate shear stress at failure, τ_f , was found to be a function of both the net normal stress and the matric suction. This approach utilizes the Mohr Coulomb failure envelope approach of finding the friction angles in two different stress spaces. Consequently, the peak shear stress would be calculated in the subsequent form when subjected to two different stress states.

$$\tau_f = c' + (\sigma - u_a)_f \tan \phi' + (u_a - u_w) \tan \phi^b \quad (29)$$

where τ_f represents the shear strength at failure, c' represents the cohesion of the soil, $(\sigma - u_a)_f$ is the net normal stress, ϕ' is the friction angle in the net normal stress space, $u_a - u_w$ is the matric suction applied to the soil, and ϕ^b is the friction angle in the matric suction stress space.

2.2.5 Axis Translation Technique

The axis translation technique was developed by Hilf (1956) to provide a way to control the degree of saturation and suction in a laboratory soil sample. This method makes use of a fully saturated High Air Entry Value (HAEV) disk to separate the air - water interface. The technique typically changes the suction by altering the air pressure that is applied to the top of the specimen and the pore water pressure below the disk. Alternatively, the pore water pressure can be altered, while keeping the air pressure constant at atmospheric pressure. A reference axis is established at a point within the sample and pore water is extracted from the fully saturated sample. The extracted water results in a decrease in water content in the sample while the increase in the matric suction is measured from the reference axis. Tracking the water content in the specimen and the applied

suction one can develop a soil water retention curve. A typical configuration of a soil sample under axis translation is shown in the following figure.

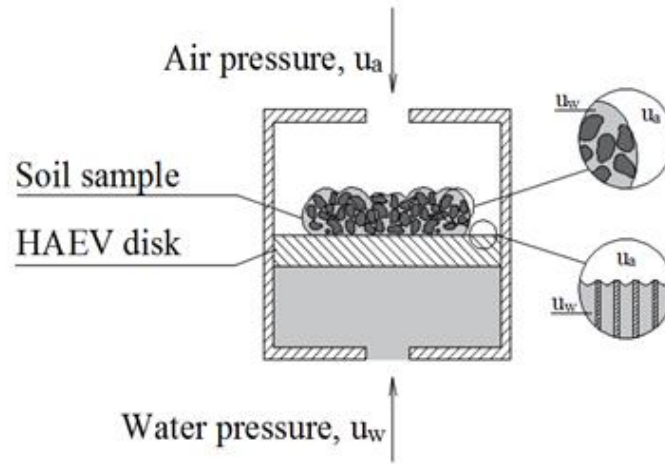


Figure 9: Typical configuration for a partially saturated soil cell chamber (after Lu and Likos, 2004)

2.3 Dynamically Loaded – Partially Saturated Materials

Numerous investigations have been conducted to study the behavior of unsaturated soils under different state conditions. In these investigations, the studies utilized different soils and types of equipment. The implications of comparing the results are readily apparent, in which different testing methods could result in diverse conclusions from different analysis techniques and equations. In an attempt to describe the overall behavior of soils, the following sections have been dedicated to past studies on the effects of different state and material variables on the dynamic behavior (ie. shear modulus and damping ratio) and seismic compression (ie. pore fluid generation, axial and volumetric strains) of unsaturated soils.

2.3.1 Previous investigations on Dynamic Soil Properties

The dynamic behavior of partially saturated soils often describes the stiffness and damping properties and has been a subject of many studies to date. Different state variables such as cyclic stress/strain ratio, frequency of loading, confining pressures, and the number of cycles in conjunction with the degree of saturation have been altered to determine the impacts of these

variables on the dynamic properties. Previous studies that have utilized bender elements to study the small strain shear modulus with respect to the effects of partially saturated soils have indicated that increasing the matric suction can induce larger observed small strain shear moduli in soils (e.g. Figure 10) (Cho and Santamarina 2001, Ghayoomi and McCartney 2011, Kumar and Madhusudhan 2012). However, there is a discord in where or whether the peak small strain moduli value occurs in regards to the degree of saturation depending on the material type. This could be due to the sample saturation techniques, tested soil points (residual values not reached or tested), effective confining pressures, etc.

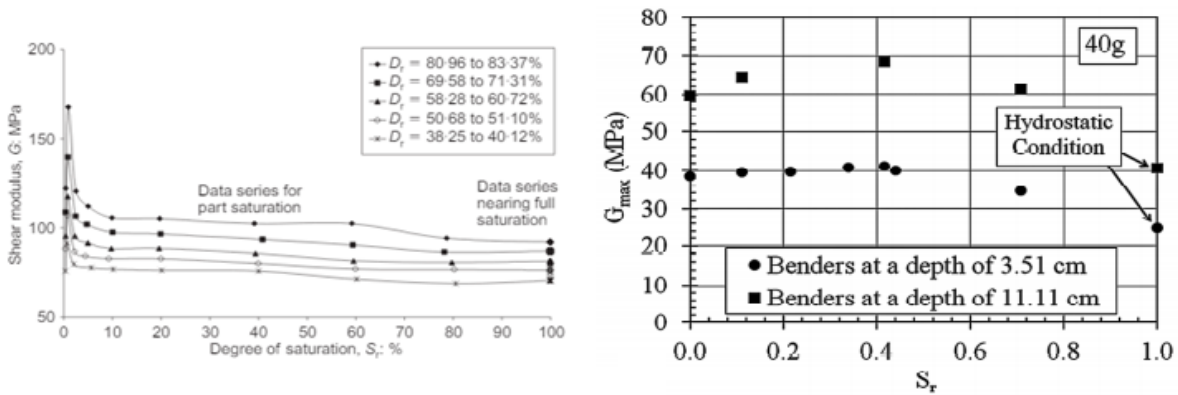


Figure 10: Effect of Saturation on G_{max} a) (after Kumar and Madhusudhan, 2012) b) (after Ghayoomi and McCartney, 2011)

The same parameter has also been examined using data from resonant column tests. These studies also confirmed the conclusion that by increasing the matric suction applied to the sample, the small strain shear moduli would increase as shown in Figure 11 (Khosravi and McCartney 2011, Hoyos et al. 2015).

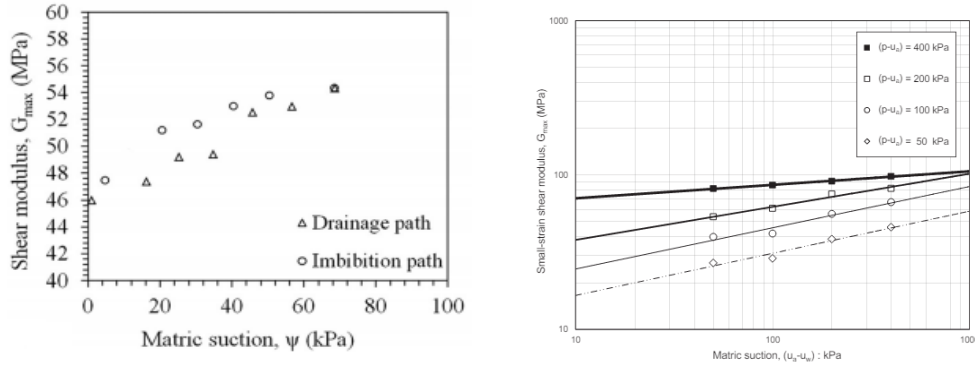


Figure 11: Effect of Matric Suction on G_{max} a) (after Khosravi and McCartney, 2011) b) (after Hoyos et al., 2015)

Medium to large strain shear modulus values have been measured using triaxial systems adapted with suction control/axis translation systems to control the degree of saturation in the sample (Cui et al. 2007, Kimoto et al. 2011, Ghayoomi et al. 2015). The results shown in Figure 12 indicated an increase in shear modulus in specimens with higher matric suctions.

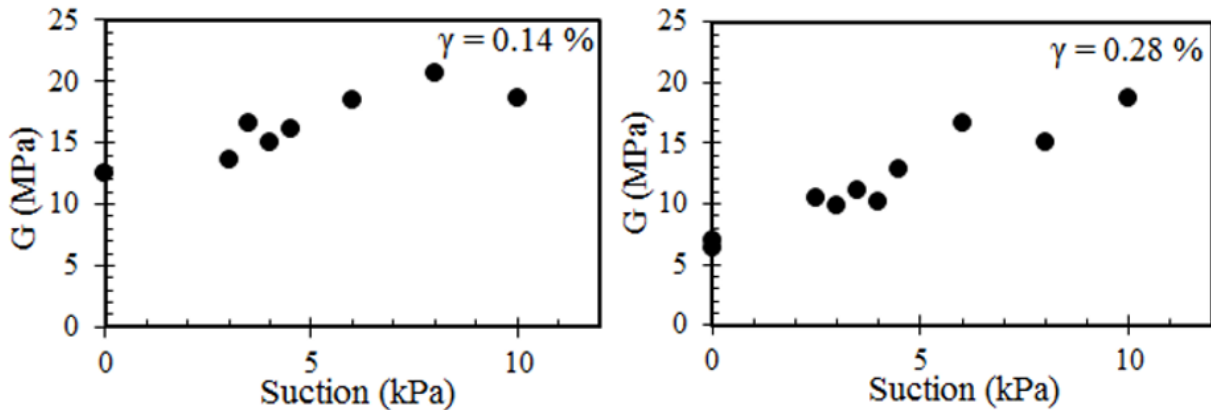


Figure 12: Recorded Shear Modulus Values of Partially Saturated Samples (after Ghayoomi et al., 2015)

Large strain shear moduli of partially saturated soils under different loading conditions (cyclic vs monotonic) have also been studied to a limited extent using commercially built direct simple shear machines (Jafarzadeh and Sadeghi 2012, Milatz and Grabe, 2015). The results of the normalized shear modulus and damping ratios obtained from Jafarzadeh and Sadeghi compared against results from other investigations is presented in Figure 13. It should be noted that different testing methods, state conditions, and soils were used by other investigations.

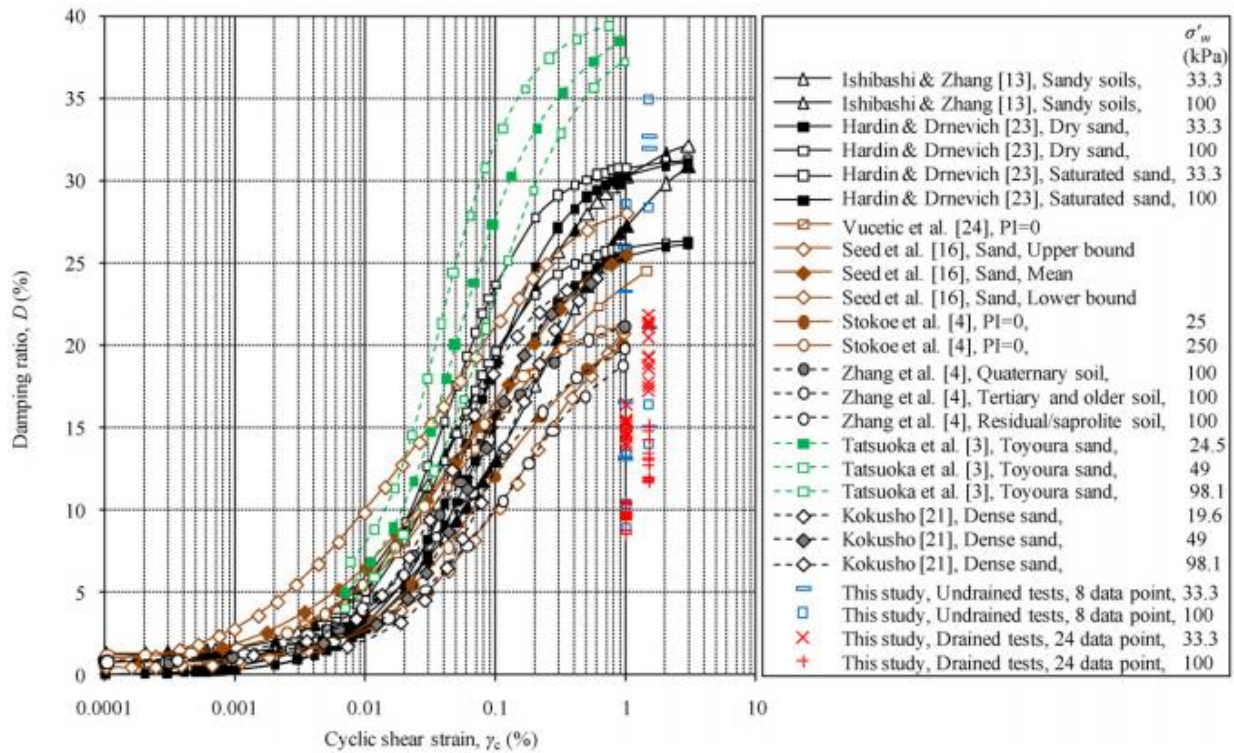
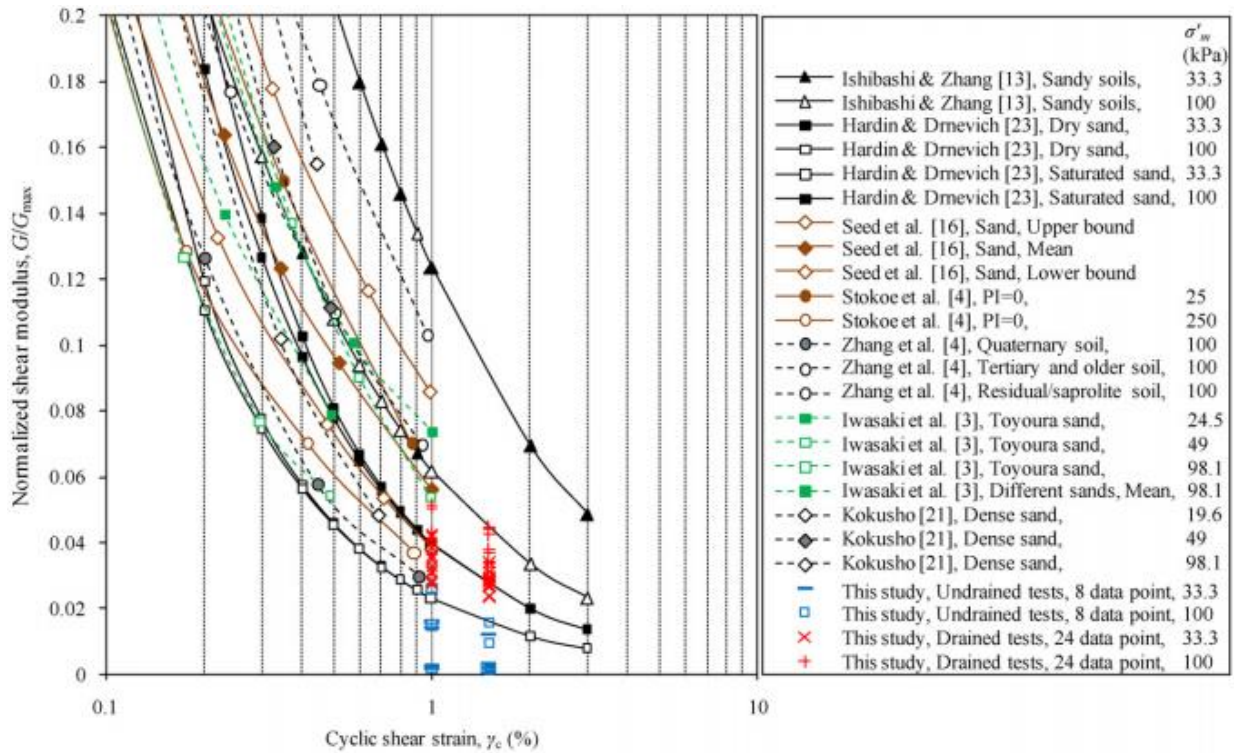


Figure 13: Results of the Normalized Shear Modulus and Damping Ratios (after Jafarzadeh and Sadeghi, 2012)

From the figure, the results from Jafarzadeh and Sadeghi indicate lower results than typical recorded results from other investigations. This is attributed to the different state conditions and testing methods used.

The damping ratios of unsaturated soils at small, medium, and large strains have been measured using resonant column and triaxial systems (Chin et al. 2010, Biglari et al. 2011, Hoyos et al. 2015). The results showed that as the matric suction increases, a stiffer soils is observed and less damping occurs (e.g, Figure 13).

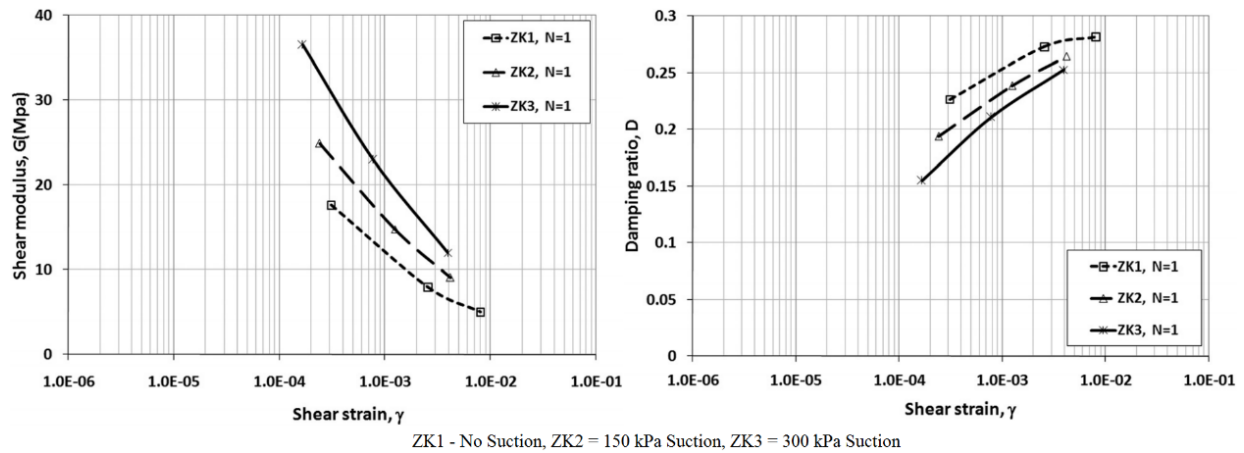


Figure 14: Shear Moduli and Damping Ratios (after Biglari, 2011)

2.3.2 Previous investigations on Seismic Compression

Seismic compression describes the volumetric/axial strain and pore fluid (both air and water) generation response of soils when subjected to dynamic loading. Previous research using direct simple shear apparatuses have shown that this behavior is linked with the composition of the soil, prepared relative density, stress history (OCR), and applied shear strain (Whang et al. 2004). The investigation led to the conclusion that the degree of saturation had a large effect on the amount of vertical deformation experienced by the soil as displayed in Figure 15. This effect was more noticeable on soils with a large amount of plastic fines than soils with a small amount of plastic fines.

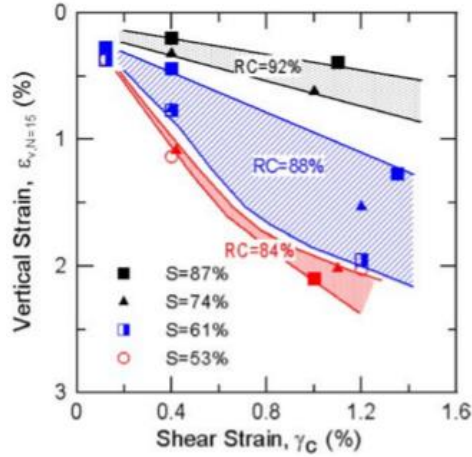


Figure 15: Effects of Relative Density and Saturation on Seismic Compression (after Whang et al., 2004)

Conversely, a study conducted by Duku et al. (2008) concluded that the degree of saturation showed no effect on the seismic compressional behavior of clean sands. A figure illustrating this effect is provided.

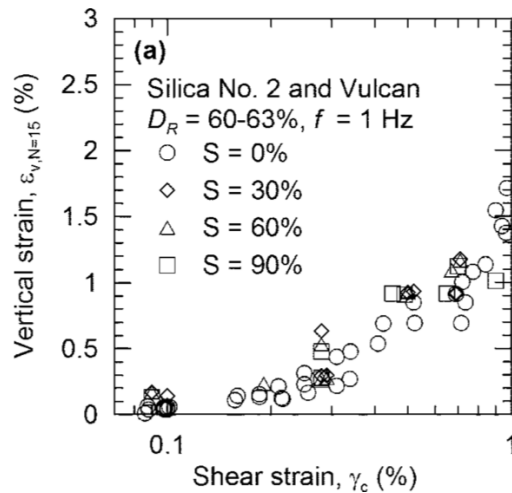


Figure 16: Lack of Effect of Saturation on Seismic Compression (after Duku et al., 2008)

It should be noted that these studies utilized a different method in order to prepare the samples. This technique (proctor compaction) could simulate a different mechanical behavior of the soil when subjected to different saturation levels. On the contrary, an investigation using a direct shear device modified to desaturate soils with the axis translation have shown that the soils experiencing higher matric suction will result in less seismic axial compression (Nishimura et al. 2010).

The importance of the drainage conditions on the pore water generation and dissipation of partially saturated soils has also been analyzed using a conventional triaxial system capable of generating dynamic earthquake motions (Sawada et al. 2006). The conclusion of the investigation was that if the maximum shear strain subjected to the soil was larger than 10%, the total volume change that was observed was not dependent on the saturation level (e.g. Figure 17). However if the shear strain was less than 10%, the drainage response affected the seismic compression experienced by the partially and fully saturated soils. Partially saturated soils were found to experience more volumetric strain during the undrained condition (during the earthquake motion) compared to fully saturated soils due to the compressional response of air in the soil matrix. Fully saturated soils exhibited more volumetric strains after the earthquake motion in the fully drained condition.

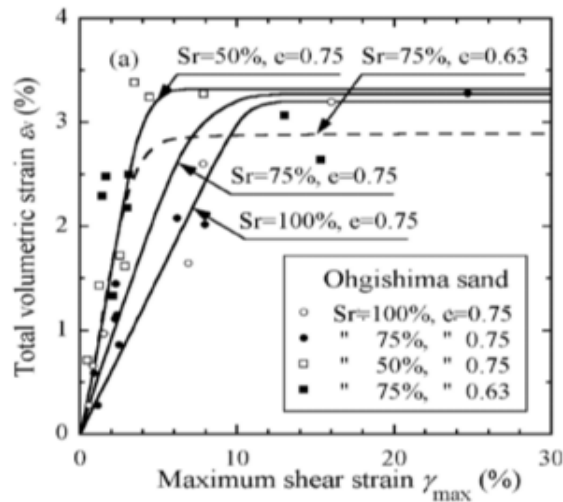


Figure 17: Effect of Saturation and Shear Strain on Volumetric Strain (after Sawada et al., 2006)

Furthermore, an empirical model developed by Ghayoomi and McCartney (2013) has been verified using centrifuge modeling to determine the total amount of settlement experienced by dry, partially saturated, and fully saturated sand layers subjected to seismic excitation. The model breaks the seismic settlement experienced by the soils in two different categories including compressional

and consolidation volumetric strains. The conclusion of this study showed that soil experienced the least amount of volumetric strains when the soil has a degree of saturation between 0.3 - 0.6 (e.g. Figure 18)

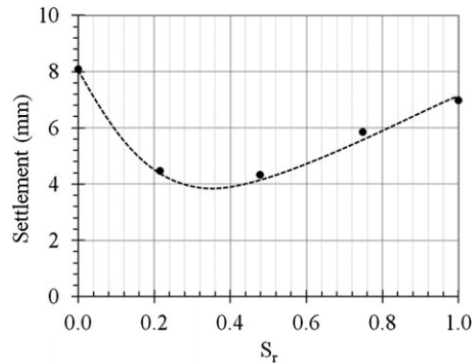


Figure 18: Effect of Saturation on Settlement (after Ghayoomi and McCartney, 2013)

2.3.3 Current Investigation on Dynamic Properties of Unsaturated Soils

The current investigation that will be conducted is unique in its own way compared to previous investigation due to the testing methods used and imparted shear strains. The axis translation technique has only been recently used to control the degree of saturation and matric suctions in soils. However, this technique has been used to test the dynamic properties in triaxial, resonant column, forced vibration, and bender element configurations which could lead to different mechanical responses (Chin et al. 2010, Biglari et al. 2011, Hoyos et al. 2015, Ghayoomi et al. 2015). Additionally, previous studies using direct simple shear systems to study dynamic properties have used the wet compaction method to control the degree of saturation (Duku et al. 2008). Previous investigations using direct simple shear apparatuses modified with the axis translation technique have tested soils at a limited amount of large cyclic shear strains (Jafarzadeh and Sadeghi 2012, Milatz and Grabe 2015). Therefore, the current investigation is essential to understand the behavior of soil when subjected to medium shear strains in a modified direct simple shear device.

CHAPTER 3

DIRECT SIMPLE SHEAR APPARATUSES

3.1 Introduction to Direct Simple Shear Machines

Although there are numerous tests to determine the dynamic properties of soils both in laboratory (ie. Cyclic Resonant Column, Cyclic Triaxial, acoustical testing), and in-situ conditions (ie. Seismic refraction and the pressuremeter), the direct simple shear apparatus is one of the more geo-mechanically preferred methods due to the direct measurements of shear stress and shear strain. It is often used to determine the liquefaction response of saturated soils subjected to medium to large strains or to understand seismic compression of compacted soils. Direct simple shear (DSS) machines allow geotechnical personnel to study the mechanical properties of soils when subjected to shear in one direction at a 1-G level (as opposed to centrifuge testing). The advantage of this test as opposed to other laboratory methods is that it best represents a soil element subjected to “simple shear”. In order to explain this, an example of a seismic shear wave example is presented.

In this conceptual example, a homogeneous soil mass lays above bedrock. A soil column is made up of individual soil elements (Figure 19a) and is considered to be in the “at-rest” condition. An earthquake motion is then introduced to the site (Figure 19b) and the bedrock moves in a lateral motion in the x – direction. A seismic shear wave (s-wave) propagates upwards (in the y - direction) through the soil column in the following form and individual soil elements (such as the one emphasized in red) are subjected to shear stresses. This response can be simulated by testing a small element of soil under similar simple shear stresses.

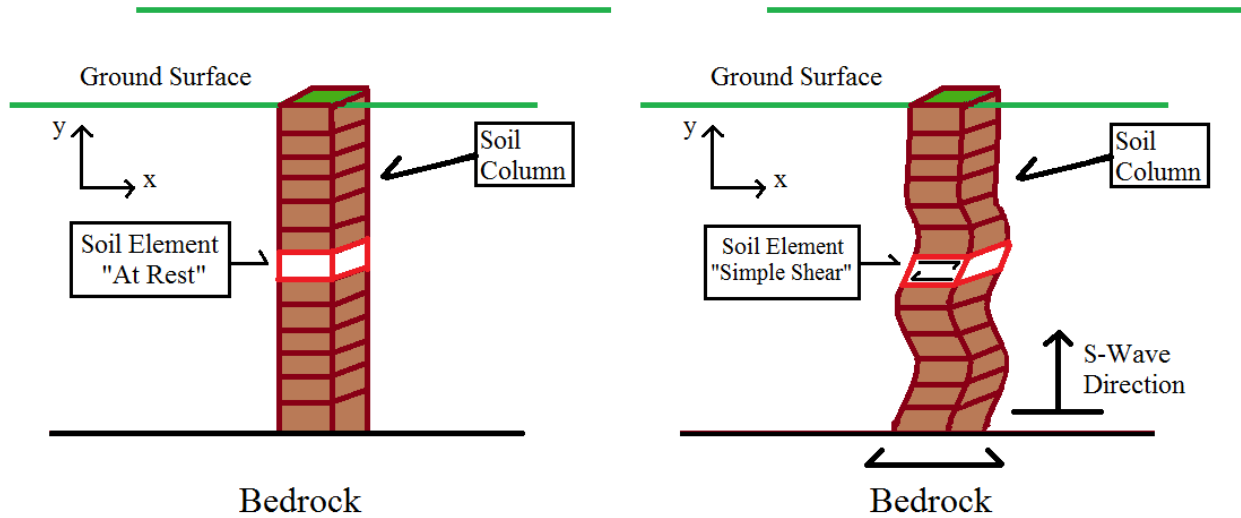


Figure 19: Conceptual Example of a Seismic Shear Wave System: a) before earthquake, b) during earthquake

3.2 Variation of DSS Machines

The main configuration of most direct simple shear apparatuses contains the same mechanical movements and measurements. These systems often keep a constant vertical pressure applied to the top of the specimen while a horizontal static or cyclic shear load is applied to the sample. Then, the corresponding forces and displacements are measured. The variations between these systems are often in the sample containment methods and dimensions. The sample confinement methods and size effects will be discussed in the subsequent sections.

3.2.1 Effects of Sample Confinement (SGI, NGI, and Cambridge)

The confining boundaries used to maintain a constant lateral volume for the soil sample consists of three different methods. The first method was developed by the Swedish Geotechnical Institute in 1936 and uses a rubber membrane to hold the sample together. A set of metal rings is then placed around the sides of the sample (Kjellman, 1951). The second method was developed by the Norwegian Geotechnical Institute; this method uses a wire reinforced rubber membrane to maintain a constant volume. The third method was developed by a researcher at the University of

Cambridge that used plates mounted with hinges to impart a uniform load across the sample (Roscoe, 1953). These confinement methods have been shown to slightly affect the residual behavior of the soil that is tested (McGuire, 2011). The confinement methods are illustrated in the next figure.

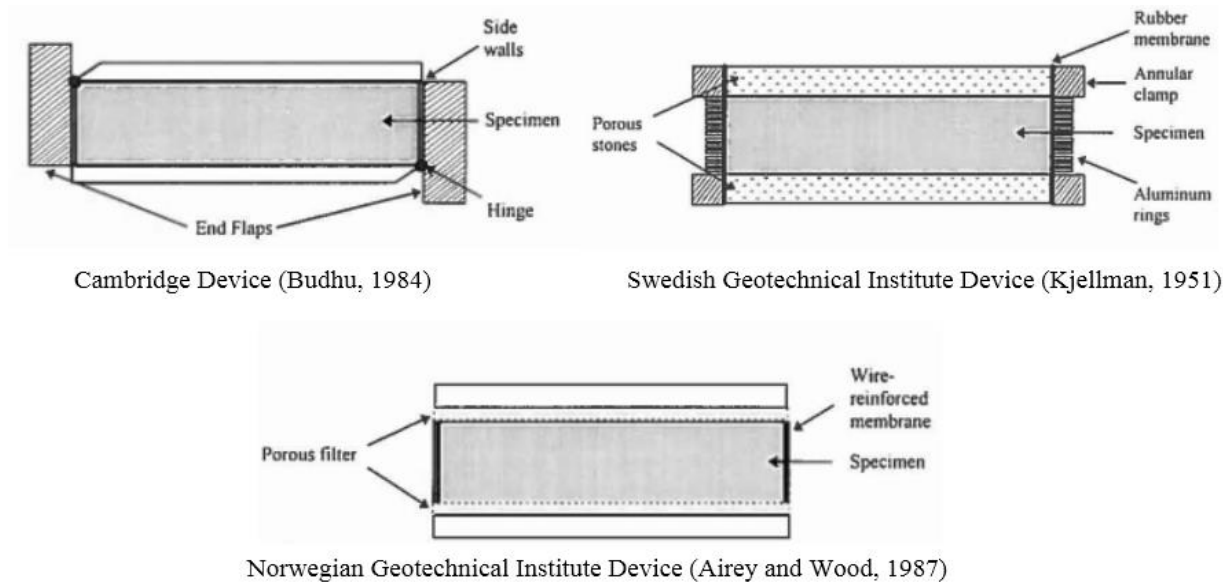


Figure 20: Cross-Sectional Views of Various DSS Apparatuses (after Dunstan, 1998)

3.2.2 Effects of Specimen Sample Size

The effects of specimen dimensions on the static stress-strain behavior have been studied by numerous researchers (Wright et al. 1978, Vucetic 1982, Budhu and Wood 1984). The results from these studies have shown that static stress-strain behavior was not influenced by the H/D ratio, nor the confinement method chosen.

However, in regards to the dynamic properties, a study conducted by Shen et al. (1977) showed that the H/D ratio affects the uniformity of the shear strain distribution along the sample. As this ratio decreases, a more uniform shear strain distribution along the boundaries of the sample can be observed. A discussion point brought up by Shen questions the capability to use the external horizontally applied strain as a basis for the dynamic response of the soil mass due to the non-uniformity of the displacement throughout the specimen.

In addition to the H/D ratio, the distribution is also affected by the percentage of wire-reinforcement (for NGI tests), the elastic modulus of the soil, the Poissons' ratio, and the applied horizontal displacement.

ASTM Standard D6528 – 07 recommends that the maximum H/D ratio to be less than 0.40 with a minimum height and diameter of 12 mm and 45 mm, respectively. A variety of researchers have modified the dimensions of the sample size to be less than the maximum H/D ratio set forth by the standard. The dimensions used for each investigation is provided in the table below.

Table 1: Dimensions of various DSS Sample Specimens

| University and Researchers | Title of Work (Year) | Type of Test | Specimen Diameter | Specimen Height | H:D ratio |
|---|---|------------------------------|--------------------------|---|---------------------|
| MIT - Imtiaz Ahmed | Investigation of Normalized Behavior of Resedimented Boston Blue Clay using Geonor DSS Apparatus (1990) | Geonor DSS - SGI - undrained | 6.7 cm (2.59 in.) | 2.3 cm (.905 in.) | 1: 2.91 |
| UMass-Amherst - D. DeGroot, C. Ladd | Undrained Multidirectional Direct Simple Shear Behavior of Cohesive Soil (1996) | Multidirection DSS - NGI | 6.7 cm (2.59 in.) | 2.3 cm (.905 in.) | 1: 2.91 |
| UCLA - M. Vucetic, G. Lanzo, M. Doroudian | Damping at Small Strains in Cyclic Simple Shear Test (1998) | DS-DSS - NGI | 6.6 cm (2.59 in.) | 2 cm (typical) | 1: 3.3 |
| UCLA - A. Mortezaie & M. Vucetic | Effect of Frequency and Vertical Stress on Cyclic Degradation and Pore Water Pressure in Clay in the NGI Simple Shear Device (2013) | NGI Undrained | 66.7 mm (2.62 in.) | 18.5 mm (.728 in.) | 1: 3.6 |
| UCDublin - N. Boylan & M. Long | Development of a Direct Simple Shear Apparatus for Peat Soils (2008) | Cambridge - Undrained | 70 mm (2.75 in.) | Variable (5 to 35 mm) or (0.197 to 1.378 in.) | 1: 14 to 1:2 |
| UNH - H.Miller | Development of Instrumentation to Study the Effects of Aging on the Small Strain Behavior of Sands (1994) | SGI - Undrained | 10.2 cm (4 in) | 2.54 cm (1 in) | 1: 4 |
| UCLA - P.M. Duku & J.P. Stewart | Digitally Controlled Simple Shear Apparatus for Dynamic Soil Testing (2007) | NGI -Undrained | 10.2 cm (4 in.) | 2 cm (typical) | 1: 5.1 |
| UC Davis - Shen et al. | An Analysis of NGI Simple Shear Apparatus for Cyclic Soil Testing (1977) | NGI - Undrained | 3.2 in. | 0.8 in | 1: 4 |
| ASTM D6528 – 07 | Standard Test Method for Consolidated Undrained Direct simple Shear Testing of Cohesive Soils (2007) | NGI - Undrained | 45 mm (min) | 12 mm (min) | 0.4 (max) or 1: 2.5 |

3.2.3 Recent work by other institutions

Over the past couple of years, a variety of new types of DSS apparatuses have been developed by universities and institutions across the world. A system developed by the University of California – Los Angeles has the capability to control and accurately impart cyclic and static loads in 3 different directions (X, Y, and Z) using an integrated and complex system of PID loops (Duku et al., 2007).

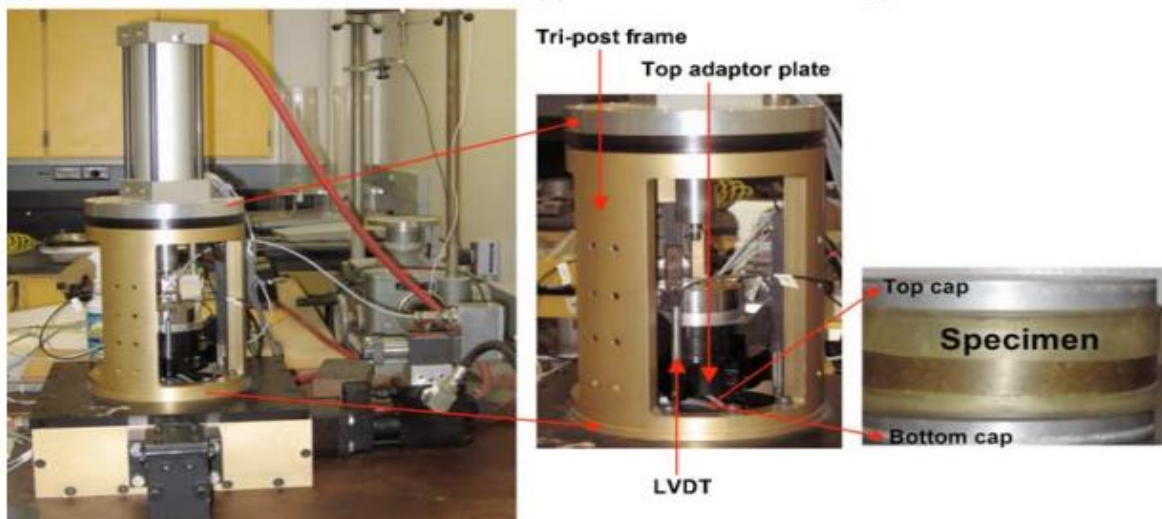


Figure 21: Digitally Controlled – Simple Shear Apparatus at UCLA (after Duku, 2007)

Another system developed at the University of California is the double specimen DSS (DSDSS). This apparatus features two parallel samples that are loaded at the same time; the main advantage of using this system was the ability of eliminate false deformation readings for a particular specimen due to system compliance and friction limitations (Doroudian and Vucetic, 1995).

At the Texas A&M University, a prototype of a multi-directional DSS system was developed with the extended ability to impart a back pressure to the system. This ability allows for the system to act essentially as a triaxial system and provides a more effective way to saturate the soil sample, while having the ability to shear the sample in a horizontal manner (Rutherford, 2012).

3.3 UNH DSS System

The Direct Simple Shear system at the University of New Hampshire was developed by Dr. Pedro de Alba and Heather Miller in 1992. The system was initially built to study the small strain behavior of Holliston 00 sand in relation to thixotropic effects. The system was then further modified by Alicia Dunstan in 1998 to effectively produce even smaller strains that could be applied to reconstructed Gulf of Mexico clay samples.

The system is comprised of multiple parts including (1) the framework, (2) vertical and horizontal actuators to provide movement, (3) a control system hardware/software and data acquisition (DAQ) system, and (4) various sensors to measure the behavior of the soil. The framework of the system is comprised of a steel frame based on top of a steel table. A set of Thomson ball slides provide a guide for the bottom platen of a soil system to be guided in a horizontal direction. Another set of slides is fixed along the sides of the soil cell to allow a vertical load to be guided onto the sample.

The vertical movement is provided by a pneumatic actuator and is regulated by a load cell and a linear variable differential transducer (LVDT). The horizontal movement is provided by a hydraulic actuator and is controlled on a Proportional Integral Derivative (PID) system in which a capacitive transducer provides horizontal distance feedback to the controller. A block diagram showing the electrical layout of the PID system and integration of the signal feedback is provided in the appendix. The following figure shows the current setup of the UNH-DSS.



Figure 22: Current Configuration of the UNH - DSS

Numerous changes have been made to the system in the last two years in order to allow the system to become operational since its last previous working state in 1998. During this time, the system required an entirely new digital controller for the horizontal actuator since the previous controller could not be located. The new controller and data acquisition system is based off of the National Instruments software LabVIEW and allows users to acquire signals, record the response, and control the sensors in the system. Additionally, the hydraulic pump to provide the accumulators and actuator with the hydraulic fluid was also replaced. The specifications of the sensors used, controller module, hydraulic equipment, data acquisition modules/chassis system, and GeoTac flow pump are provided in the appendix.

In the previous system, the user interface allowed users to designate whether the system was load or displacement controlled for cyclic testing. The current setup allows users to designate the amplitude of the displacement (strain-controlled), however it is not setup for load (stress) controlled testing at this stage.

The soil sample configuration is based off of the Swedish Geotechnical Institute (SGI) DSS setup. The soil sample is confined by a series of silicon/teflon coated metal rings that are stacked. The soil sample is 10.16 cm (4 inches) in diameter and approximately 2.54 cm (1 inch) in height. The vertical piston can produce pressures of up to 137.412 kPa (20 psi) onto the sample, pressures above this limit will cause leaks in the piston seals. The damper system consists of two springs and a steel beam to provide stability to the hydraulic piston; it can be modified with different sets of springs to provide a stable loading condition for different strain ranges. The current damper configuration is limited to net horizontal movements between $4.305 \cdot 10^{-4}$ cm ($1.695 \cdot 10^{-4}$ inches) and $1.506 \cdot 10^{-3}$ cm ($5.9 \cdot 10^{-4}$ inches).

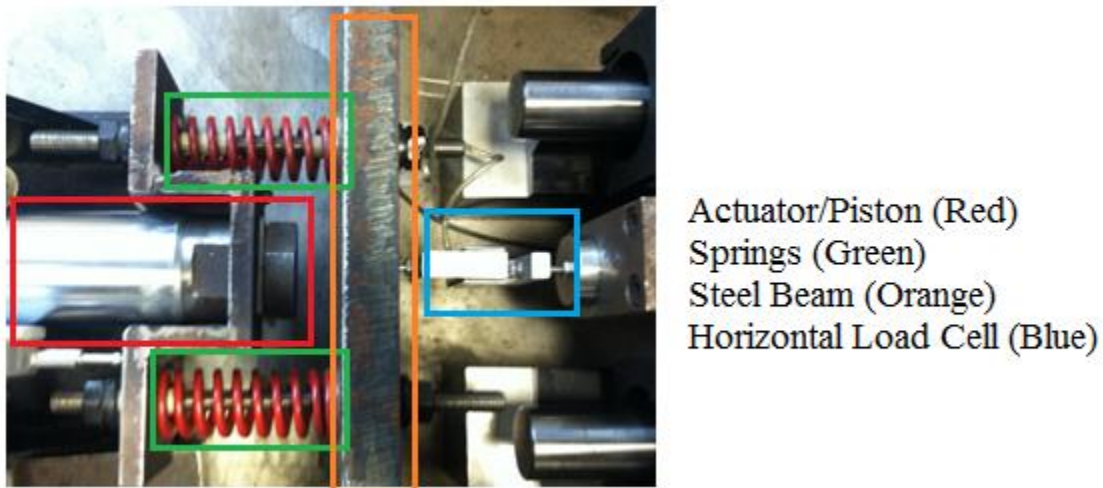


Figure 23: Current damper configuration for horizontal movement (top view)

The technique of controlling the horizontal loading is also known as closed loop PID control. This technique uses a controller integrated into the computer to send a signal to the servo-amplifier and then to the servo-valve attached to the hydraulic piston/actuator. The piston motion is then transferred through the damper system previously mentioned. The motion is transferred to the horizontal load cell to one side of the bottom table (which rests on top of the Thomson slides) and to the soil sample (built on top of the bottom table). On the other side of the bottom table is a

capacitance transducer that records and provides (distance) feedback to the computer and controller. The signal is then used to make adjustments to the servo-amplifier to complete the cycle over again.

A full schematic of the UNH Direct Simple Shear System with the position of the labeled pumps, actuators, sensors, piping, and soil chamber is provided in the following figure.

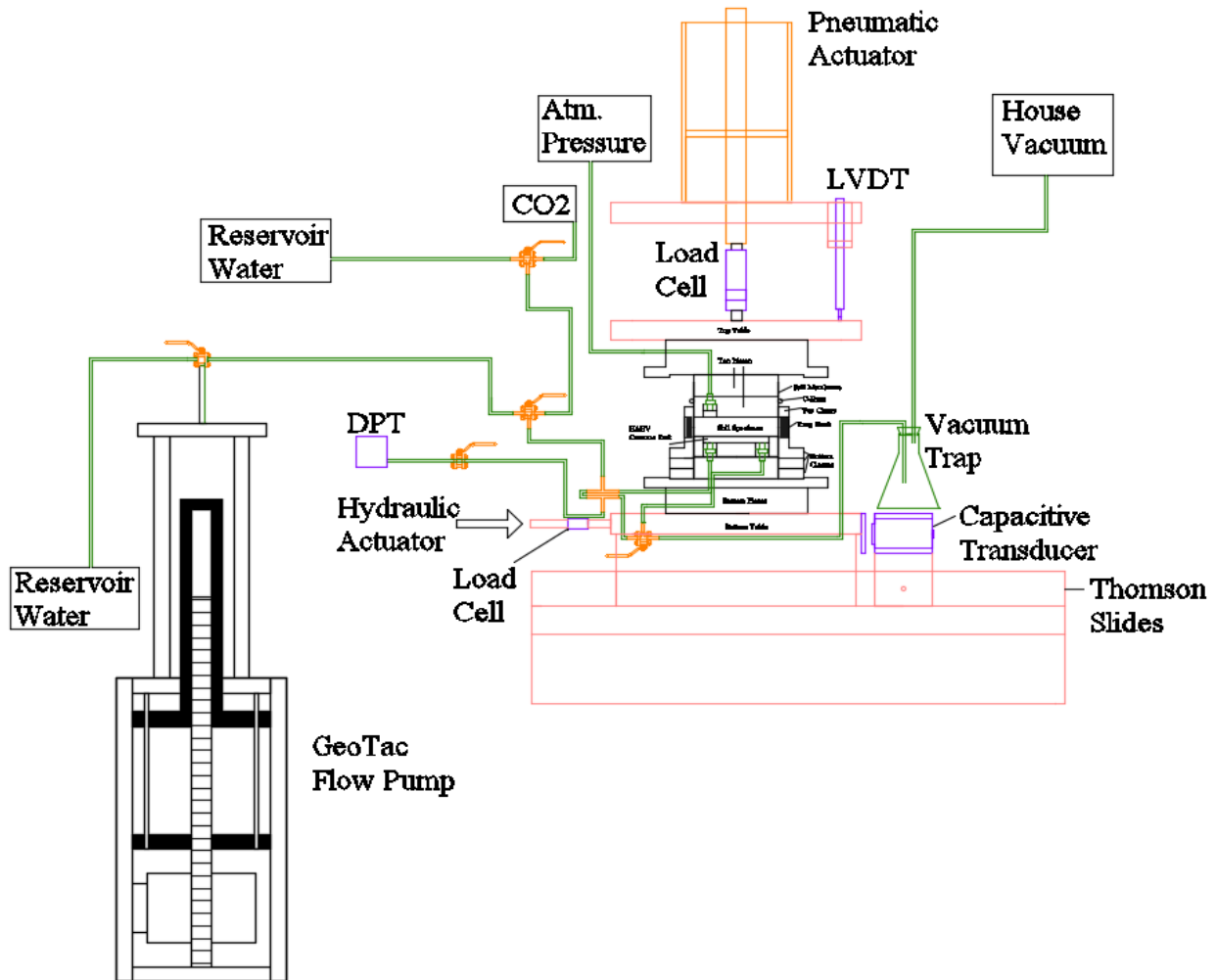


Figure 24: DSS Schematic Architecture: Full System

3.4 Modification for Partially Saturated Soils

In order to accurately control the degree of saturation in partially saturated soils using axis translation technique, a High Air Entry Value (HAEV) ceramic disk is often utilized. This disk

allows the flow of water to enter through the bottom, while prohibiting air (past a threshold value) to enter through the top. The HAEV ceramic disk that is incorporated into the bottom platen in the UNH – DSS is rated at ½ bar (50 kPa). The outer edges of the disk are epoxied to the platen to ensure that air cannot penetrate between the interface of the disk and platen. The bottom platen also includes a water channel and compartment underneath the disk to allow the user to flush out any air that may be trapped. The modified bottom platen is shown in the next figure, while the schematic and dimensions for the platen and the adapter can be found in the appendix.



Figure 25: Modified Base Platen w/ embedded HAEV ceramic disk

In addition to the modification to the soil sample cell, a Geotac Digiflow Automated Flow Pump was incorporated into the system. This pump allows users to control the water pressure, u_w beneath the HAEV ceramic disk and thus the matric suction in the soil cell. Additionally, a calibrated differential pressure transducer measures the difference in pore air pressure at the top (atmospheric) and pore water pressure or matric suction at the bottom of the sample. Depending on the stage of the test, various valves can be opened and switched in order to allow certain conditions to be applied. Specifications on the flow pump are provided in the Appendix section. The piping network is shown in the following schematic.

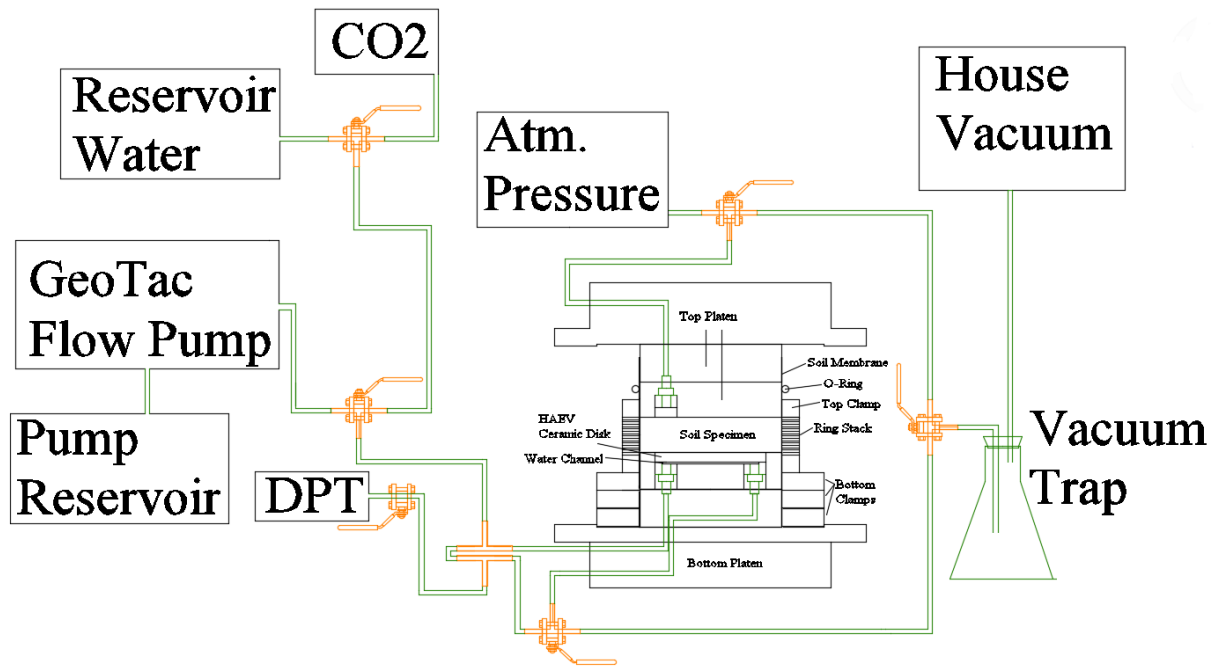


Figure 26: Soil Cell with Piping Schematic

CHAPTER 4

SAMPLE PREPARATION & TESTING

4.1 Testing Material Properties

F-75 Ottawa silica sand was used for this investigation. This sand is classified as a clean poorly graded (SP) soil according to the Unified Soil Classification system. The grain size distribution curve was created by performing a sieve analysis in accordance with ASTM C136-14 and is shown in the subsequent figure. The coefficient of uniformity, C_u and curvature, C_c were both determined from this figure.

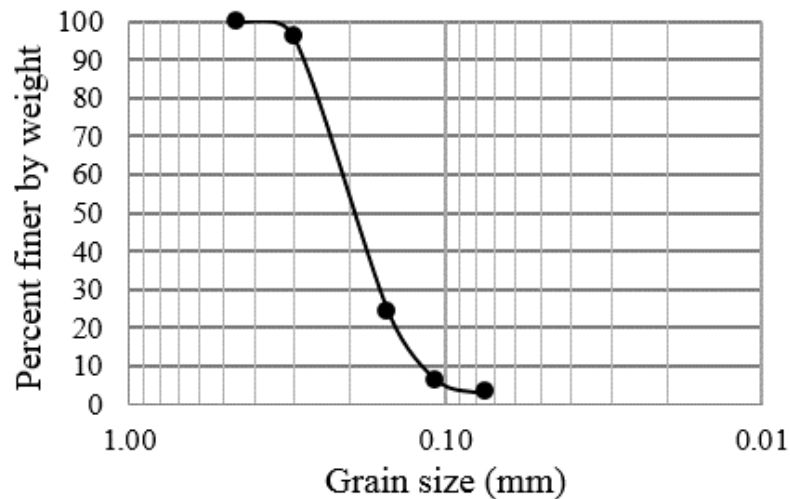


Figure 27: Grain Size Distribution of F75 Ottawa Sand (after Suprunenko, 2015)

Additionally, the sand's maximum and minimum densities were determined using ASTM D4253 and ASTM D4254, respectively. Results from these tests were shown to be lower than other published values (Hargy, 2011). To be consistent with other test analyses that used the same soil, the properties of the sand for e_{min} , e_{max} , ρ_{min} , and ρ_{max} are based off a previous study that utilized the same soil. The friction angle for the sand was determined through an average of 3 static triaxial

tests prepared at a relative density of 45% (Suprunenko, 2015). A summary of the geotechnical properties of the tested sand are presented in the following table.

Table 2: Various properties of F75 - Ottawa Sand

| Property | Value |
|--|--------------|
| Specific Gravity | 2.65 |
| e_{min}, e_{max} | 0.486, 0.805 |
| $\rho_{min}, \rho_{max} \text{ (kg/m}^3\text{)}$ | 1468, 1781 |
| Coefficient of Uniformity | 1.83 |
| Coefficient of Curvature | 1.09 |
| Prepared Specimen Relative Density | 45% |
| Friction Angle ($^{\circ}$) | 40 |

4.2 Sample Preparation

The soil sample was constructed on top of a bottom platen using the following procedure. Various aluminium collar rings were attached to the platen and were used to clamp a soil membrane around the base of the soil sample. Vacuum grease and O-rings were attached to the membrane to create a seal. A stack of Teflon coated aluminium rings was then inserted onto the sample and made flush with the base. A vacuum mold was installed onto the platen and the membrane was stretched over the top of the mold. A picture of the assembled bottom system before sample preparation is shown in Figure 28.

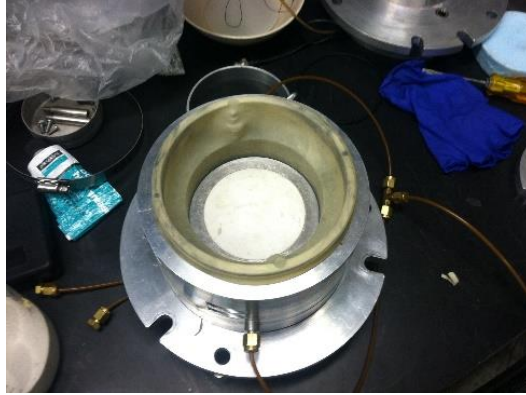
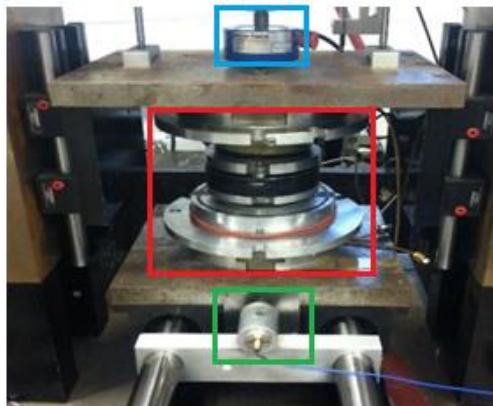


Figure 28: Bottom platen of cell with assembled vacuum mold

A piece of filter paper was then inserted inside the membrane. Ottawa sand was then dry pluviated into the mold to the desired density. It is then levelled off and another piece of filter paper was inserted on top of the sand. The height of the sample is recorded into a spreadsheet. A regular porous disk was placed on top of the filter paper and guiding rods were then installed around the edges of the bottom platen. The top platen was then slowly lowered onto the guide rods and on top of the porous disk. An annular clamp was then installed to secure the membrane to the top platen. The vacuum mold was then removed. The soil sample was inserted into the DSS system and clamped into place using T-Clamps that are embedded into the top and bottom platens of the soil chamber. The guide rods were then removed at the end. A picture of a fully assembled soil chamber in the DSS system is shown in Figure 29. A step by step procedure outlining the entire sample preparation and testing procedure is also provided in the appendix.



Vertical Load Cell (Blue)
Soil Chamber (Red)
Capacitance Transducer (Green)

Figure 29: Soil Sample Chamber installed in the DSS system

4.3 Vertical Consolidation

After inserting the sample into the apparatus, a vertical load is applied to the sample by manually adjusting an air regulator. The values of the consolidation of the sample are acquired manually by reading values of the LVDT and load cell in the LabVIEW interface. These values are then presented in a spreadsheet. The vertical consolidation of the sample results in changes of the height of the sample and thus a change in relative density (varies sample to sample, typically from 3% - 20%). To account for this change in density, the vertical deformation was used to adjust the tested relative density.

One of the implications of using the current DSS system is the approximation of the vertical load. In the previous system, the application of the vertical load utilized a pneumatic servo-valve system to create a PID loop with the designated load. In the current system, the manual use of an air regulator results in a vertical load with a variance of 5 - 10%. In order to consider the effects of variance in the system, a normalization process was used. Further details on this process will be provided in analysis section.

4.4 Sample Saturation and desaturation to the target matric suction

A variety of tests were conducted on multiple samples. In general, there were 6 types of tests that were conducted regarding the degrees of saturation; these tests consisted of a completely dry, fully saturated, and multiple partially saturated tests (w/ matric suctions at 4 kPa, 5kPa, 6kPa, 8kPa, and 10 kPa).

It should be noted that when soils are subjected to partially saturated and fully saturated conditions, the air pressure in the sample was kept at atmospheric conditions, while the water pressure below the HAEV disk was kept at a “constant” pressure using the flow pump. To verify this state when the cyclical loading was applied, the pore water pressures (PWP) were recorded

using values provided by the DPT. Fully saturated soils were kept under the same conditions (as the partially saturated soils) and were subjected to the flow pump's active control of maintained constant PWP below the HAEV disk. However, when subjected to a cyclic load, excess pore water pressures could build up since the flow-pump may not have had time to extract water from the sample in time. This would result in "partially" drained conditions for both unsaturated and "fully" saturated soils. This effect could be considered an issue if the excess pore water pressures are large as it directly affects the stress inside the soil element, however further analysis is presented in a later section of this thesis.

In order to fully saturate the samples, de-aired water was flushed through the bottom of the specimen. The height of the water in the tank was considered to ensure that a quick condition did not occur during this process. Unlike a triaxial system in which back pressure saturation can be achieved by applying a confining cell pressure to the sample, the water level (saturation level) in the DSS sample was checked by reading a value from a calibrated differential pressure transducer (DPT). The flow of water was cut from the tank and the sample water level was allowed to equilibrate. Full saturation was assumed when the DPT reading was higher than the top of the sample.

Samples considered to be "fully saturated" may only be 87 – 93% saturated, whereas Skempton's B – value method of saturation allows samples to have a degree of saturation of 95 - 99%. In order to be consistent with the implications of the "fully saturated" soils, the obtained SWRC was consistent with the same method of saturation. However, fully saturated specimens in this study are more accurately "nearly saturated"

The desaturation of the sample to the target matric suction was conducted using the axis translation technique. The valves connecting the sample to the flow pump were opened and the

pump extracted water from the sample. In a similar fashion, the SWRC was created using a similar procedure. The software that controls the flow pump is shown in the ensuing figure and allows users to track, control, and record the volume and pressure of the pump.

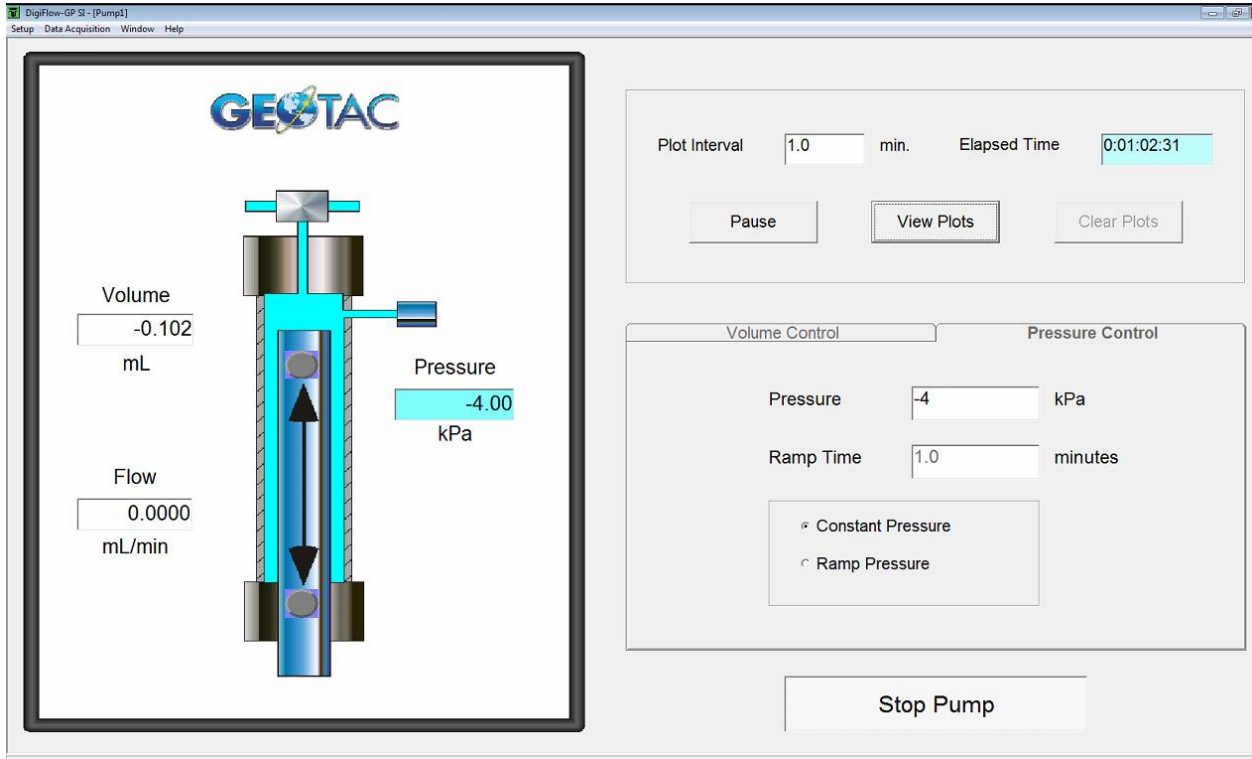


Figure 30: GeoTAC software for the DigiFlow Pump

The procedure for the SWRC measurement consisted of extracting water from the sample at constant increments of applied suction. Values of the extracted water volumes and readings from the DPT were taken once the sample was determined to be at a steady state condition (when the flow of water was less than 0.0002 mL/min). Matric suction values were calculated by establishing a reference pressure at the middle of the soil sample and subtracting the reference pressure from the values read from the DPT at a steady state condition. The results of the SWRC are shown in the next figure. The following van Genuchten parameters were then determined by fitting the curve on top of the experimental data. The experimental data was also compared to previous

investigations that also utilized the same material subjected to partially saturated conditions. These parameters are presented in Table 3.

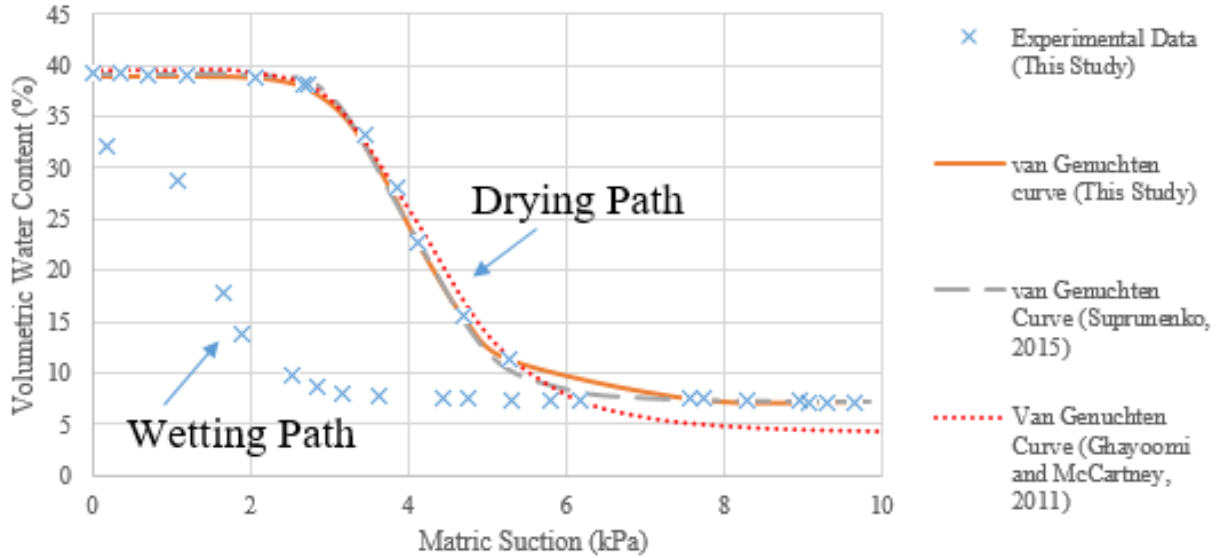


Figure 31: Soil Water Retention Curve of F75 Ottawa Sand

Table 3: van Genuchten Parameters of F75 Ottawa Sand

| van Genuchten Parameters | Current Study | Suprunenko, 2015 | Ghayoomi and McCartney, 2011 |
|-----------------------------|---------------|------------------|------------------------------|
| Alpha, α | 0.25 | 0.25 | 0.24 |
| N | 8 | 9 | 7 |
| Residual Water Content (%) | 7.15 | 7.2 | 4 |
| Saturated Water Content (%) | 38.9 | 39.2 | 39.5 |

The initial soil water retention curve was based on a soil sample that was prepared at a relative density of 45%. However, after vertical consolidation, the relative density increased in each specimen. Therefore it was necessary to complete a SWRC when the sample was in the DSS chamber. A comparison of the volumetric water content in the sample verse matric suction is shown in the next figure.

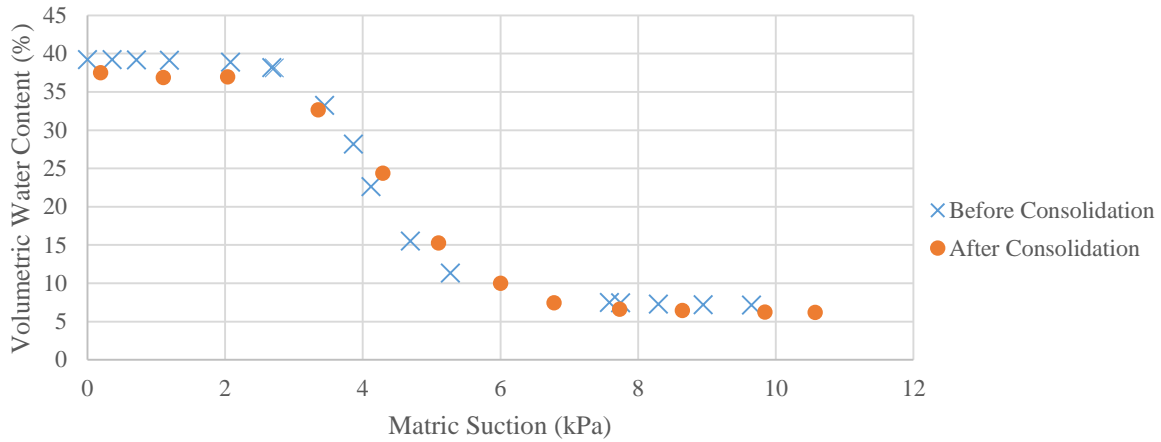


Figure 32: Comparison of SWRC before and after consolidation

It is apparent from the figure, that the volumetric content is slightly affected by the consolidation stage in the test. This is mainly due to the amount of water that the can fill the voids of the sample with a lower porosity, however when comparing the degrees of saturation of the entire specimen, it is apparent that the degree of saturation is not significantly affected by the consolidation stage.

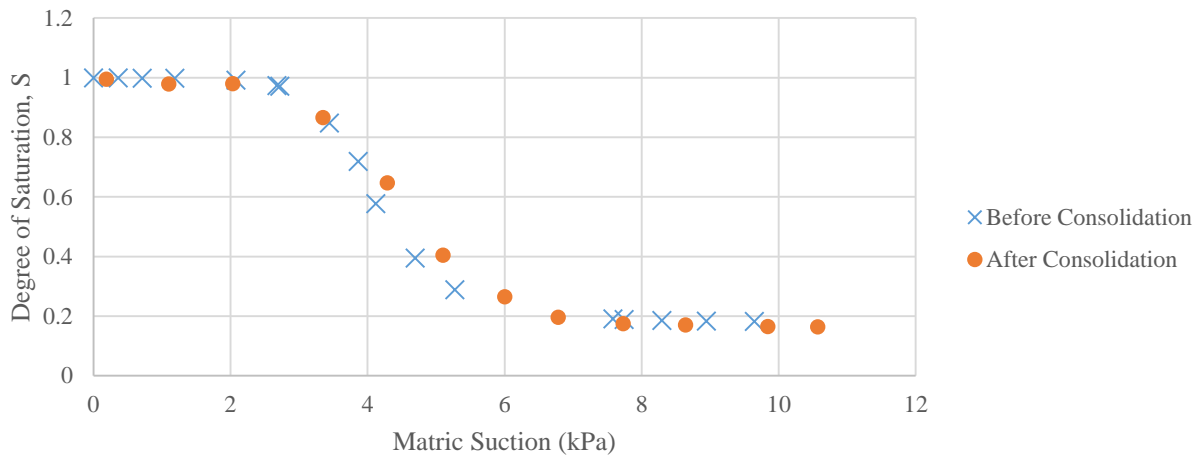


Figure 33: Degree of Saturation before and after consolidation

In addition to the soil water retention curve obtained from testing, the fitted van Genuchten for the tested soil is compared against the HAEV ceramic disk to show the relation of how the disk separates the air – water interface is shown in Figure 34.

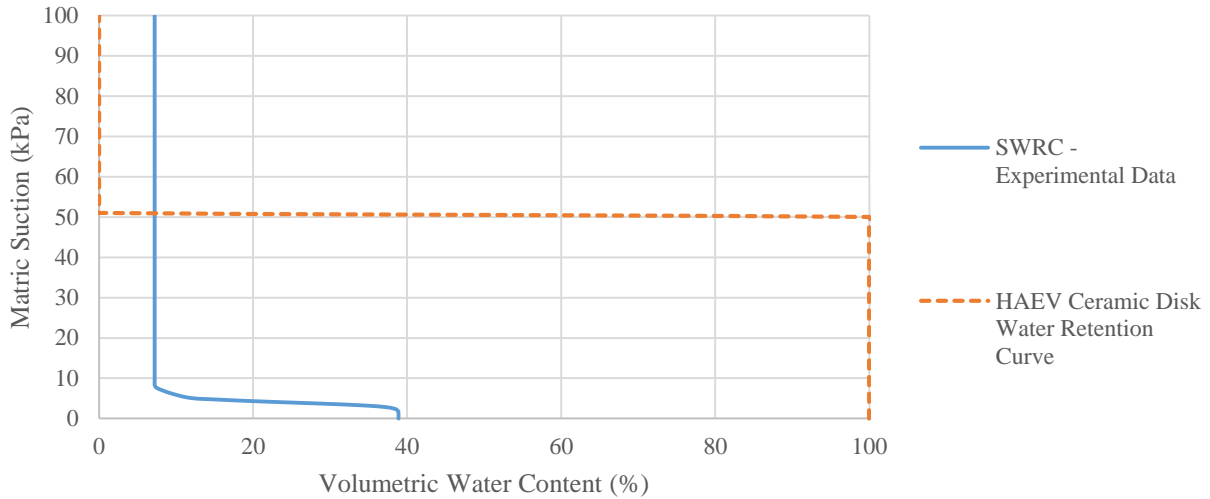


Figure 34: van Genuchten curve vs HAEV threshold

It should be noted that the van Genuchten curve is extrapolated to extremely high values of matric suction in order to show the limits of the HAEV disk. From this figure, it is readily apparent that the HAEV disk rated at 50 kPa is sufficient enough for this soil to reach residual water contents without passing the threshold value of the disk.

4.5 Applying cyclic loads (Direct Simple Shear Testing)

In order to start cyclical testing, the hydraulic actuator is started. It should be noted that when turning the hydraulic actuator on, a pressure on the springs – steel beam and damper system causes a slight monotonic load that is not taken into consideration. The effect is unavoidable since the pump cannot be turned on for an extended period of time (due to a slow apparent leak of hydraulic oil between the seals of the servovalve/actuator).

After the designated degree of saturation is reached, the program *LabVIEW (shaker-daq-main.vi)* is opened. The program interface (before a test is run) is shown in the following figure.

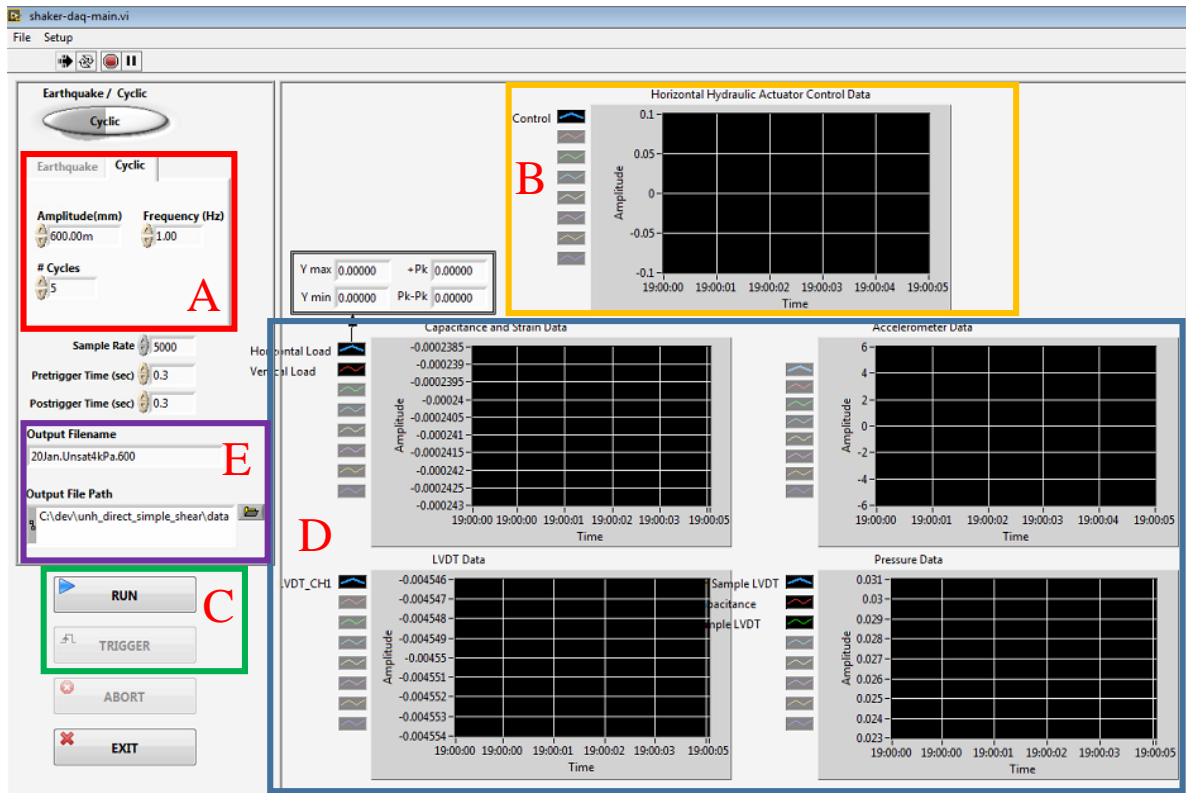


Figure 35: User Interface of UNH-DSS Data Acquisition System and Control

In the interface, the designated amplitude, frequency, and duration of the control signal is inputted into the software (Box A). The control signal that is sent to the actuator is shown in Box B. Live signals from the sensors are initiated when the “Run” button is pushed. The horizontal loading is initiated when the “Trigger” button is engaged by the user and feedback from the various sensors are then recorded (Box D). The recorded signals are exported into a destination path shown in Box E as an Excel file. Although the control signal amplitude is designated by the user, slight variations between the recorded motion and control signal exist between tests with the same amplitude. These variations are accounted for when normalizing the shear modulus values. The motion is applied to the sample using the technique described in the previous chapter.

4.6 System Mechanical Compliance Corrections

4.6.1 Top Table Movement

It was observed from multiple tests and a previous investigation that there is movement in the top table (attached to the top of the sample cell). Although the primary cause is not fully understood, it is suspected that this motion is induced by the attachment of the damping system to the loading frame. In the previous system developed by Dunstan, the effect of the top table movement was considered for correcting the net displacement of the sample. Through a compiled amount of tests, the top table movement was simultaneously recorded for each test. On average, the top table motion was found to contribute 61.5% to the net cyclic motion. For example, a sample that was subjected to a horizontal distance of 0.0006 inches at the bottom of the sample, would have 0.000225 inches of movement at the top. The net motion would be the top motion subtracted from the bottom motion, resulting in a net movement of 0.000375 inches. The recorded motions were compiled into the subsequent figure and a polynomial function to best estimate the top table movement as a function of the bottom table movement was obtained.

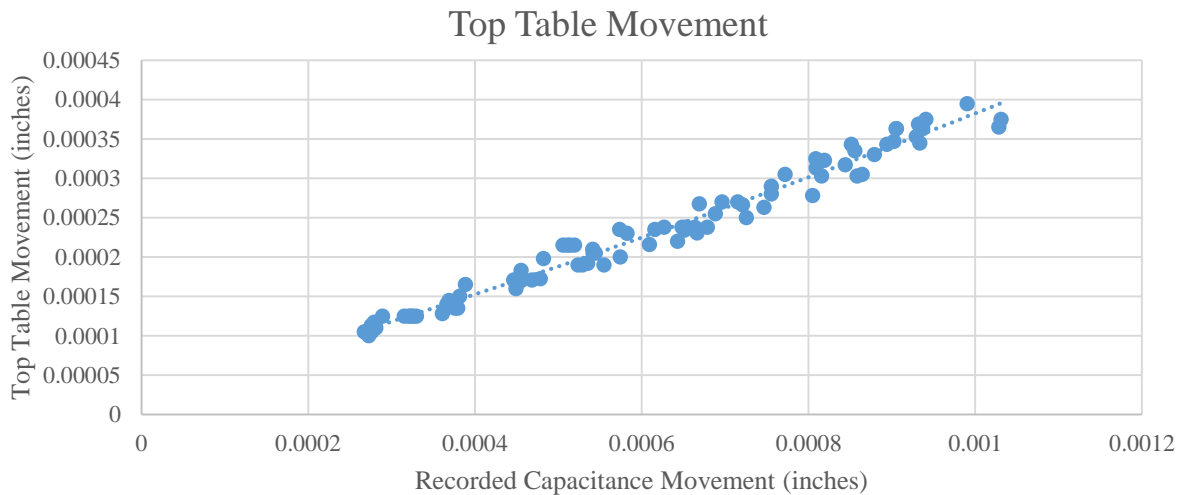


Figure 36: Correlation between the top and bottom table movement

$$y = 55.36x^2 + 0.306x + (2.15 \cdot 10^{-5}) \quad (30)$$

In this equation, y is the top table movement and x is the recorded horizontal motion captured by the capacitance transducer from the bottom table movement. The net horizontal motion subjected to the sample would be the top table movement subtracted from the recorded capacitance motion. In order to apply this concept to the cyclical horizontal motion, a sine wave with the same period and time delay of the control signal is overlapped onto the recorded capacitance signal. The recorded motions from the top sample LVDT and capacitance transducer were found to be in sync with no noticed delay when the horizontal motion was applied. The amplitude of the top table movement is provided by Equation 30. The resulting signal represents the net horizontal motion of the sample. The position of the top sample LVDT is presented in the subsequent figure.

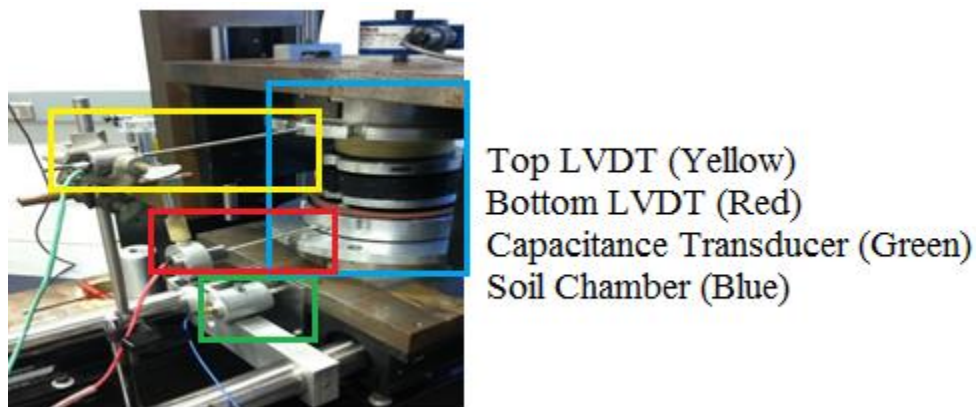


Figure 37: Top and Bottom LVDT sensors for distance corrections

4.6.2 Friction Response Correction

Although the system utilizes a set of low friction Thomson slides in order to provide guidance for bottom of the sample, there is internal resistance that would contribute force to the sample. To account for this resistance, a water sample was created. Since water does not have a shear resistance, the response of the sample would indicate the amount of force required to move the bottom table. The results of the water sample tests and correlation between the movements and force is presented in the ensuing graph.

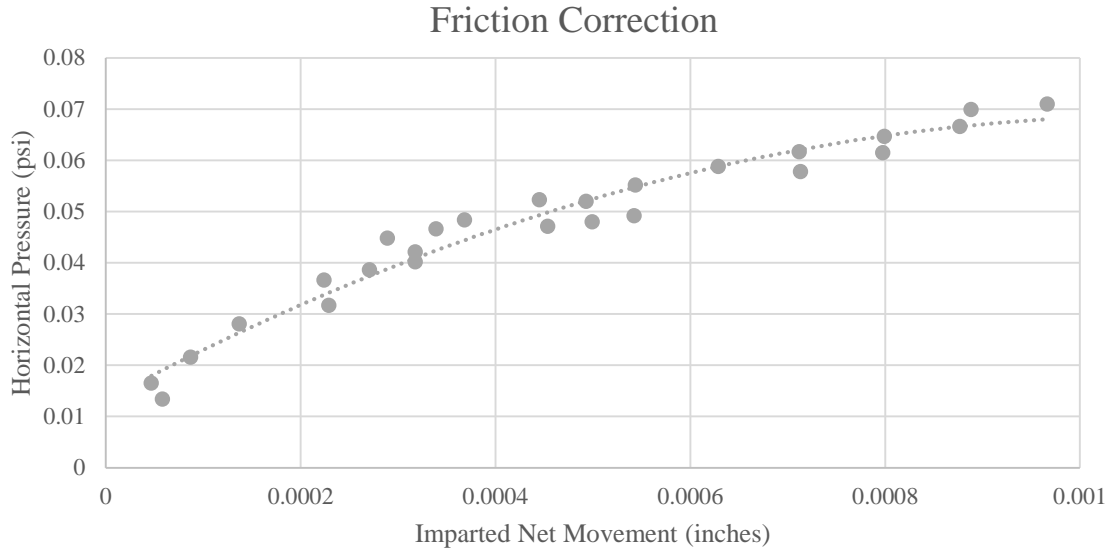


Figure 38: Correlation between Frictional Resistance and Net Horizontal Movement

$$y = -46619x^2 + 101.65x + 0.0133 \quad (31)$$

In this polynomial equation, y represents the frictional resistance (psi) and x represents the imparted net movement (inches) derived from the previous top table correction. Similar to the top table correction, the frictional resistance is subtracted from the response of the load cell using a similar equivalent sine wave approach.

4.7 Testing Program

Samples were prepared at a relative density of 45%. The vertical consolidation stage of the test subjected soils to be vertically confined with an approximate pressure of 50 kPa. The testing program for this investigation used two different methods in saturating and testing the soil. One of the approaches tested soil samples under the same applied amplitude (shear strain) and varied the degrees of saturation (Samples A1 – A3). The other approach tested samples with the same applied matric suction and varying strain amplitudes (Samples B1 – B7). The samples were sinusoidally loaded at a frequency of 1 Hertz for a duration of 5 cycles. The frequency of 1 Hertz was chosen for this study because it often represents similar conditions to the soil when subjected to moderate

seismic earthquakes with a similar dominant frequency (e.g. 1994 Northridge Earthquake, 1999 Chi – Chi Earthquake). A summary of test parameters is provided in the table below.

Table 4: Summary of Test Parameters

| | | |
|---|---|---|
| Sample Prepared Relative Density (*) | 45% | |
| Total Vertical Confining Pressure | ~ 50 kPa | |
| Sample Name | Applied Matric Suction (kPa) | Applied Normalized Shear Strain (%) |
| A1 | Dry, Saturated, 4 kPa, 8 kPa, 10 kPa | 0.02 |
| A2 | Dry, Saturated, 4 kPa, 6 kPa, 8 kPa, 10 kPa | 0.032 |
| A3 | Dry, Saturated, 4 kPa, 6 kPa, 8 kPa | 0.04 |
| B1 | Dry (0 kPa Suction) | 0.017, 0.029, 0.035, 0.04, 0.045, 0.05, 0.055, 0.059 |
| B2 | Fully Saturated (0 kPa Suction) | 0.017, 0.023, 0.029, 0.035, 0.04, 0.045, 0.05, 0.055 |
| B3 | 4 kPa | 0.017, 0.023, 0.029, 0.035, 0.04, 0.045, 0.05, 0.055, 0.059 |
| B4 | 5 kPa | 0.017, 0.023, 0.029, 0.035, 0.04, 0.045, 0.05, 0.055 |
| B5 | 6 kPa | 0.017, 0.023, 0.029, 0.035, 0.05, 0.055, 0.059 |
| B6 | 8 kPa | 0.017, 0.023, 0.029, 0.035, 0.04, 0.045, 0.05, 0.055, 0.059 |
| B7 | 10 kPa | 0.017, 0.023, 0.029, 0.035, 0.04, 0.045, 0.05, 0.055, 0.059 |

* Although the sample is prepared at this density, an increase in D_R between (3 – 20%) can occur after the vertical consolidation stage.

CHAPTER 5

DATA INTERPRETATION & ANALYSIS

5.1 Data Analysis

The output from the LabVIEW program incorporates the readings from the various sensors in a single Microsoft Excel file. The recorded signals are then post-processed using Matlab scripts. The post-processing scripts are included in the Appendix. The results of the electrical feedback signals after the cyclic horizontal load was triggered can be seen in the next figure. The transformation of the electrical feedback signals (in millivolts) to recorded parameters (in terms of standard units, ie. lbs, inches, etc.) were obtained by calibrating each sensor individually.

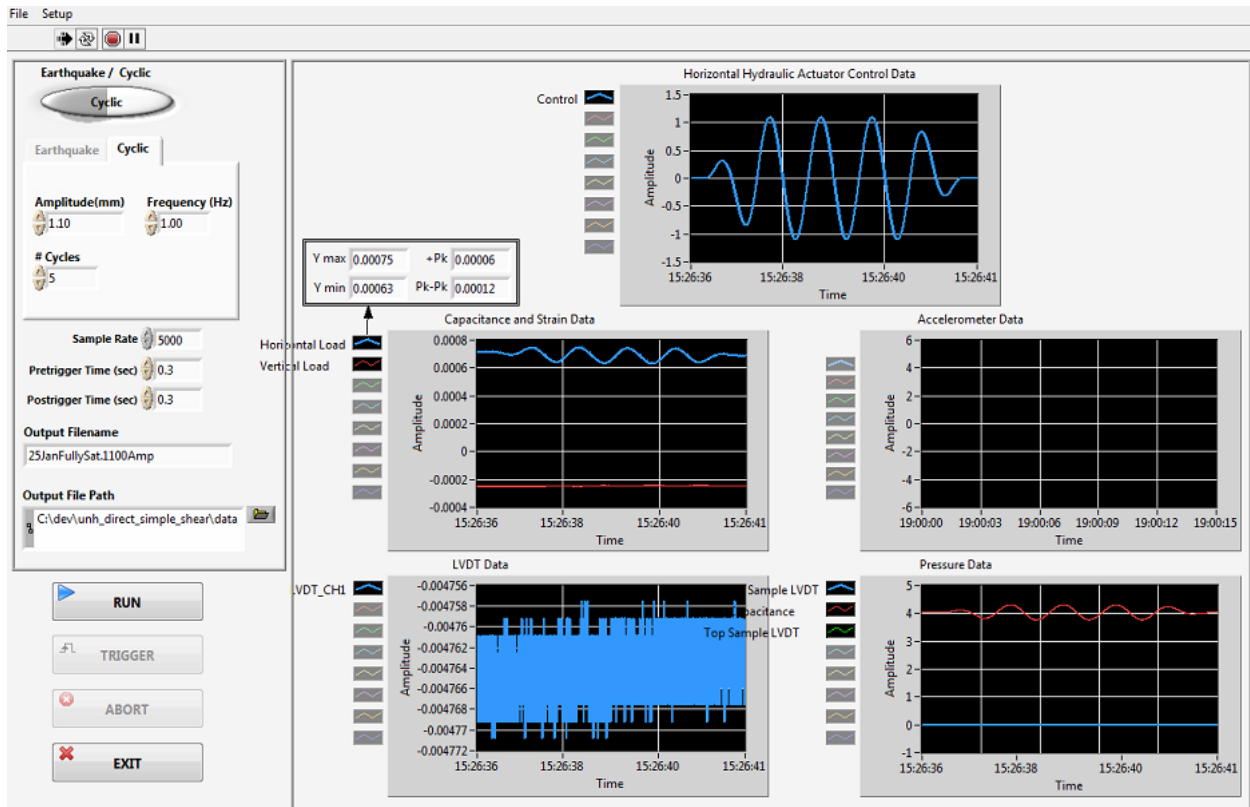


Figure 39: DAQ signals of various sensors after a cyclic test

In order to accurately analyze the results of the tests, some of the signals required some post – processing to eliminate noise. These signals were filtered by using the Matlab functions “moving average” and “smooth”. One of the implications of using these functions is that the function averages data from the previous number of specified recorded values, thus a time delay for the specified number of sample points is recorded. Although this effect is minimal, this results in a delay in the recorded response and the behavior of the soil. Signal filtering was applied to the readings of the top LVDT and the vertical confining load.

The obtained signals for the horizontal motion were modified for the top table movement and frictional resistance response mentioned in Chapter 4. Examples of response of the load cell and net – motions are provided in the following figures. These motions have been transformed from the electrical signals to the corresponding parameters. The shear strain response is shown in the next figure.

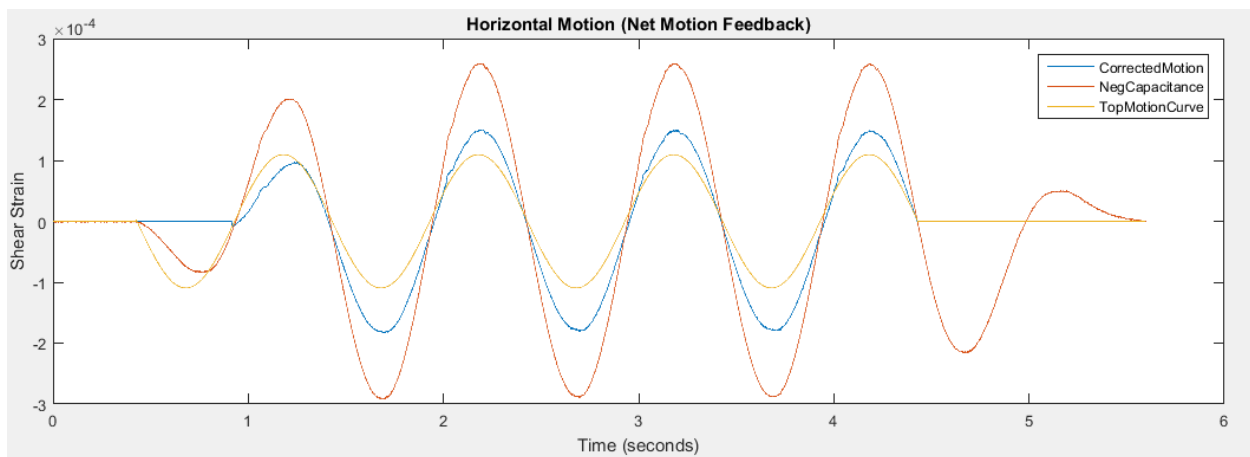


Figure 40: Recorded Horizontal Motion Feedback

According to Figure 40, the horizontal motion of the soil is converted from a distance reading to strain by dividing the value by the recorded height of the sample. The recorded shear strain by the capacitance transducer is shown in orange. The correction accounting for the top table motion is shown in yellow; the sinusoidal amplitude for this correction was established using Equation 30 and the average shear strain amplitude from Cycles 2 – 4 of the capacitance reading (in orange).

The corrected net shear strain of the sample (shown in blue) would be the top table correction shear strain subtracted from the capacitance shear strain. It should be noted that time syncing was involved by matching the correction curve and feedback peak to peak since there was not a noticeable delay in the top table and capacitance transducer movement. This motion is then used for the calculation of the frictional response and then used to correct the shear stress response as shown in the following figure.

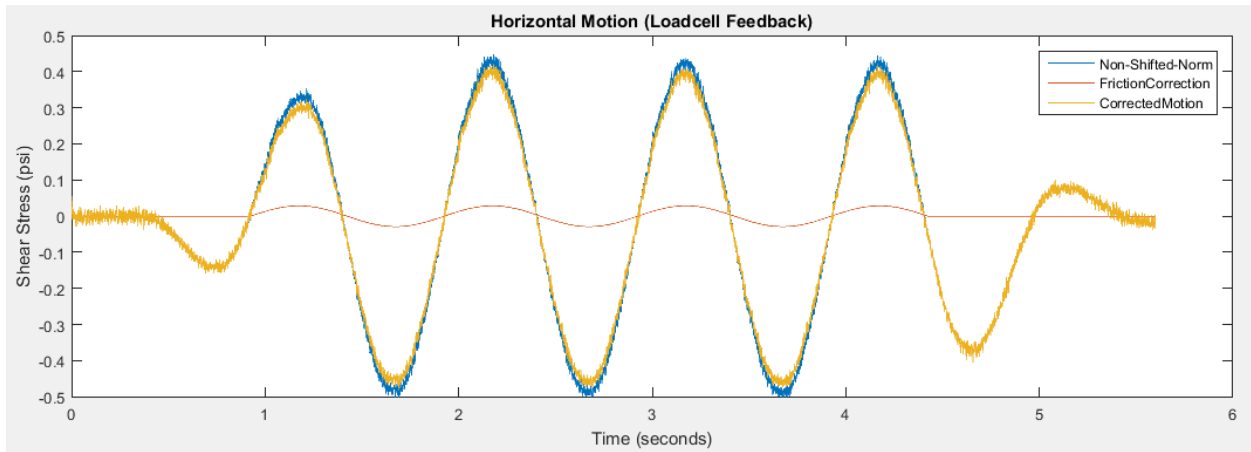


Figure 41: Recorded Horizontal Stress Feedback

This figure shows the progression of the shear stress produced from the horizontal actuator through the duration of the cyclical test. The horizontal load (recorded from signals by the horizontal load cell) is divided by the sample area to produce the shear stress (as shown on the y – axis). The signal in blue depicts the recorded data and the signal in orange is the correction for frictional correction. The amplitude for the sinusoidal friction correction is based off of average net displacement (cycles 2 – 4) determined from previous plot and Equation 31. The frictional correction is then subtracted from the recorded motion to form the shear stress response of the soil (shown in yellow).

The net shear strain and corrected shear stress response of the soil (as previously shown) is plotted against one another and the soil responses over the course of cycles 2 – 4 are plotted. The incorporation of noise from the horizontal load cell is readily apparent from Figure 41. The

initial determination of the seismic properties are calculated from the hysteresis loops that are formed for cycles 2 – 4.

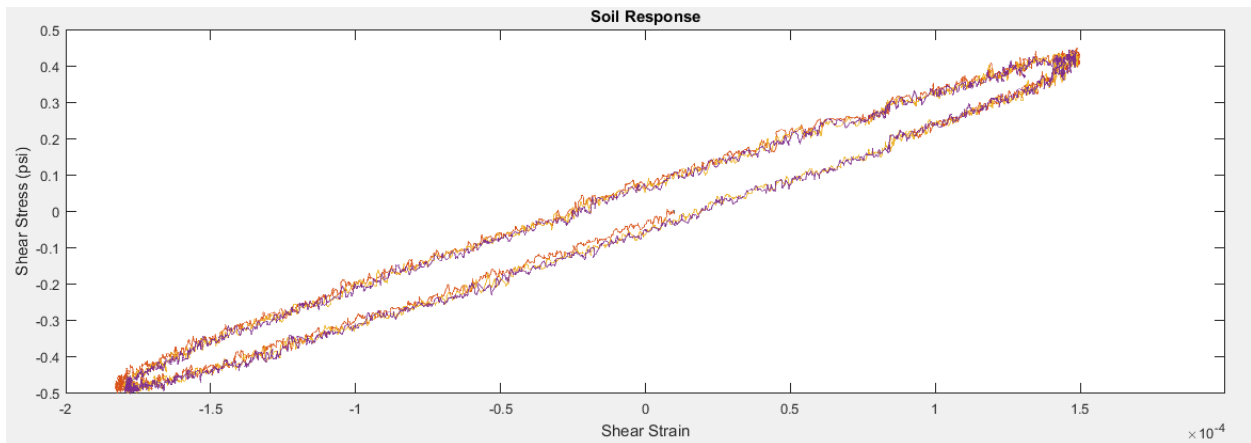


Figure 42: Soil Response of a partially saturated soil

The dismissal of the dynamic properties for cycles 1 and 5 is mainly due to the ramping portions of the loading scheme from the control signal that is provided in the program. Reference lines are overlapped onto the hysteresis loop, shown in Figure 43, to provide insight on how the dynamic properties were calculated.

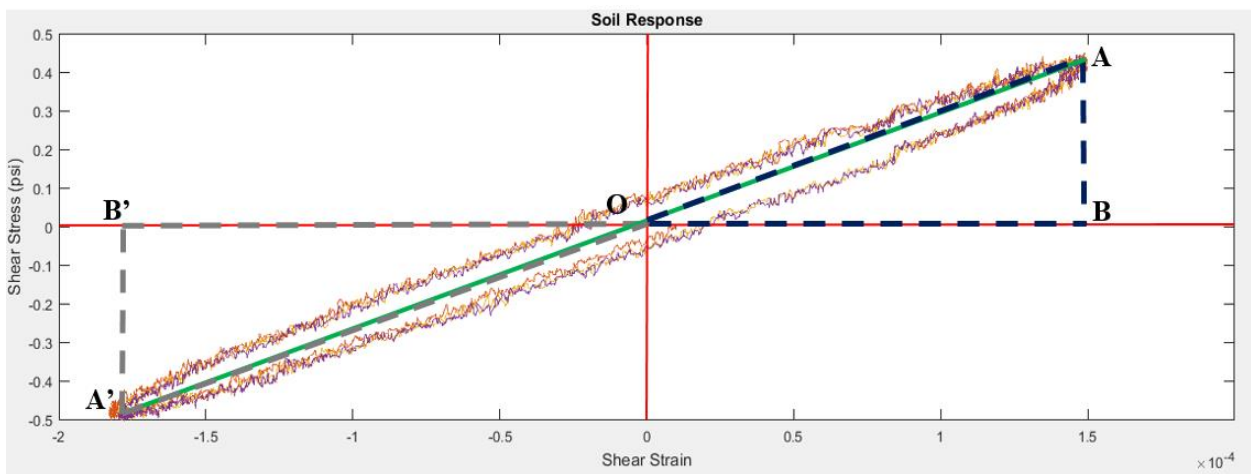


Figure 43: Soil Response with Reference Lines for the Dynamic Property calculations

It should be noted that in this figure the reference line is drawn for the average shear strain modulus and damping ratio. The secant shear modulus, G_{sec} was calculated by taking the slope of line A-A'

for each cycle. The individual shear modulus for each cycle was then averaged. The damping ratio was calculated using the following equation for each cycle and then averaged.

$$\zeta = \frac{1}{2\pi} * \frac{\text{Area of Hysteresis Loop}}{\text{Area of Triangle OAB} + \text{Area of Triangle OA'B'}} \quad (32)$$

It should be noted that in this equation, the area of the hysteresis loop represents the energy dissipated into the soil structure, while the areas OAB and OA'B' represent the stored energy in the soil element. These areas are calculated within the MATLAB script for each cycle.

5.2 Modification of the G_{sec} values

The preliminary results of the secant shear modulus are based off of the net shear strains measured by the capacitance transducer. The shear strains are based off the motion that is inputted by the user. However, slight discrepancies can exist between two tests with the same inputted signal. To account for this effect, as well as the compliance issues due to the variation in the top table load and relative density. It is imperative to modify these measured values in order to compare results between two different tests subjected to the same motion.

The modification of these values are conducted using a combination of equations established by Seed and Idriss (1970) and Oztoprak and Bolton (2013). Recall the following formula for the shear modulus.

$$G = 1000K_2(\bar{\sigma}_m')^{0.5}$$

This equation is a function of the effective mean confining pressure, and K_2 which is a function of K_{2max} and F' which in turn are functions of relative density and shear strain. The modification of the shear modulus would then be in the following form.

$$\frac{G_{modified}}{G_{unmodified}} = \left(\frac{\bar{\sigma}_{m,modified}}{\bar{\sigma}_{m,unmodified}} \right)^{0.5} * \left(\frac{K_{2,modified}}{K_{2,unmodified}} \right) \quad (33)$$

In this equation, G_{modified} represents the modified G_{sec} value, $G_{\text{unmodified}}$ represents the recorded values from the test, $\bar{\sigma}_{m,\text{modified}}$ is the modified confining pressure, $\bar{\sigma}_{m,\text{unmodified}}$ is the recorded value of average effective confining pressure over the duration of the test. $K_{2,\text{modified}}$ is a value based on the modified density and strain, and $K_{2,\text{unmodified}}$ is a value based off the relative densities and strains recorded in the test.

The values were modified for the total vertical pressure of 50 kPa which corresponds to a mean confining pressure of 28.57 kPa for a dry test. The formula for the effective mean confining pressure is provided.

$$\bar{\sigma}_m = \frac{1}{3}(\sigma_v + (2 * (1 - \sin(\varphi')) * \sigma_v)) \quad (34)$$

In this equation, $\bar{\sigma}_m$ represents the mean confining pressure through the test, σ_v is the average vertical pressure through the duration of the cyclical load portion of the test, and φ' is the friction angle of the sand (which was determined from triaxial testing). Since the total vertical pressures are averaged through the duration of the test, the effect of the pore fluid (matric suction or water pressures in some cases) response within the sample becomes vital when determining the effective pressure in the soil (using Equation 28). This is important for both partially and fully saturated soils to show that the matric suction or water pressure in the soil did not drastically change during the duration of the cyclic loading. The confirmation of this condition is presented in the next chapter.

The modification of the relative density, D_r , and applied cyclic shear strains, γ_c , are accounted for in the K_2 portion of the equation. The K_2 parameter is a function of the $K_{2,\text{max}}$ and F' values are shown in the subsequent set of equations

$$K_2 = K_{2,\text{max}} * F' \quad (35)$$

$$K_{2,\text{max}} = (0.6 * D_R) + 16 \quad (36)$$

$$F' = \frac{G}{G_{max}} \quad (37)$$

The formulation of K_{2max} is based off of empirical data from a study conducted by Seed and Idriss (1970) and is dependent on the relative density of the soil. F' represents the degree of reduction in the shear modulus degradation curve. This value is also a function of the shear strain. Oztoprak and Bolton's equation for the degradation of shear modulus was used with the material properties (coefficient of uniformity) and state variables (void ratio and relative density) provided in Chapter 3. The shear modulus degradation parameter, F' is presented over a series of strains in the subsequent figure.

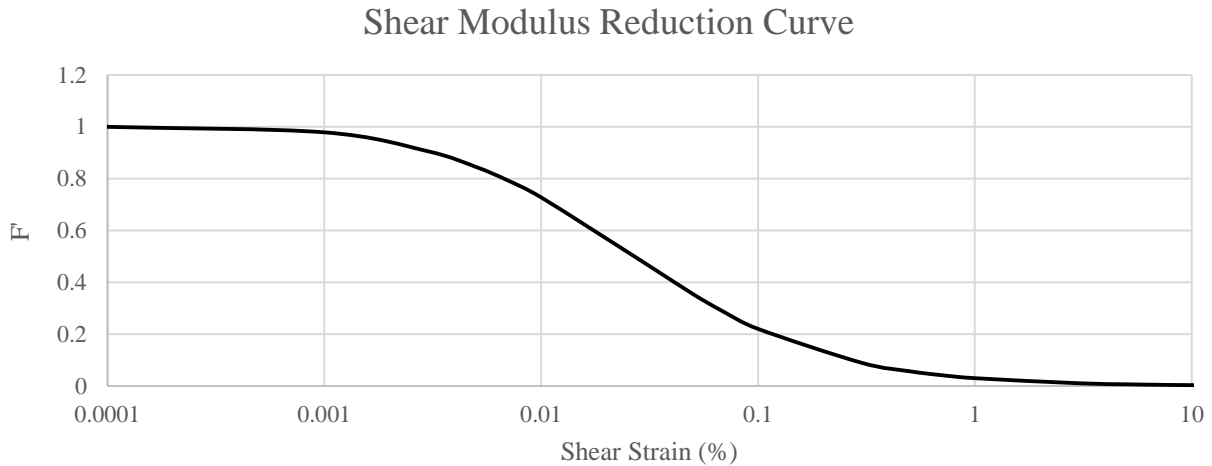


Figure 44: Shear Modulus Reduction Curve of F75 Ottawa Sand (after, Oztoprak and Bolton 2013)

In order to better explain the modification process, an example is presented. A soil sample is subjected to the vertical consolidation stage (of 50 kPa) and the relative density changes from 45% to 53%. The sample is then saturated and desaturated to partially saturated conditions (of 4 kPa matric suction). It is then sinusoidally loaded with a cyclical shear strain amplitude of “0.032%”. The actual recorded signals after the MATLAB post processing show that the shear strain subjected to the sample was 0.0315%, the average total vertical stress was 48.35 kPa (effective stress at 50.59 kPa using Equation 28), and the calculated average shear modulus from the hysteresis loops was 15.87 MPa. The mean effective confining stress would be 28.91 kPa.

Using the equations 35 – 37 and Figure 44, the $K_{2\text{modified}}$ value would be 19.75 (for D_R at 45%, and strain at 0.032%), $K_{2\text{unmodified}}$ value would be 22.12 (for D_R 53% and strain at 0.0315%), $\bar{\sigma}'_{m,\text{modified}}$ value would be 28.57 kPa, $\bar{\sigma}'_{m,\text{unmodified}}$ value would be 28.91 kPa, and $G_{\text{unmodified}}$ value would be 15.87 MPa. Inputting these values into the modification equation (e.g. Equation 33) would result in a G_{modified} value of 14.08 MPa. These values are summarized in the Table 5 to show the recorded and modified values used for Equation 33.

Table 5: Summary of Modification Process for Shear Modulus Value

| Modification Parameter | Unmodified (Recorded) Value | Modified Value |
|--|------------------------------------|-----------------------|
| Vertical Effective Confining Pressure (kPa) | 50.59 | 50 |
| Mean Effective Confining Pressure | 28.91 | 28.57 |
| Shear Strain Amplitude | 0.0315% | 0.0320% |
| Relative Density | 53% | 45% |
| K2 Value | 22.12 | 19.75 |
| Average Shear Modulus (MPa) | 15.87 | 14.08 |

This modification process was used for all of the samples in order to compare the shear modulus values against each other on the same shear strain level and to eliminate compliance issues due to relative densities and changes in confining pressures. The modification process for the shear modulus values was found to contribute anywhere from 6.3% to 36.7% with an average of 19.7% from the recorded value. The contribution amount was dependent on how much the recorded value (e.g. confining pressure, shear strain, and relative density) deviated from the intended value. It should be mentioned that other approaches looking at the effects of only the confining pressure or relative density and shear strain were considered, but were not used for the presentation of results.

5.3 Modification of Damping Ratio Values

The modification of the damping ratio, ζ is based off of the modification process used for the shear modulus values. Since the damping ratio and the shear modulus have been known to have a reciprocal trend from one another, the ratio between the values was assumed to be in the following form,

$$\frac{\zeta_{modified}}{\zeta_{unmodified}} = \frac{G_{unmodified}}{G_{modified}} \quad (38)$$

where, $\zeta_{modified}$ is the modified damping ratio (with regards to density, shear strain, and confining pressure), $\zeta_{unmodified}$ is the calculated average damping ratio from the hysteresis loops, $G_{unmodified}$ is the recorded G_{sec} value from the hysteresis loops, and $G_{modified}$ is the modified shear modulus mentioned in the previous section.

To demonstrate this modification process, the previous example will be recalled upon for continuity purposes. The damping ratio calculated from the previous examples hysteresis loops yielded a value of 0.0651. The modified and unmodified shear modulus values were 14.08 MPa and 15.87 MPa, respectively. Using the aforementioned equation, the modified damping ratio would yield a value of 0.0734.

5.4 Determination of the G_{max} and ζ_{max} values

The small strain shear modulus, G_{max} and large strain damping ratio, ζ_{max} are often required to distinguish a normalized approach of comparing soils dynamic properties under different conditions. In the following sections, the equations and methods used for determining these values are explained. The modulus reduction curve (G/G_{max}) and increasing trend of the damping ratio (ζ/ζ_{max}) over a wide range of strains with the normalized data from this investigation are presented in the next chapter.

5.4.1 Determining the Small Strain Shear Modulus, G_{max}

Similar to the method for the modification of the shear modulus values detailed in the previous section, the small strain shear modulus, G_{max} was calculated using the empirical equation established by Seed and Idriss (e.g. Equation 6). Recall the following equation for the small strain shear modulus

$$G_{max} = 1000K_{2,max}(\bar{\sigma}'_m)^{0.5}$$

Recall that in this equation, $K_{2,max}$ is an empirical value based off of the relative density of the sand and, $\bar{\sigma}'_m$ which is the effective mean confining pressure of the sample. For each test, the value for G_{max} changed for each different degree of saturation and matric suction applied to the sample due to the change in effective stress (e.g. Equation 26), while the $K_{2,max}$ parameter remained consistent for each test (for $D_R = 45\%$).

5.4.2 Determining the Large Strain Damping Ratio, ζ_{max}

The determination of the large strain damping ratio utilized the empirical formula established by Seed and Idriss (e.g. Equation 19). Recall that the formula was dependent on the saturation level of the test, in which x was 33 (for dry condition) and 28 (for fully saturated condition). Since the results of this investigation tested soils at different degrees of saturation from a dry to fully saturated state, the assumption on the progression of the x value changed linearly over the course of saturation was made. Therefore, the equation was altered into the following form,

$$\zeta_{max} = (33 - 5(S_R)) - 1.5(\log(N)) \quad (39)$$

In this equation, ζ_{max} represents the maximum damping ratio, S_R is the degree of saturation, and N is the number of cycles. In addition to the degree of saturation assumption, the value of N was assumed to be 3, since the damping ratios were averaged over the course of three cycles. Since the

degree of saturation was different for each test, the maximum damping ratio was calculated for each case.

CHAPTER 6

RESULTS & DISCUSSION

The results from the investigation are presented in two sections, seismic compression and dynamic properties. The seismic compression results are broken into the pore fluid response of the soil and the progression of axial strain exhibited by soils subjected to increasing shear strains. The dynamic properties include the modified shear modulus values, damping ratios, and normalized shear modulus values (G/G_{max}) and normalized damping ratio results (ζ/ζ_{max}). The presentation of these properties are separated to correspond with the testing methods used (A and B series).

6.1 Seismic Compression Results

6.1.1 Pore Fluid Response

As it was mentioned in Chapters 4 and 5, the pore water response was measured by the DPT to ensure that partially saturated and fully saturated soils were tested under drained or, practically, partially drained conditions throughout dynamic testing. The results indicated that changes in the PWP were not considered to be significant. The pore water pressure response for two fully and two partially saturated soils subjected to two different cyclic motions are presented in Figure 45.

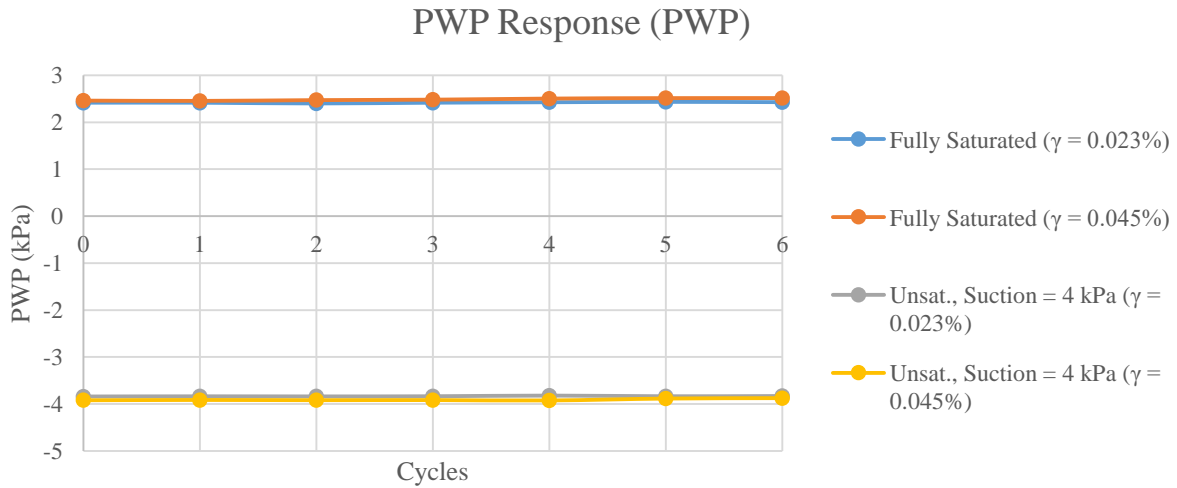


Figure 45: Pore Water Pressure Response over Cyclical Testing

The graph shows the PWP response in partially and fully saturated soils during cycles 1 - 5 of cyclical loading. It should be noted that the plots include an additional 2 cycles of readings (1 cycle for pre testing - Cycle 0, and 1 cycle for post testing – Cycle 6) to show the pressures before and after the test. It can be observed that in both cases (saturated and partially saturated soils), a slight change in PWP is noticeable, however the magnitude in relation to the applied pressures was considered minimal through the duration of the test. This was also the observed trend for the other partially saturated soils (5 kPa, 6 kPa, 8 kPa, and 10 kPa). However, in order to provide a more accurate picture of the extent of the change in pore pressures, Figure 46 provides a more detailed look into the “change” in PWP response previously presented in Figure 45.

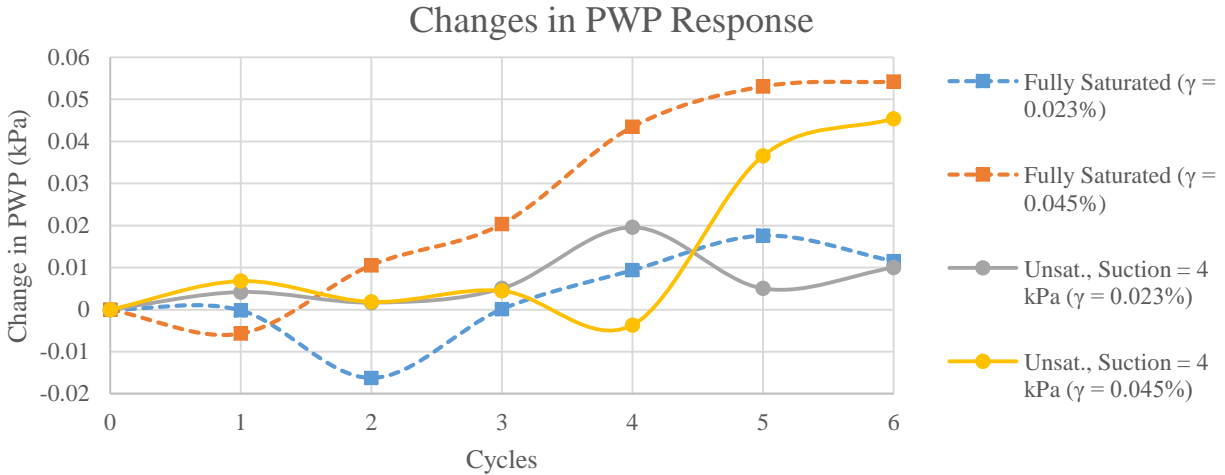


Figure 46: Changes in Pore Water Pressure Response during Loading

The effect of imparted shear strain (as denoted by the percentages in the legend) on the effect of PWP is displayed for both conditions; the trend indicates that higher shear strains result in larger changes in PWP. At smaller strains, the change is considered to be much insignificant. This trend corresponds well with previous investigations. The results from the testing should be taken with a considerable amount caution since the resolution of the DPT falls in the range of the changes in PWP recorded. The resolution is rated at 0.1% F.S. (full span) or 0.1 kPa, therefore the recorded changes may actually be noise instead of the actual pressure change in the sample.

6.1.2 Axial/ Volumetric Strain Response

The multistage seismic compression results were calculated from the changes in height before and after a dynamic test was conducted. The term “multistage” describes the loading pattern that was used for testing, in which larger and larger motions were subjected to the same specimen under the same degree of saturation. The vertical deformations were then used to calculate the axial strains that the sample experienced. Since the sides of the samples were confined, the axial strains are approximately equivalent to the volumetric strains. The results are presented for samples B1 – B7 in Figure 47.

Multistage Seismic Compression

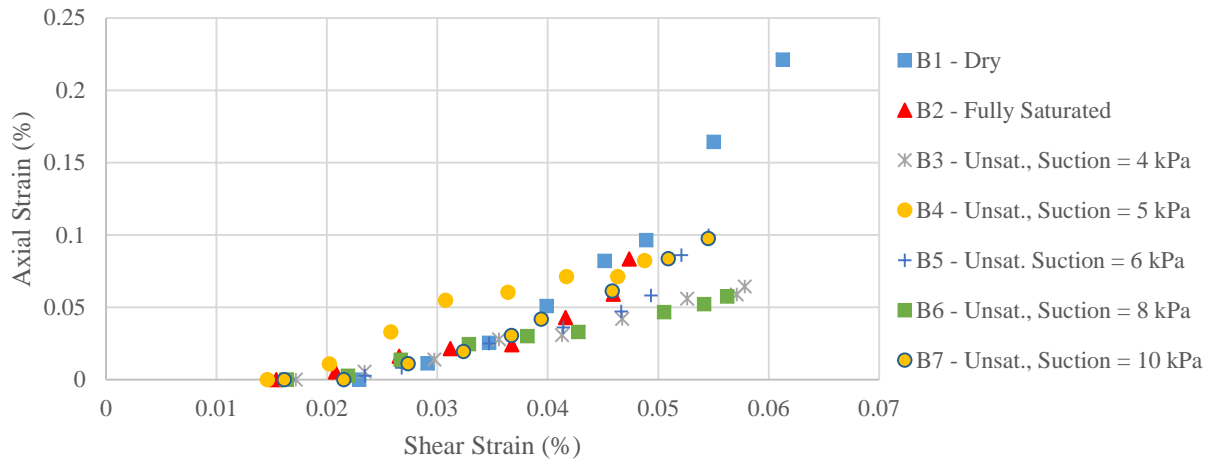


Figure 47: Multistage Seismic Compression Results

The results from the multistage testing of the B series show the relation between the amounts of axial strains estimated from the vertical settlement and applied shear strains. In this plot, the applied shear strains were not modified using the technique explained in the previous chapter where the recorded shear strains were matched with the strains experienced by the soil. From this plot, one can observe that matric suction had no significant impact on the vertical strains when the shear strain is less than 0.037%. However, at larger shear strain values, the dry sand sample (B1) experienced the most settlement while partially saturated soils (B3 – B7) experienced the least amount of axial strain. The compressional axial strains exhibited by sample B4 suggests that there may have been an error in reading the vertical deformation from the sensor since it displays a different trend from the remainder of the tests (at $\gamma \sim 0.025\%$). With the exception of sample B4, the approximation of the volumetric shear strain threshold, γ_{tv} , is between 0.017% and 0.023% and is in agreement with values suggested by Hsu and Vucetic (2004), although it should be noted that these sample were tested at a slightly different relative densities.

6.2 Results of the Dynamic Properties

The results of the dynamic properties are presented for the different methods of dynamic testing.

Sample series A(1 -3) tested samples at the same relative shear strain level, while adjusting the degree of saturation between tests. Sample series B (1 – 7) maintained the same degree of saturation, while testing the samples over a range of shear strain values. The presentation of the strain dependent shear modulus, G and the damping ratio are presented in the following sections.

6.2.1 Results from Sample Series A

The results from sample series A is presented in two different manners. One method is plotting the modified shear modulus values vs the degree of saturation (e.g. Figure 48). Using this figure one can show the distinction of the location of the fully saturated and dry shear modulus as both have zero suction. However, at the lower end of saturation ($S < 0.01$), it is difficult to distinguish the difference between dry vs residual shear moduli values. The alternative way of presenting the results is to plot the shear modulus against the matric suction values (e.g. Figure 49). This figure allows researchers to understand the effects of matric suction on the shear modulus. The difficulty associated with this data presentation is that the fully saturated and dry results of the shear modulus values are both located at 0 kPa for matric suction. Therefore, it is necessary to present the data in two different ways as shown in the ensuing figures.

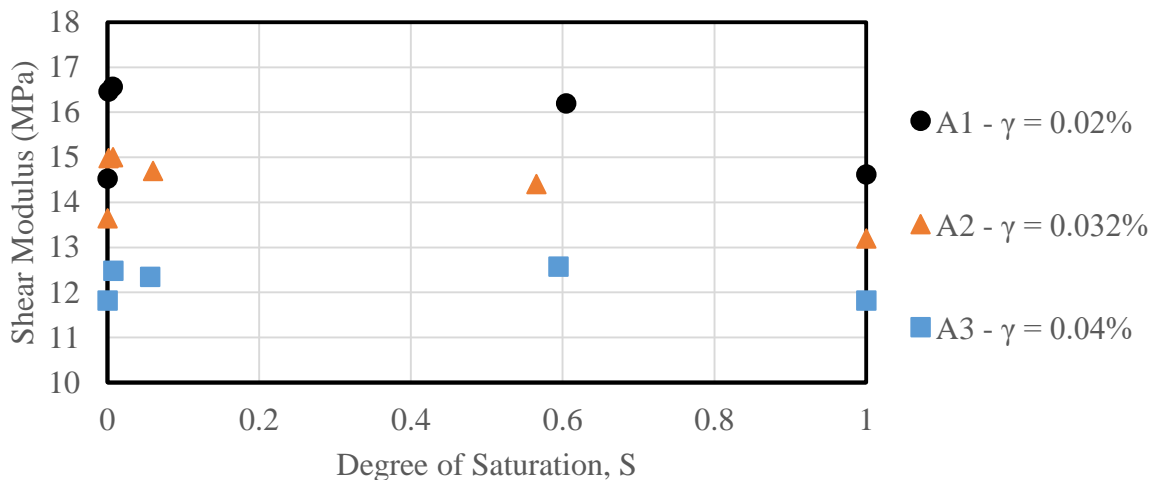


Figure 48: Modified Shear Modulus Values vs Degree of Saturation

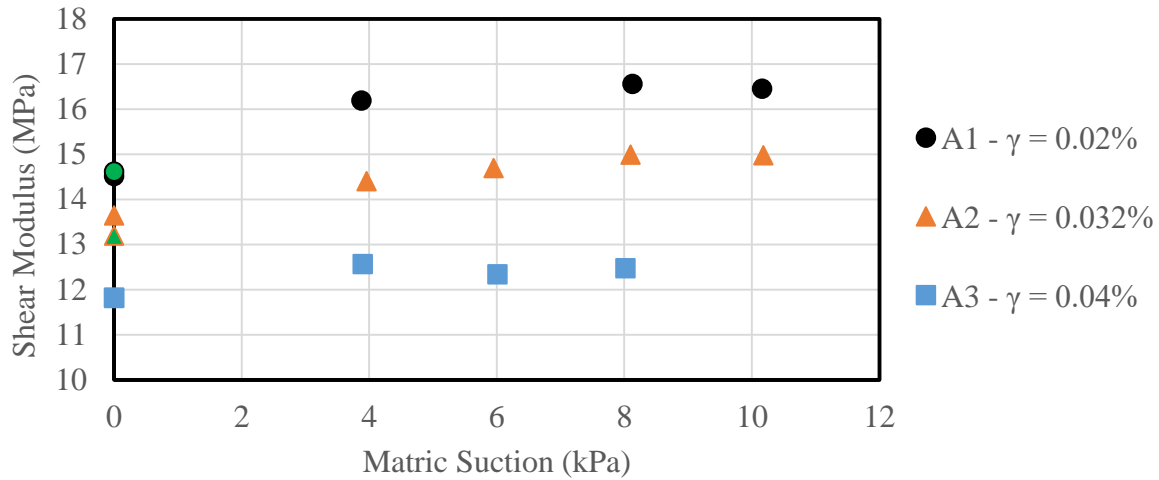


Figure 49: Modified Shear Modulus vs Matric Suction (fully saturated soils are denoted with green fill)

These plots show the clear effects of partially saturated soils on the shear modulus and confirm conclusion from studies by Cui et al. (2007), Hoyos et al. (2015), and Suprunenko (2015) that indicate that higher values of matric suction in the soil matrix can contribute an increase in value on the secant shear modulus. The peak shear modulus value over the range of the suctions indicate that the maximum value occurs when samples are subjected to a matric suction of 8 kPa. However, a slight decrease in the shear modulus value when transitioning from 8 kPa to 10 kPa can be noticed. The degradation of the shear modulus is apparent from the position of the data points. Samples subjected to larger strains (i.e. Sample A3) correspond with lower shear modulus values than samples with smaller induced shear strains (i.e. Sample A1). A normalized approach in presenting the shear modulus is displayed in the following figure. In this figure, the values of the modified shear modulus are normalized with the dry shear modulus value obtained for the sample.

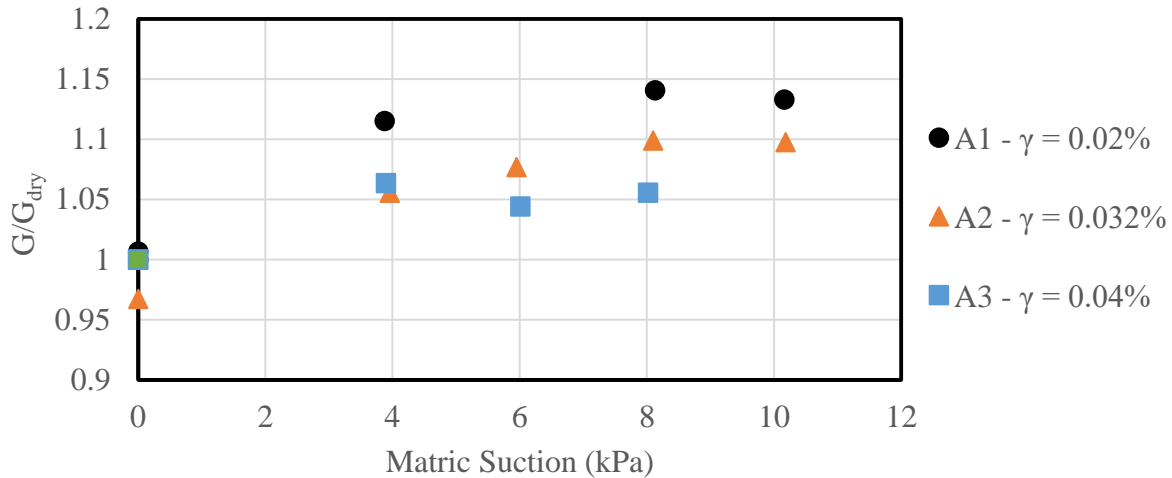


Figure 50: Normalized Shear Modulus w/ respect to Dry Shear Modulus, A-series

The contributions to the stiffness from the matric suction can be seen to contribute a partial amount to each soil sample. It should be noted that the dry samples would be normalized to a value of 1, while contributions or deductions to the stiffness would read as values larger or smaller than 1. At smaller shear strains (e.g. A1), the matric suction has a maximum contribution of ~14% over the dry sample stiffness. However, at larger shear strains (e.g. A3), the contribution of matric suction at 8 kPa to the stiffness response is roughly 5%.

In the following figures, the damping ratios corresponding to data points in Figures 51 and 52 are presented in forms similar to the previous two (i.e. Damping ratio versus Degree of Saturation and Matric Suction). It is important to note that the damping ratio reflects the inverse trends occurring within the stiffness/shear modulus calculations since the properties are inversely related. Also, mechanically it has been proven that stiffer soils generally result in lower damping values.

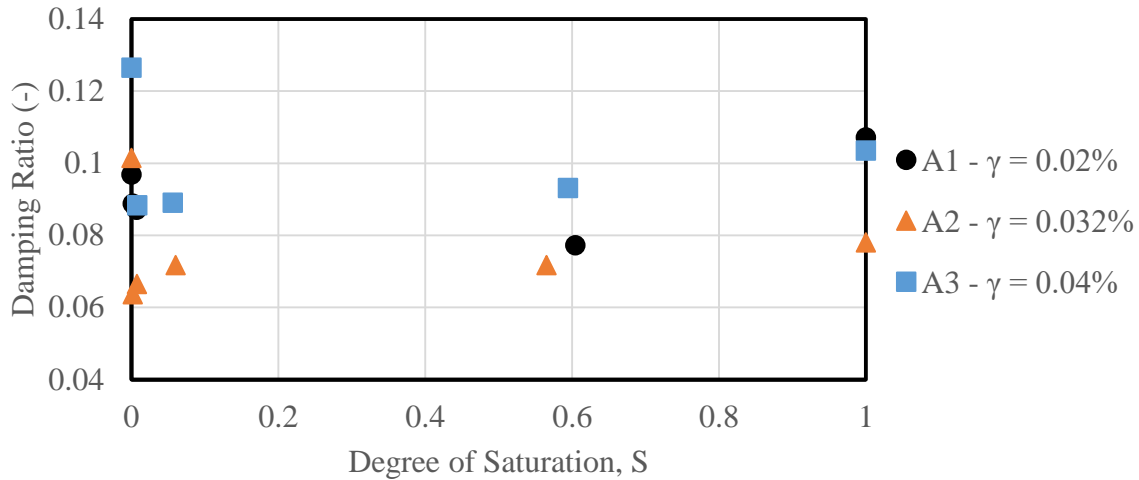


Figure 51: Modified Damping Ratio vs Degree of Saturation

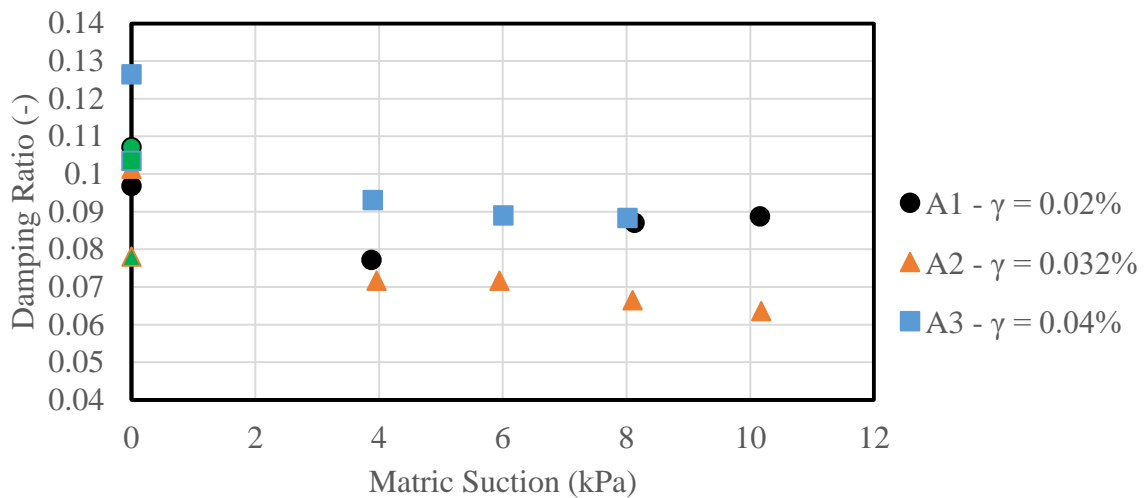


Figure 52: Modified Damping Ratio vs Matric Suction (fully saturated soils denoted in green)

In these figures, a decrease in damping ratio can be observed when the specimen was subjected to higher suctions (w/ the exception of series A1; although in this series partially saturated soils exhibit lower damping values). The lowest damping occurs for partially saturated soils, while the peak damping value is shown at the dry condition. This corresponds well with the properties observed for the shear modulus values (such that the values reflect lower damping values for higher suction values). This observation corresponds well with previous conclusions by other researchers (Biglari et al. 2011, Kimoto et al. 2011).

6.2.2 Results from Sample Series B

The presentation of the results from Sample Series B is presented in a form to show the shear modulus over a range of shear strain for samples subjected to the same matric suction. It should be noted that the shear modulus values have been modified using the techniques described in the previous chapter. The shear modulus response for Sample Series B is shown in the next figure.

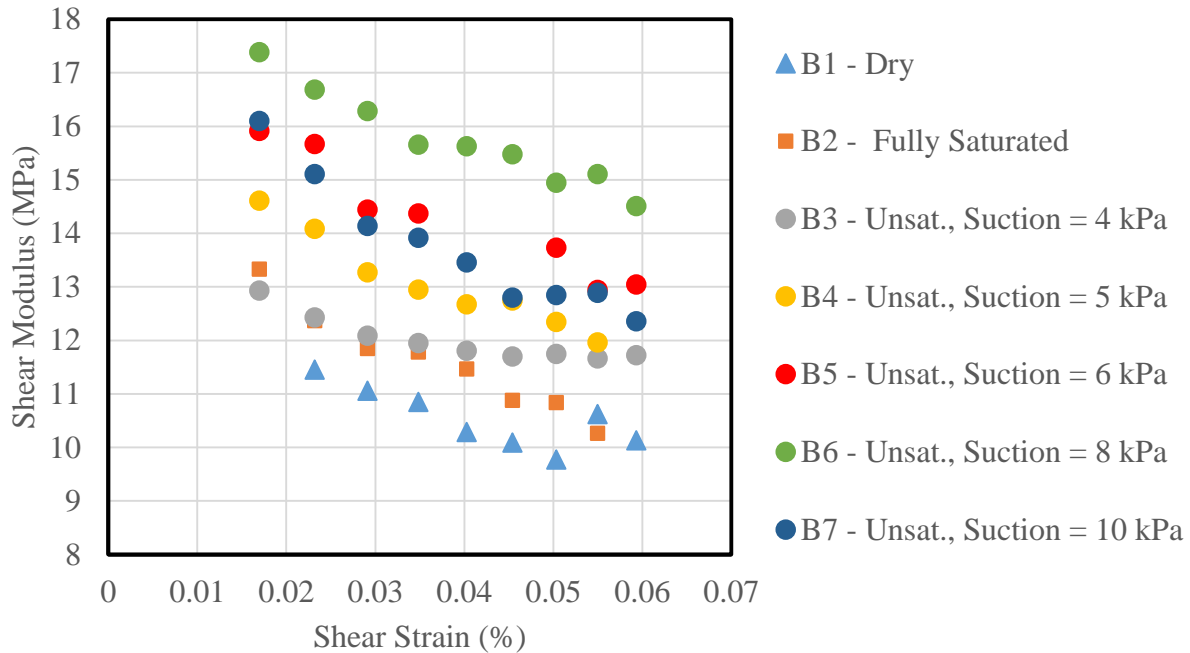


Figure 53: Shear Modulus vs Shear Strain

A clear depiction of the degradation in shear modulus values when higher shear strains are applied to the sample can be observed from the test results. These results confirm the ability of this DSS machine to measure a decrease in shear modulus values when changing the shear strain values slightly, as well as the previous results from sample series A. The data illustrates that partially saturated soils yield higher shear modulus values over soils at fully saturated and dry states, with peak values occurring at 8 kPa matric suction at the same shear strain level. Potential outliers for this sample series include B3 (at shear strains < 0.04%) as it shows a smaller shear modulus value than the nearly saturated condition. Alternatively, it may suggest that the saturated sample, may

not actually be fully saturated but instead “nearly” saturated as it was discussed earlier. The same argument can be used to explain why the fully saturated soils resulted in higher shear modulus than in the cases of dry soils while it was expected to be the same. The data set also shows the decrease in stiffness when the matric suction transitions from 8 kPa to 10 kPa, this observation is consistent with sample series A. This may suggest that a different mechanical response may be enacted within the soil even though the two values are essentially at the same residual value of saturation. The decrease in mechanical response (i.e. stiffness) of the soil may be caused by the decrease of inter-particle stress within the soil. Capillary attraction may fall off in magnitude (when going from 8 kPa to 10 kPa of Matric suction) as the interfaces between water and soil particles lose continuity, which would then result in a lower shear modulus value.

The damping ratio vs shear strain response for sample series B is shown in the ensuing figure.

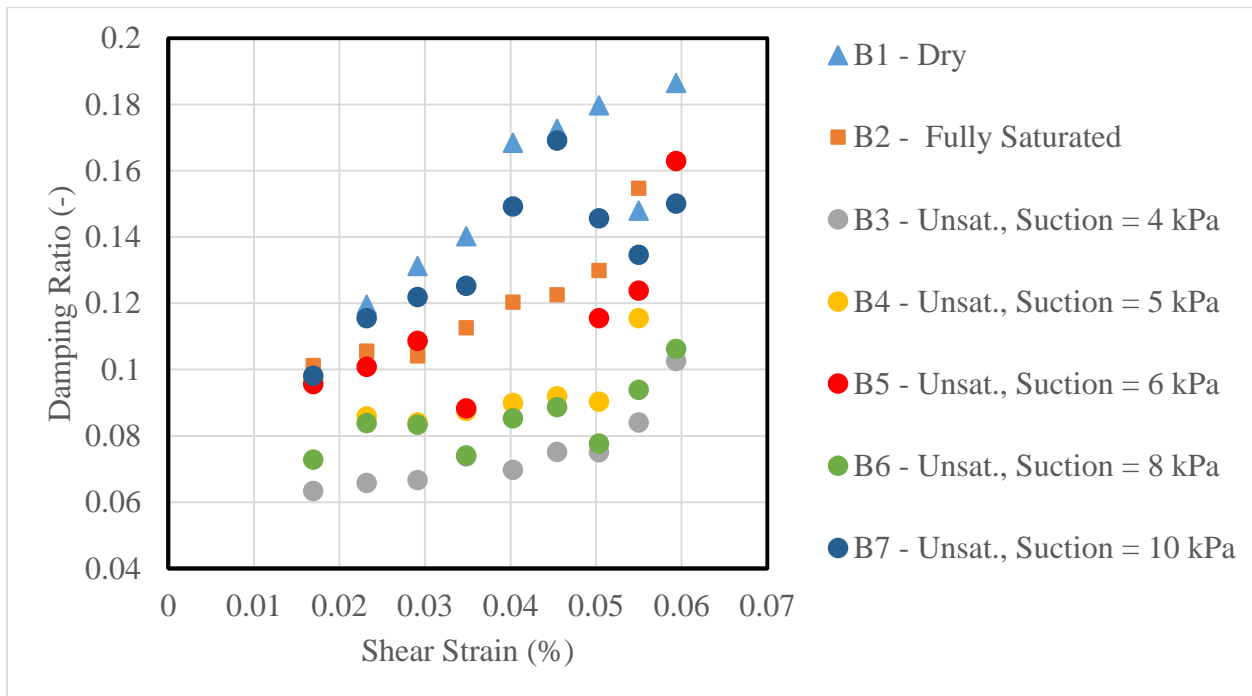


Figure 54: Damping Ratio vs Shear Strain

Similar to the observed trends from sample series A, the results from the sample series B reflect the trend of higher damping ratios when subjected to higher shear strains. Furthermore, the depiction of the highest damping was exhibited by the dry soil samples, while unsaturated soils displayed less damping. It should be noted that the damping ratio for sample B7 exhibits high damping. This may confirm the findings that a loss in capillary attraction is exhibited in the soil structure when transitioning from 8 kPa to 10 kPa of matric suction. Concurrently, the behavior of the soil could act like a dry soil, displaying a high damping ratio. It is apparent that the trend between the damping ratio and the degree of saturation is not consistent between series A and B, this may be due to differences in testing methods and the modifications made to the damping ratios that account for the confining pressure, density, and applied shear stress. In addition, previous researchers have also occasionally observed irregular trends in damping ratio patterns for different degrees of saturation (Jafarzadeh et al. 2012)

6.3 Shear Modulus Reduction and Damping Curves

The degradation of the shear modulus and increase in the damping ratio are presented in the following sections. In order to present these results, the determination of the small strain shear modulus, G_{max} and maximum damping ratio, ζ_{max} were calculated through the methods mentioned in the previous chapter. The recorded values determined through testing were then used to establish the ratios G/G_{max} and ζ/ζ_{max} .

The shear modulus reduction values are compared against values obtained through a curve established by Oztoprak and Bolton (2013). The parameters for the curve are as follows: $C_u = 1.83$, $e = 0.6605$, $p' = 28.57$ kPa, $p_{atm} = 101.3$ kPa, and $D_R = 0.45$.

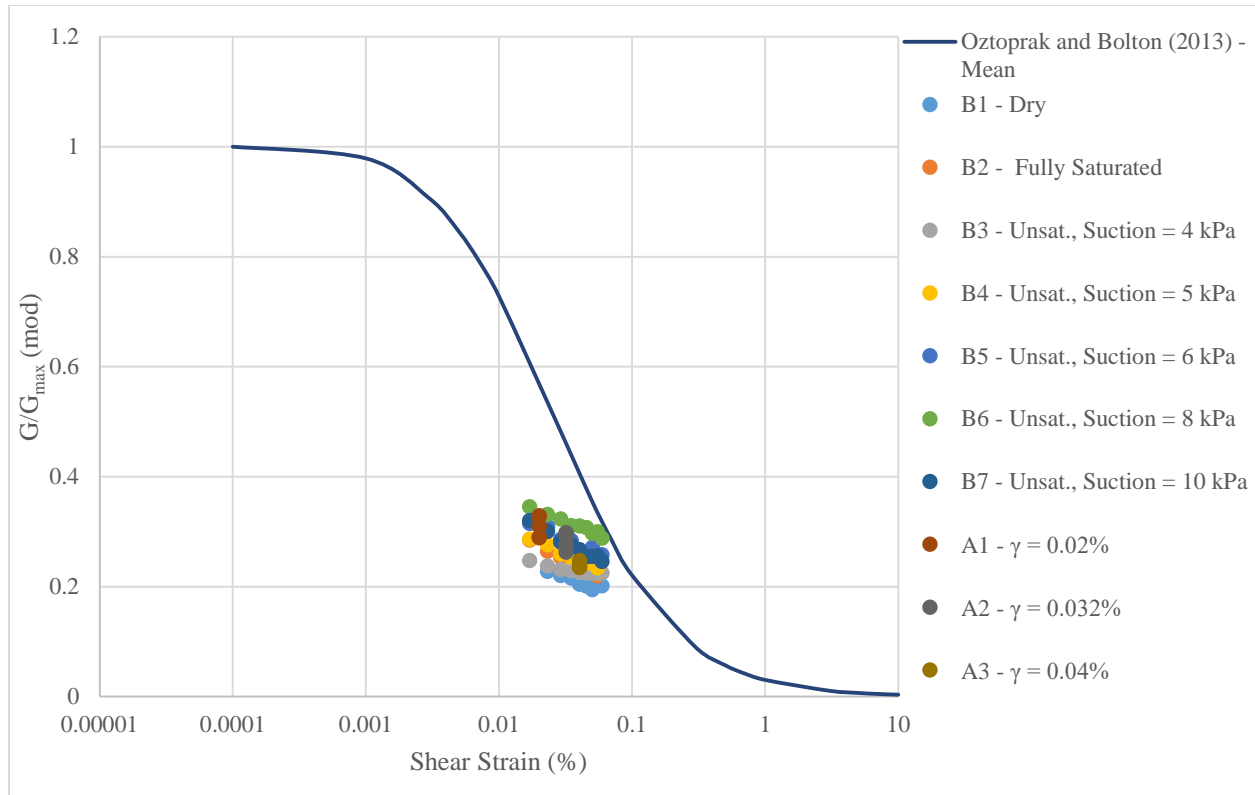


Figure 55: G/G_{max} vs Shear Strain

This plot suggests that the values of the shear modulus, G , measured by this DSS system are less than the ones that can be predicted from empirical relations. This finding would be consistent with past studies on the machine conducted by Dunstan (1998) and Miller (1994). Alternatively, it may suggest that the empirical relation for the value of the small strain shear modulus G_{max} established by Seed & Idriss may overestimate the small strain modulus associated with this sand. It should be taken into account that the empirical values for the shear modulus by Seed & Idriss and the modulus reduction from Bolton and Oztoprak were based off of results from different testing methods (i.e. Resonant Column, torsional shear, and triaxial cell). Although it is not imperative that the data should fall on the normalized line established by Oztoprak and Bolton, the data should reflect the rate of degradation as shown by the curve in this particular set of shear strain values. However, considering the scatter available in the proposed empirical relations the measured values are in approximately acceptable range, especially in higher strain levels.

The relation of the ζ/ζ_{\max} curve established by the Hardin and Drnevich (1972) was used (e.g. Equation 20) in combination with the shear modulus reduction curve by Oztoprak and Bolton (2013). The measured values were normalized by the approximate ζ_{\max} and compared with the empirical formula in Figure 55.

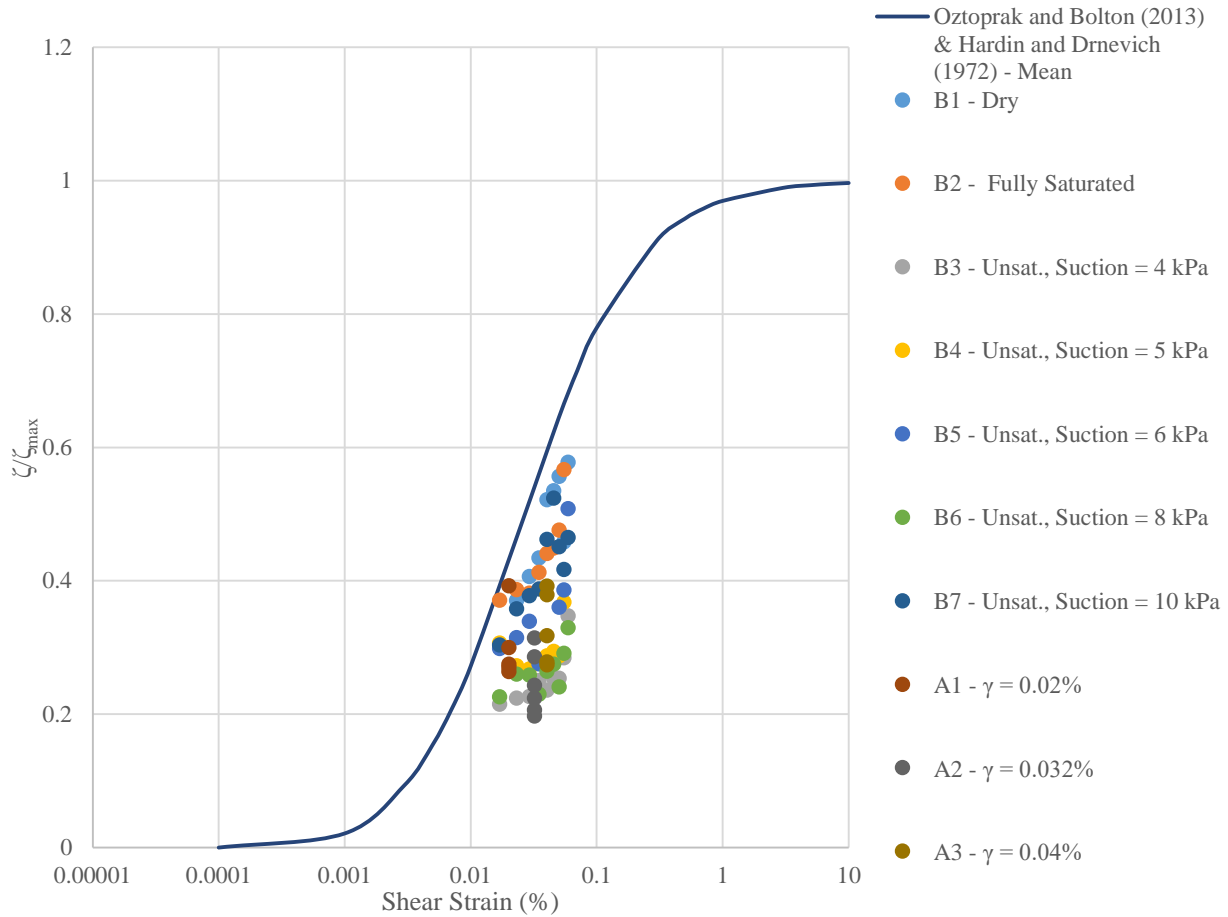


Figure 56: ζ/ζ_{\max} vs Strain

The empirical normalized damping significantly overestimates the measured values. This variance is more severe than what was observed in shear modulus mainly because the normalized relation was not from one study on one soil and under one state condition. Especially the maximum damping estimated from Seed and Idriss' equation was very approximate. Certainly, the damping ratio study requires further future attention.

CHAPTER 7

SUMMARY AND CONCLUSIONS

7.1 Summary

The recent renovation made to the Direct Simple Shear Apparatus at the University of New Hampshire has restored the ability to test soils under dynamic motions. These renovations include: installing a new hydraulic pump, horizontal control system, data acquisition system, various sensors, and user interfaces (LabVIEW and GeoTac Software). Additionally, the soil chamber has been modified to enable users to use the axis translation technique to control the degree of saturation and suction to soil specimens.

The investigation conducted on a clean sand shows the effect of the degree of saturation and matric suction on the seismic compression and dynamic properties of partially saturated soils. The behavior of pore water pressures in partially and fully saturated soils show the ability of the flow pump to maintain relatively constant pressures when subjected to these shear strain levels. The volumetric threshold shear strain is not dependent on the degree of saturation and was found to occur at a value between 0.017% and 0.023%. However, when subjected to shear strains larger than the volumetric threshold shear strain, the overall axial strain results indicate that partially saturated soils experienced less deformation than dry soil.

The importance of the saturation and testing methods (sample series A vs B) can lead to significant differences in the amount of increase in shear moduli that the matric suction can contribute to the soil structure. The shear modulus values were found to increase when subjected to higher matric suctions with a peak shear modulus value occurring when a sample was subjected to 8 kPa of matric suction. These values were larger than the shear modulus values recorded by

dry and fully saturated samples. Alternatively, the partially saturated soils displayed lower damping ratios compared to dry and fully saturated soils. An interesting observation was noted when soils were subjected to 10 kPa of matric suction; in which, decreases in the shear modulus and increases in the damping ratios suggest a loss of capillary attraction in the soil structure when transitioning from 8 kPa to 10 kPa of matric suction.

The viability of the DSS as a means to record reasonable results for the dynamic properties was confirmed by the observation of the degradation of the shear modulus with increasing shear strains. Concurrently, the corresponding damping ratio values increased as the applied shear strains increased.

7.2 Conclusions

In conclusion, the following lessons can be deduced from the results of this research:

- Partially saturated soils exhibit a stiffer mechanical response than dry and fully saturated soil and will deform less than dry samples.
- Partially saturated soils exhibit less damping than dry soils.
- Soils subjected to higher shear strain values exhibit lower stiffness values, while soils subjected to lower shear strains display higher stiffness values.
- Soils subjected to higher shear strain values exhibit higher damping values, while soils subjected to lower shear strains display lower damping values.

7.3 Potential Research/Modifications for the Future

Although the apparatus is able to distinguish the changes in dynamic properties over a small range of applied shear strains and different saturation conditions, it is recommended that for future tests, studies and modifications should be made to the system to address the relatively low value of recorded shear modulus values. It is suspected that the movement recorded by the vertical load

and LVDT and that this may have an effect on the shear modulus values due to an introduced moment in the system. In order to address this issue the need to establish active control in vertical loading would need to be developed.

Numerous modifications should be conducted by altering the LabVIEW software architecture. It is recommended that the user should be familiar with software engineering or have an outside professional make the necessary changes. These changes should include restoring the ability to run stress controlled tests (using the horizontal load cell as feedback in the PID control loop) and controlling the vertical load. An additional pneumatic servo-valve is available and was previously used for controlling the vertical load. However, it was not integrated into the LabVIEW software. The additional servo-valve would allow users to actively control the vertical load applied for vertical consolidation or maintain constant vertical pressure when running the dynamic portion of the test.

Further improvement to the soil sample cell could be made for the confirmation of results from this investigation. A pressure transducer could be installed to the top of the sample to track the changes in pore air pressure. Alternatively, instead of changing the PWP below the disc to control the matric suction, the air pressure at the top of the specimen could be changed to test samples at the same suction level. The sample rate of the DPT should be increased to record the behavior of the PWP between cycles. The incorporation of an additional bender element into the already modified bottom platen could also allow users to reincorporate the already existing bender element embedded into the top platen of the sample. The re-establishment of the acoustical system would allow the measurement of the small strain shear modulus values.

A completely different approach of creating a new soil cell that would users to apply a pressure surrounding the sample could also have some advantages. One such would be that water

surrounding the cell could prevent the potential for air diffusion from occurring around the sides of the sample. Additionally, an induced cell pressure would allow users to achieve high degrees of saturation using Skempton's B – Value saturation technique.

REFERENCES

- Airey, D. W., and D. M. Wood. "An Evaluation of Direct Simple Shear Tests on Clay." *Géotechnique* 37.1 (1987): 25-35. Print.
- ASTM D6528-07, Standard Test Method for Consolidated Undrained Direct Simple Shear Testing of Cohesive Soils, ASTM International, West Conshohocken, PA, 2007, www.astm.org
- Biglari, M., Jafari, M.K., Shafiee, A., Mancuso, C., and D'Onofrio, A. "Shear Modulus and Damping Ratio of Unsaturated Kaolin Measured by New Suction-Controlled Cyclic Triaxial Device." *Geotechnical Testing Journal*. 34.5 (2011): 1-12. Web.
- Budhu, Muniram. "Nonuniformities Imposed by Simple Shear Apparatus." *Canadian Geotechnical Journal*. J. 21.1 (1984): 125-37. Web.
- Chin, K. B., Leong, E. C., and Rahardjo, H. "Cyclic Behaviour of Unsaturated Silt in Suction-controlled Simple Shear Apparatus." *Unsaturated Soils*. 1 (2010): 65-70. Print.
- Cho, G.C., and Santamarina, J. C. "Unsaturated Particulate Materials—Particle-Level Studies." *Journal of Geotechnical and Geoenvironmental Engineering* 127.1 (2001): 84-96. Web.
- Cui, Y.J, Tang, A.M, Marcial, D., Terpereau, J.M, Marchadier, G. and Boulay, X. "Use of a Differential Pressure Transducer for the Monitoring of Soil Volume Change in Cyclic Triaxial Test on Unsaturated Soils." *Geotechnical Testing Journal* 30.3 (2007): 1-7. Web.
- Das, Braja M. *Principles of Soil Dynamics*. Boston: PWS-Kent Pub., 1993. Print.
- Darendeli, B. M. "Development of a new family of normalized modulus reduction and material damping curves" Diss. U. of Texas - Austin. 2001. Web
- Doroudian, M., and Vucetic, M. "A Direct Simple Shear Device for Measuring Small-Strain Behavior." *Geotechnical Testing Journal* 18.1 (1995): 69-85. Web.
- Duku, P. M., Stewart, J. P., Whang, D. H., and Venugopal, R. "Digitally Controlled Simple Shear Apparatus for Dynamic Soil Testing." *Geotechnical Testing Journal*. 30.5 (2007). Print.
- Duku, P. M., Stewart, J. P., Whang, D. H., and Yee, E. "Volumetric Strains of Clean Sands Subject to Cyclic Loads." *Journal of Geotechnical and Geoenvironmental Engineering*. 134.8 (2008): 1073-1085. Web.
- Dunstan, Alicia H. *Laboratory Simulation of Earthquake Loading on Clay*. Thesis. University of New Hampshire, 1998. Print.

- Genuchten, M. Th. Van. "A Closed-form Equation for Predicting the Hydraulic Conductivity of Unsaturated Soils." *Soil Science Society of America Journal* 44.5 (1980): 892. Web.
- Ghayoomi, M., and McCartney, J.S. "Measurement of Small-Strain Shear Moduli of Partially Saturated Sand during Infiltration in a Geotechnical Centrifuge." *Geotechnical Testing Journal* 34.5 (2011): 103608. Web.
- Ghayoomi, M., McCartney, J.S., and Ko, H.Y. "An Empirical Methodology to Estimate Seismically Induced Settlement of Partially-Saturated Sand." *ASCE Journal of Geotechnical and Geoenvironmental Engineering* 139.3 (2013) p. 367-376.
- Ghayoomi, M., Suprunenko, G., and Mirshekari, M. "Cyclic Triaxial Test to Measure Strain-Dependent Shear Modulus of Unsaturated Sand." *ASCE International Journal of Geomechanics* (Under-Review - 2016). Web.
- Hall, J. R., Jr., and Richart, F. E., Jr. "Dissipation of Elastic Wave Energy in granular Soils." *ASCE Journal of the Soil Mechanics and Foundations Division*. Vol. 89, No. SM6. 1963. p. 27 - 56.
- Hardin, B. O., and Richart, F. E., Jr. "Elastic Wave Velocities in Granular Soils." *Journal of the Soil Mechanics and Foundations Division*, ASCE, Vol. 89, No. SM1, pp. 33 -65.
- Hargy, Jay. *Measuring Residual Strength of Liquefied Soil with the Ring Shear Device*. Thesis. University of New Hampshire, 2011. Print.
- Holtz, R. D., and Kovacs, W. D. *An Introduction to Geotechnical Engineering*. 2nd ed. Upper Saddle River, NJ: Pearson, 2011. Print.
- Hoyos, L. R., Suescún-Florez, E.A., and Puppala, A.J. "Stiffness of Intermediate Unsaturated Soil from Simultaneous Suction-controlled Resonant Column and Bender Element Testing." *Engineering Geology*. 188 (2015): 10-28. Print.
- Hsu, Chu-Chung, and Vucetic, M. "Volumetric Threshold Shear Strain for Cyclic Settlement." *Journal of Geotechnical and Geoenvironmental Engineering* 130.1 (2004): 58-70. Print.
- Idriss, I.M., and Seed, H.B. "Seismic Response of Horizontal Soil Layers." *ASCE Journal of the Soil Mechanics and Foundations Division*. 94.4 (1968): 1003-031. Print.
- Ishibashi, I. and Zhang, X. (1993). "Unified Dynamic Shear Moduli and Damping Ratios of Sand and Clay," *Soils and Foundations*. Vol. 33, No. 1, pp.182-191.
- Jafarzadeh, Fardin, and Sadeghi, H. "Experimental Study on Dynamic Properties of Sand with Emphasis on the Degree of Saturation." *Soil Dynamics and Earthquake Engineering*. 32.1 (2012): 26-41. Print.

- Kimoto, S., Oka, F., Fukutani, J., Yabuki, T. and Nakashima, K., "Monotonic and Cyclic Behavior of Unsaturated Sandy Soil Under Drained And Fully Undrained Conditions." *Soils and Foundations*. 51.4 (2011): 663-81.
- Kjellman, W. "Testing the Shear Strength of Clay in Sweden." *Géotechnique*. 2.3 (1951): 225-32. Web.
- Khosravi, A., and McCartney, J. S. "Resonant Column Test for Unsaturated Soils with Suction– Saturation Control." *Geotechnical Testing Journal*. 34.6 (2011): 103102. Print.
- Kramer, Steven L. *Geotechnical Earthquake Engineering*. Upper Saddle River, NJ: Prentice Hall, 1996. Print.
- Kumar, J., and Madhusudhan, B.N. "Dynamic Properties of Sand from Dry to Fully Saturated States." *Géotechnique*. 62.1 (2012): 45-54. Print.
- Lu, Ning, Godt, J. W., and Wu, D. T. "A Closed-form Equation for Effective Stress in Unsaturated Soil." *Water Resources Research Water Resources. Res.* 46.5 (2010): n. pag. Web.
- Lu, Ning, and Likos, W. J. *Unsaturated Soil Mechanics*. Hoboken, NJ: J. Wiley, 2004. Print.
- Masing, G. "Eigenspannungen and Verfestigung Beim Masing," *Proceedings, Second International Congress of Applied Mechanics*. (1926) p. 332 – 335
- McGuire, Seth T. "Comparison of Direct Simple Shear Confinement Methods on Clay and Silt." Thesis. University of Rhode Island, 2011. Kingston: U of Rhode Island, 2011. Web.
- Menq, F. Y. "Dynamic Properties of Sandy and Gravelly Soils." Diss. U. of Texas – Austin, 2003. Web.
- Milatz, M., and Grabe, J. "A New Simple Shear Apparatus and Testing Method for Unsaturated Sands." *Geotechnical Testing Journal*. 38.1 (2015): 9-22. Print.
- Miller, Heather J. "Development of Instrumentation to Study the Effects of Aging on the Small Strain Behavior of Sands." Diss. U of New Hampshire, 1994. Print.
- Nishimura, T., Shahrour, L., and Bian, H.B. "Investigation of the behavior of an unsaturated sand using a cyclic direct shear device." *Unsaturated Soils*. 1 (2010): 329 – 334. Print.
- Oztoprak, S., and Bolton, M.D. "Stiffness of Sands through a Laboratory Test Database." *Géotechnique*. 63.1 (2013): 54-70. Print.
- Sawada, S., Tsukamoto, Y., and Ishihara, K. "Residual Deformation Characteristics of Partially Saturated Sandy Soils Subjected to Seismic Excitation." *Soil Dynamics and Earthquake Engineering*. 26.2-4 (2006): 175-182. Web.

- Seed, H. B., and Idriss, I. M. *Soil Moduli and Damping Factors for Dynamic Response Analyses*. Rep. 10th ed. Vol. 70. Berkeley: Earthquake Engineering Research Center, 1970. Print.
- Shen, C. K., Sadigh, K., and Herrmann, L. R., "An Analysis of NGI Simple Shear Apparatus for Cyclic Soil Testing," *Dynamic Geotechnical Testing, ASTM STP 654*, American Society for Testing and Materials, 1978, pp. 148 – 162.
- Suprunenko, Ganna. *Suction-Controlled Cyclic Triaxial Test to Measure Strain-Dependent Dynamic Shear Modulus of Unsaturated Sand*. Thesis. University of New Hampshire, 2015. Print.
- Terzaghi, K., Peck, R.B., and Mesri, G. *Soil Mechanics in Engineering Practice*. New York: Wiley, 1996. Print
- Vucetic, Malden, and Lacasse, S. "Specimen Size Effect in Simple Shear Test." *Journal of the Geotechnical Engineering Division* 108.12 (1982): 1567-585. UNH Illiad. Web.
- Whang, D.H., Stewart, J.P., and Bray. J.D., "Effect of Compaction Conditions on the Seismic Compression of Compacted Fill Soils." *Geotechnical Testing Journal*. 27.4 (2004): 11810. Web.
- Wright, D.K., Gilbert, P.A and Saasa, A.S. "Shear devices for determining dynamic soil properties." *Proc. Spec. Conf. Earthquake Engineering and Soil Dynamics*, ASCE, Pasadena, 2, (1978) p.1056 – 1075. Web.

APPENDIX

Appendix A: List of Sensors and Instrumentation

Appendix B: Dimensions of the Modified Platen

Appendix C: DSS Control System – Block Diagram

Appendix D: Sample Preparation Procedure

Appendix E: Various Procedures (from Vertical Consolidation to Cyclic Testing)

Appendix F: MATLAB Code for post-processing analysis

Appendix A: List of Sensors and Instrumentation

Horizontal Equipment

- Measurement of Horizontal Load
 - Interface SSM Sealed S-Type Load Cell
 - Rated at +/- 250 lbf capacity
- Measurement of Horizontal Motion (Capacitance Movement)
 - MTI Instruments Capacitance Probe Model ASP – 500M – CTA
 - 0.500 μm range
 - 20 mV/ μm sensitivity
 - MTI Instruments AccuMeasure 9000 Capacitance Sensor Amplifier
- Measurement of Horizontal Movement (Top Sample Movement)
 - Schaevitz/ Measurement Specialties MHR 050 Series
 - +/- 0.05 inch range
 - 3.15 V/V/Inch

1. Vertical Equipment

- Measurement of Vertical/Normal Load
 - Interface 1500 Low Capacity Low-Profile Load Cell
 - Rated at +/- 300 lbs capacity
- Measurement of Vertical Displacement
 - Sensotec AC – AC Ultra Precision Model PLVX LVDT
 - +/- 0.2 inch range
 - 5.08 mV/V/0.001” output sensitivity

2. Saturation System

- Validyne Model P55 Differential Pressure Transducer
 - Rated at 100 kPa
 - +/- 5 Vdc signal
 - 0.1% Sensitivity Rating
- Geotac Flow Pump
 - 75 mL Water Reservoir Capacity
 - 100 kPa Pressure Transducer

3. Data Acquisition System

- National Instruments - SCXI 1000 Chassis
 - SCXI - 1314 & 1520 Strain Gauge Module (Load Cells)
 - SCXI – 1315 & 1540 LVDT Module (Distance Readings)

4. Mechanical Equipment

- National Instruments Controller
- Hydraulic Equipment

- Hydraulic Actuator (specifications unknown)
- Hydraulic Accumulators
- Hydraulic Pump – Custom Built by NH Hydraulics
 - Rated at 1 GPM at 2700 PSIG
 - Electric Motor – 2 HP, 1800 RPM
 - 110/220/1/60 VAC
 - Oil Reservoir
 - 7 Gallons w/ oil level & temperature sight glass
- MOOG Servovalve Model 760 – 101A
- MOOG Servo-Amplifier Model G122 – 829 – 001

- Interlaken Model 3611 – 1500-1 Pneumatic Actuator
 - 2 inch stroke
 - 4 inch cylinder bore

Appendix B: Dimensions of the Modified Platen

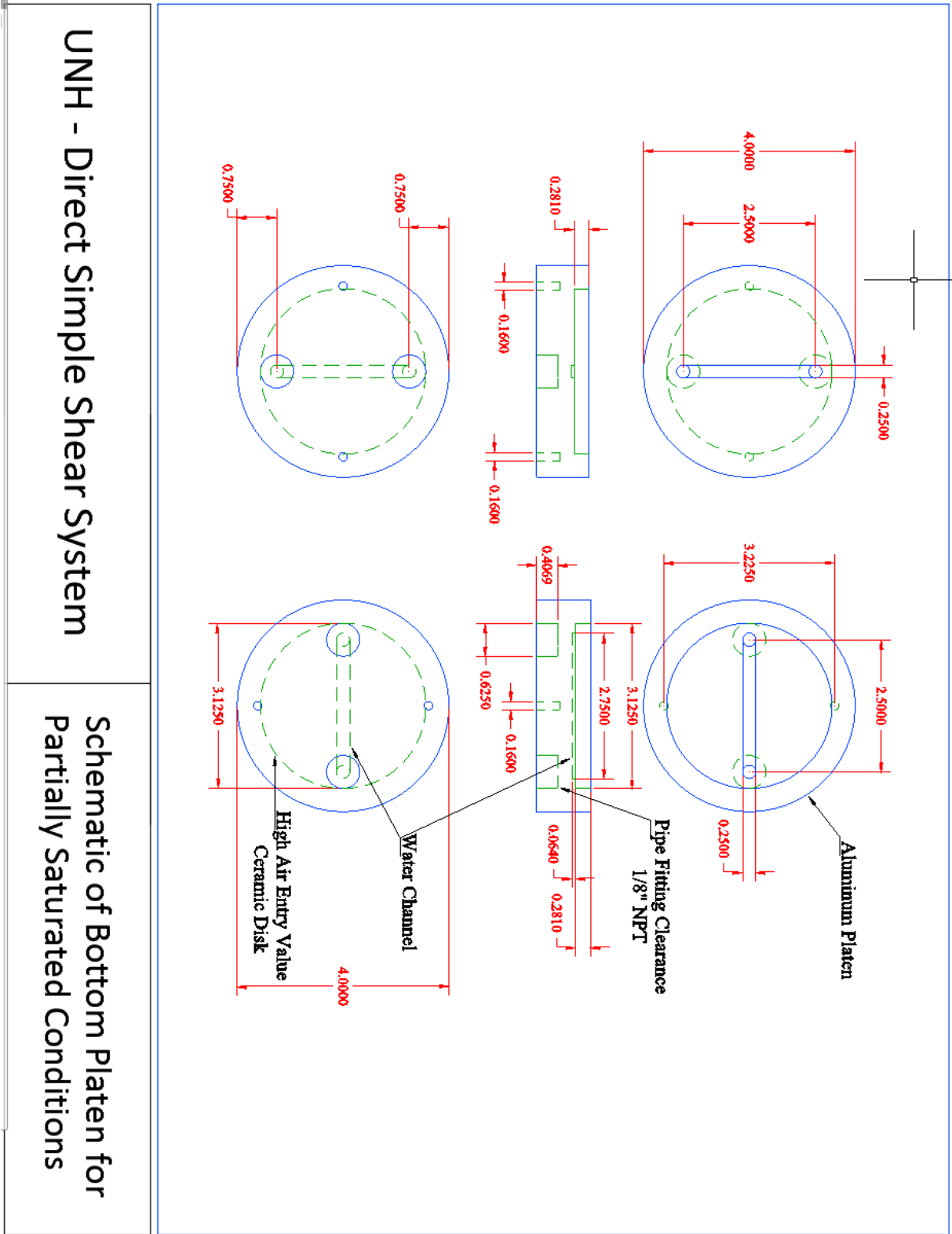


Figure B1: Modified Bottom Platen Dimensions

UNH - Direct Simple Shear System

Schematic of Bottom Platen for Partially Saturated Conditions

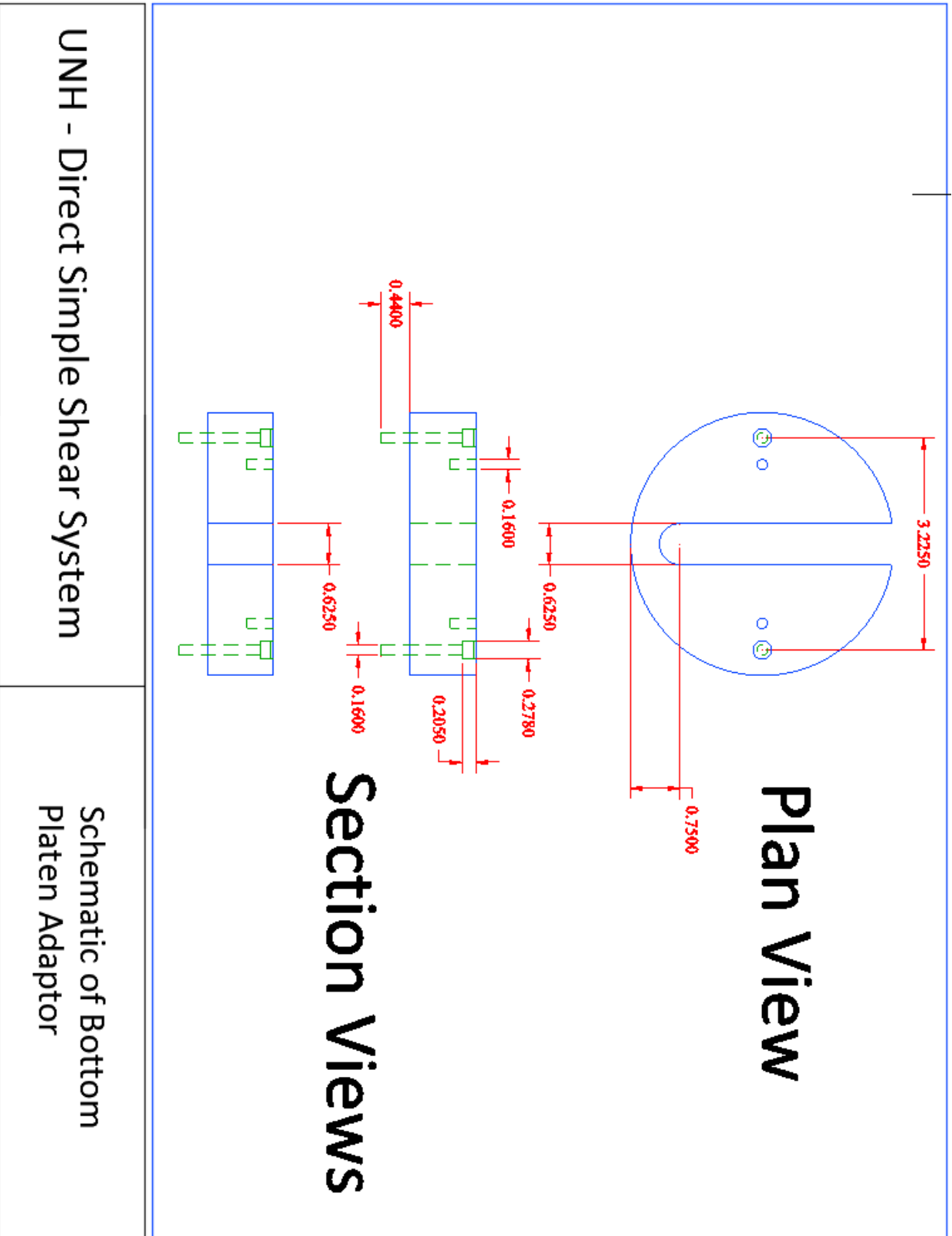


Figure B2: Bottom Platen Adaptor Dimensions

Appendix C: DSS Control System – Block Diagram

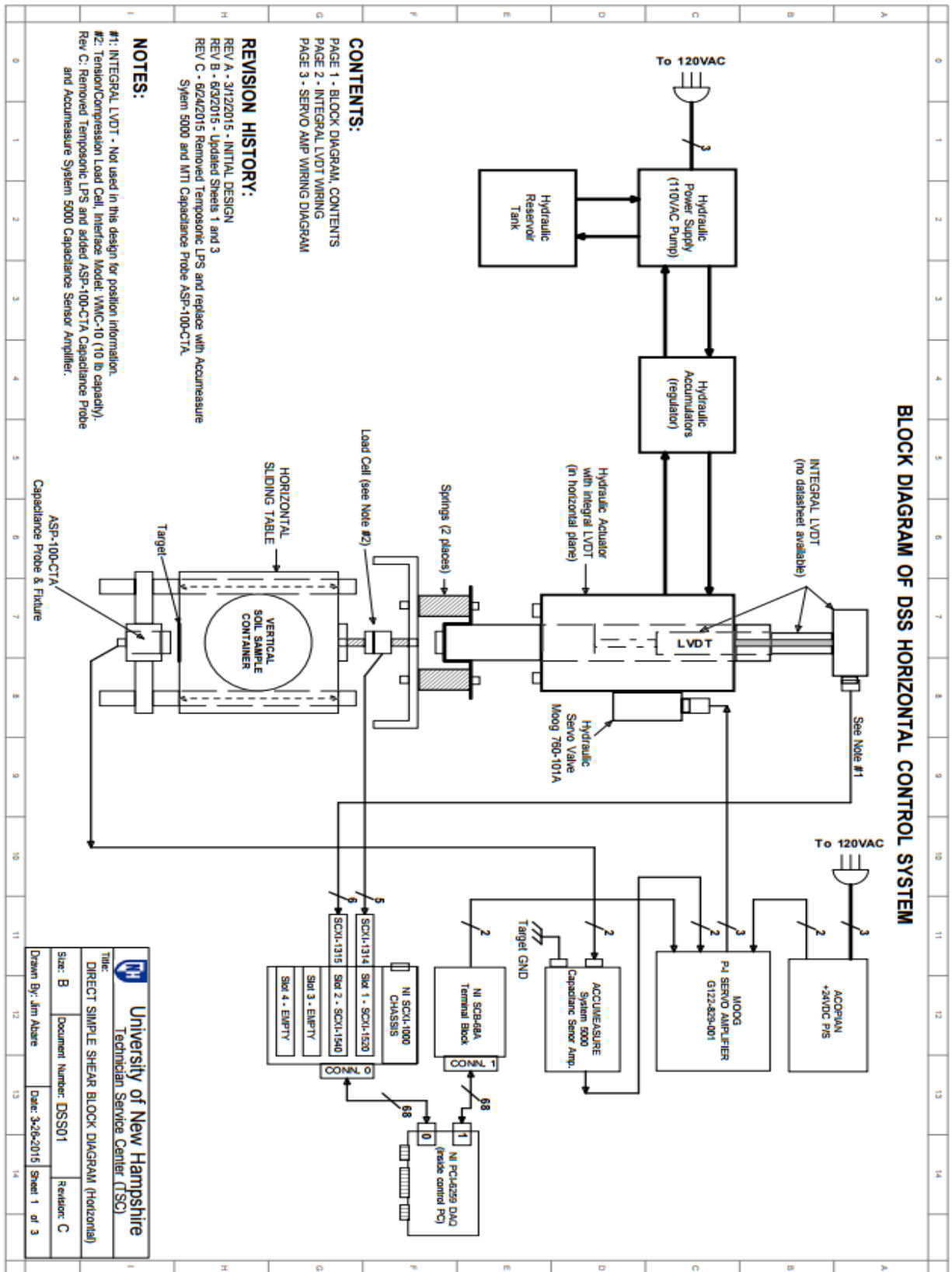


Figure C1: Block Diagram of the Horizontal Control System

Appendix D: Sample Preparation Procedure

- 1) Set the bottom platen (#1 & #2) on a level surface and apply vacuum grease around the circumference of the soil pedestal.

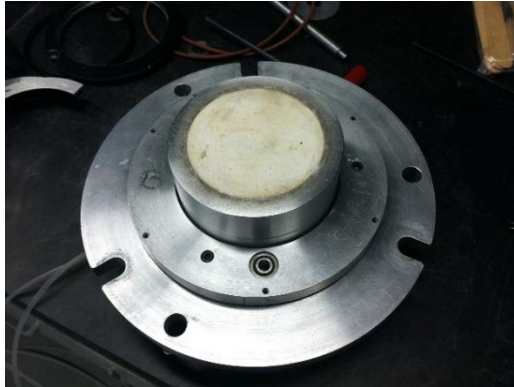


Figure D1: Modified Platen with embedded HAEV Ceramic Disk

- 2) Use a 6 – inch soil membrane to cover the bottom soil pedestal.

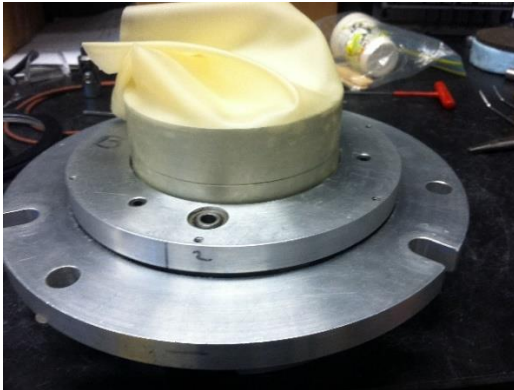


Figure D2: Attached Soil Membrane around Soil Pedestal

- 3) Install annular clamp (#3) to the soil pedestal.

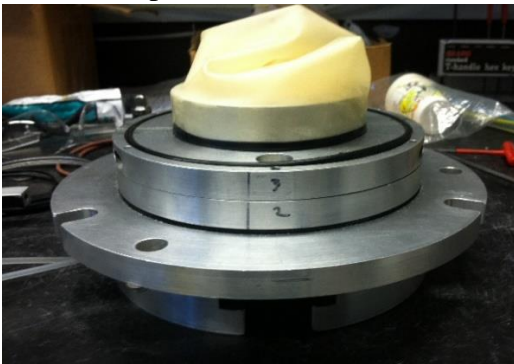


Figure D3: Bottom pedestal with annular clamp (#3)

- 4) Place 3 rings, 2 O-rings, and an annular clamp around the extended bottom platen. It is important to make sure the top of the annular clamp is level with the top part of the modified base platen.

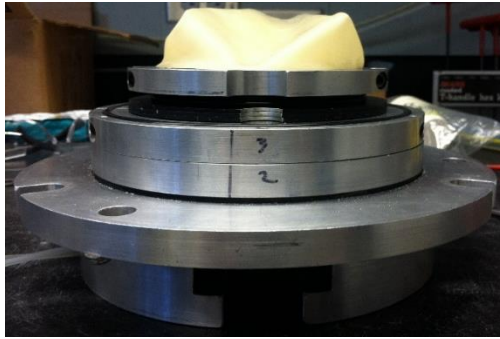


Figure D4: Various shims to allow clamp to be level with pedestal

- 5) Install the 1st part of the vacuum mold (#4) and insert 6 hex screws to make sure the bottom part of the mold is secure. Tighten the hex screws in a crisscross fashion (similar to changing a tire) and then tighten the two bolts on the side. Insert an O-Ring on top of the mold.

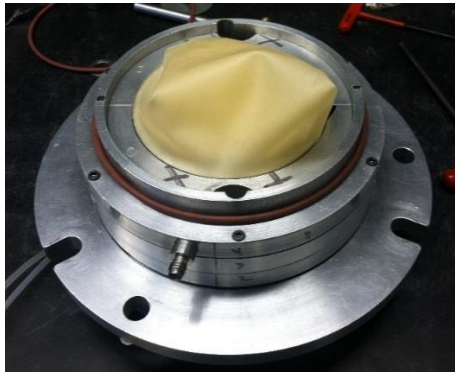


Figure D5: 1st part of Vacuum Mold

- 6) Insert the ring stack and make sure that the sample is approximately 1" tall. A guide rod can be used to straighten out the rings as shown in the following figure.

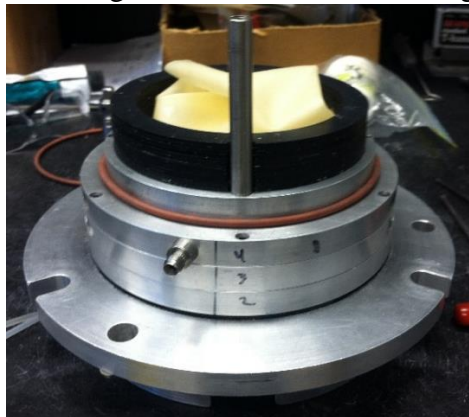


Figure D6: Ring-stack with guide rod

- 7) Install the 2nd part of the vacuum mold (#5). Insert another O-ring onto the vacuum mold.

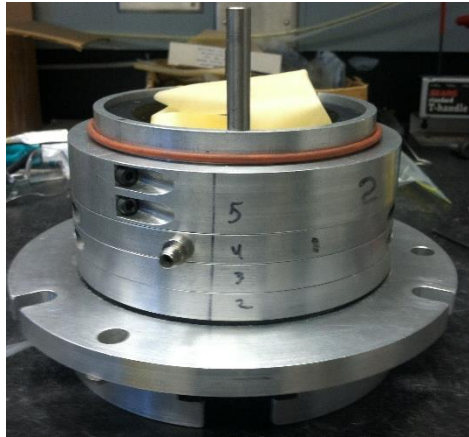


Figure D 7: Soil Sample with 2nd part of vacuum mold

- 8) Install the 3rd part of the vacuum mold (#6).

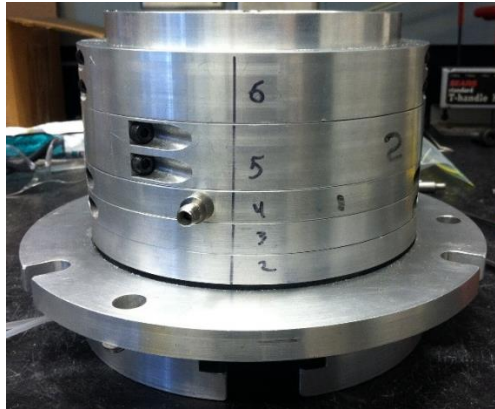


Figure D8: Soil Sample with 3rd part of vacuum mold

- 9) Stretch the soil membrane around the top of the mold and attach the vacuum lines to the mold and apply suction. The membrane should stick to the insides of the mold without any folds or wrinkles. Then, insert a piece of filter paper on top of the soil pedestal.

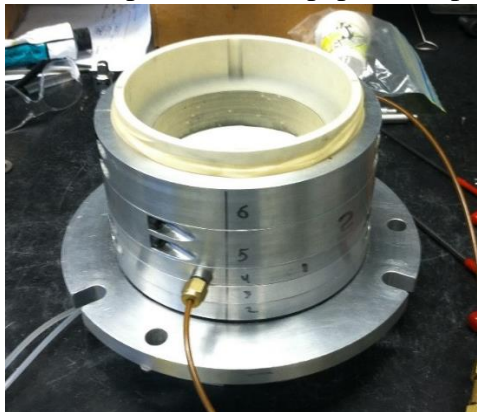


Figure D9: Stretched soil membrane around vacuum mold

- 10) Place a bag around the perimeter of the vacuum mold and clamp it around the sides to catch any sand that may fall around the sides during the sand pluviation stage.



Figure D10: Soil Sample prepared for Sand Pluviation

- 11) Measure and record the initial height of the sample from the pedestal to the top of the ring stack at three different places. Use a funnel, washer, string, and bolt to pluviated the sand into the mold. To achieve 45% Relative Density, the height of the sand to fall was found to be 21.5 inches with a 0.25 inch washer opening.



Figure D11: Sand Pluviation/Raining

- 12) Once pluviation was complete, the soil should be leveled out (using a card or piece of paper) and then insert a piece of filter paper on top of the soil. The vacuum clamp and bag can then be removed and three guide rods should then be attached to the bottom plate.

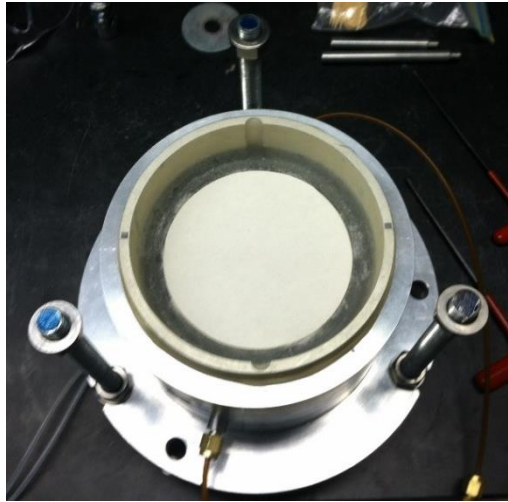


Figure D12: Sand and filter paper with installed guide rods

- 13) Before placing the top plate onto the sample, place 2 O-rings around the top platen and use vacuum grease around the perimeter. Slowly lower the top platen onto the sample until it makes contact with the soil sample. Adjust the platen to make sure it is level with the soil surface by using a level tool.

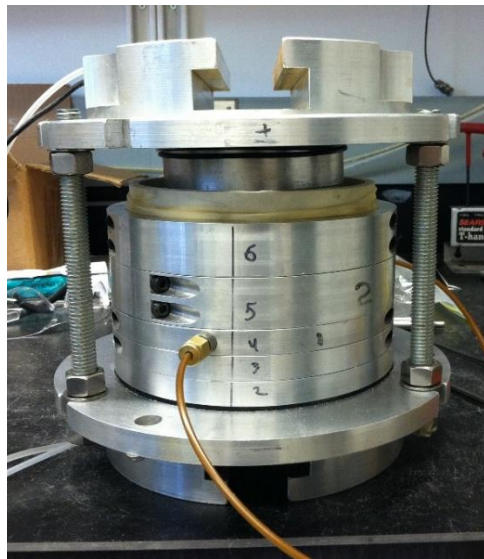


Figure D13: Top Platen w/ O-Rings installed on top of soil sample

- 14) Flip the soil membrane onto the top platen and remove the top piece of the vacuum mold (#6).

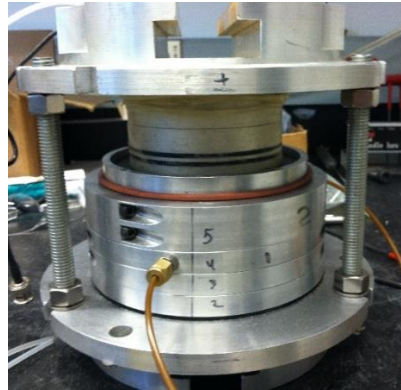


Figure D14: Soil Membrane attached to lowered top platen

- 15) Move one of the O-rings down towards the ring stack. Install the top collar and then move the other O-Ring on top of the collar. Remove the vacuum lines and slowly move the sample towards the DSS.

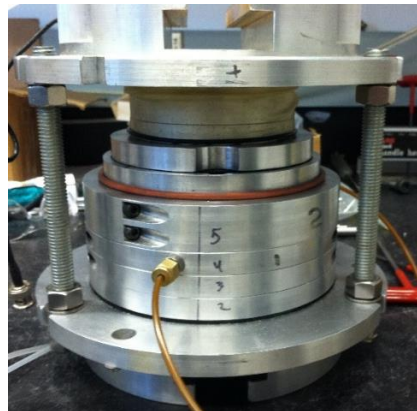


Figure D15: Installed annular clamp attaching membrane to top platen

- 16) Insert the sample into the DSS by matching the T-Clamps into position. The top table may need to be raised. This can be achieved by adjusting the air regulators on the left side of the apparatus.

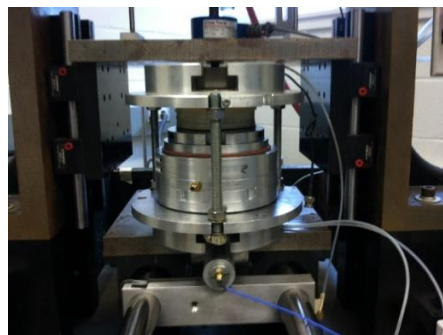


Figure D16: Lining the soil sample up with the T-Clamps

- 17) Once the sample is lined up with the T-Clamps, gently push the specimen into place. Make sure that the water lines located at the top and bottom of the soil sample do not get caught in between the top table or the bottom table. Tighten the four hex bolts connecting the T-clamps to the top and bottom table (2 bolts each).

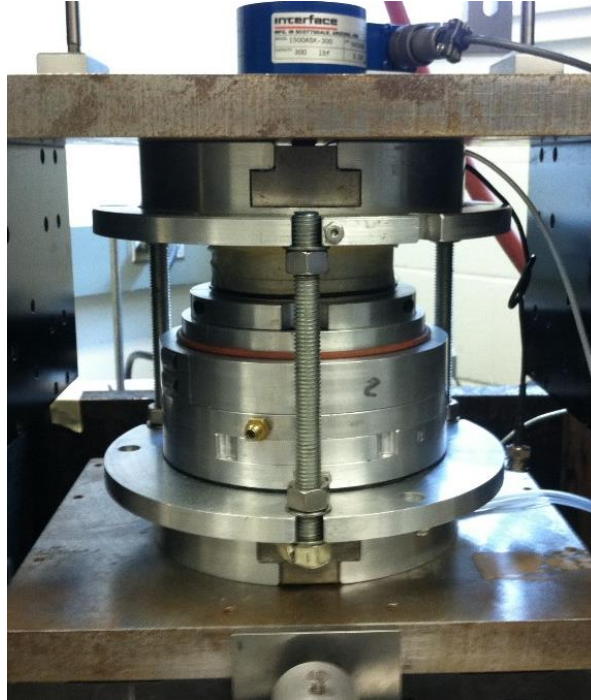


Figure D17: Installed Soil Sample in DSS

- 18) Remove the 2nd part of the mold (#5), this process should be done with extreme caution as to not disturb the soil sample rings surrounding the soil.

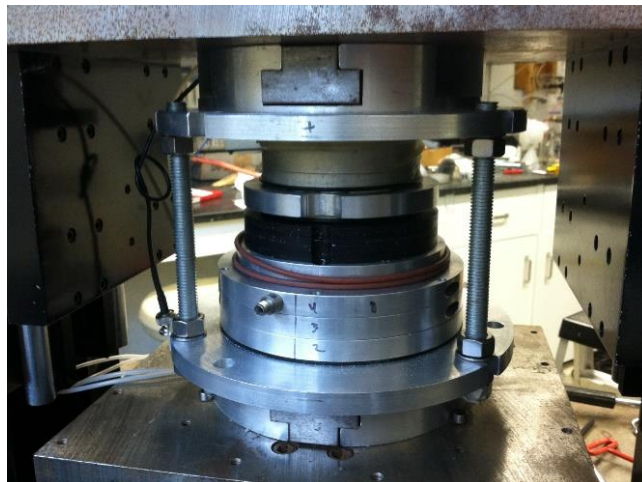


Figure D18: Soil Sample with 2nd part of vacuum mold removed

19) Before removing the last piece of the vacuum mold, install the top table LVDT. Start the program LabVIEW and start the 1st reading of the vertical consolidation stage (see next section). Lower the screws on the guide rods, so that a very small vertical load is applied. Then start removing the 6 hex screws attaching the vacuum mold to the base. Remove the two side bolts and mold very carefully. Then remove the guide rods completely. The sample is then ready for the remainder of vertical consolidation.

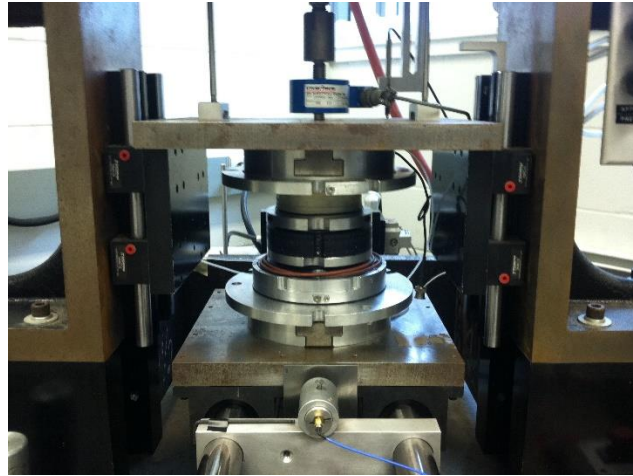


Figure D 19: Fully Prepared Soil Sample in DSS


Appendix E: Various Procedures (from Vertical Consolidation to Cyclic Testing)

Vertical Consolidation Procedure

- 1) Remove the bottom 2 sections of the mold, as carefully as possible.
- 2) Once the sample is inside of the DSS chamber, install the vertical LVDT and capacitance transducer. The capacitance transducer should be approximately 4.6 mV (as read by the voltmeter on the side) to the target.



Figure E1: Air Regulator for Top Load Control

- 3) Start the program *LabVIEW* (*Windows Desktop > Direct Simple Shear – Shortcut > shaker-daq-main.vi*). Turn on the necessary sensors (*Setup > Sensor Setup > Check the following boxes: LVDT_CH1, Vertical Load, Top Sample LVDT, and Bottom Sample LVDT > Save/Exit*). Establish the connection between the software and sensors by pressing the “” button underneath the *Setup* button. Start manually recording the loads and displacements by signaling *Run* function in the program. Manually record these values into an Excel Sheet.
- 4) At steady increments, slowly increase the pneumatic air regulator (located to the right of the desktop) and read/record in the corresponding values from the LVDT and Vertical Load cell.
- 5) Once the target pressure is reached (usually ~50 kPa -> 0.00023 mV on the Vertical Load Cell), the sample is ready for saturation or testing depending what condition the user chooses.
- 6) Install the Top Sample LVDT and Bottom Sample LVDT. This is accomplished by setting the magnetic gauge stand a set distance away. By looking at the sensor readout in *LabVIEW* and carefully adjusting the two LVDT coil assembly positions, the sensors should be within +/- 0.1 mV readings of the 0 mV reading.

Saturation and Desaturation Procedure

- 1) Connect the two pipes from the bottom of the sample to the valves connecting the water reservoir and to the flushing pipe. The top tube can connect to the vacuum valve or left open to the atmosphere. Open the valve to allow water from the reservoir to the bottom of the sample. Open the valve to the vacuum trap. This configuration is shown below and is used to flush any air that may exist beneath the HAEV.

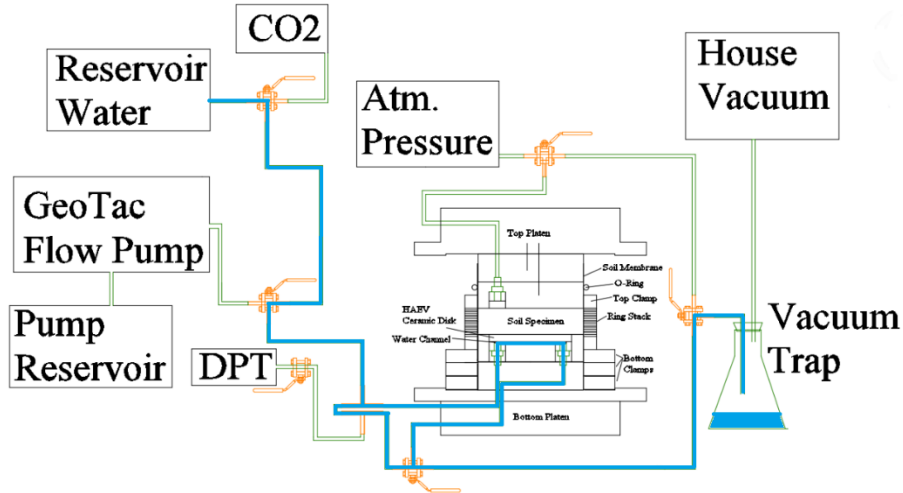


Figure E2: Water Path for Flushing Procedure

- 2) Close the valve to the vacuum trap and allow water to travel up through the HAEV and up through the soil sample. The top sample tube can be left open to the atmosphere or to the vacuum. This process should be left for a couple hours/overnight. Additional flushing periods should be conducted if any air is trapped beneath the HAEV. Careful consideration should be taken to make sure the vacuum trap does not reach its limit. The valves should allow water flow in the following configuration.

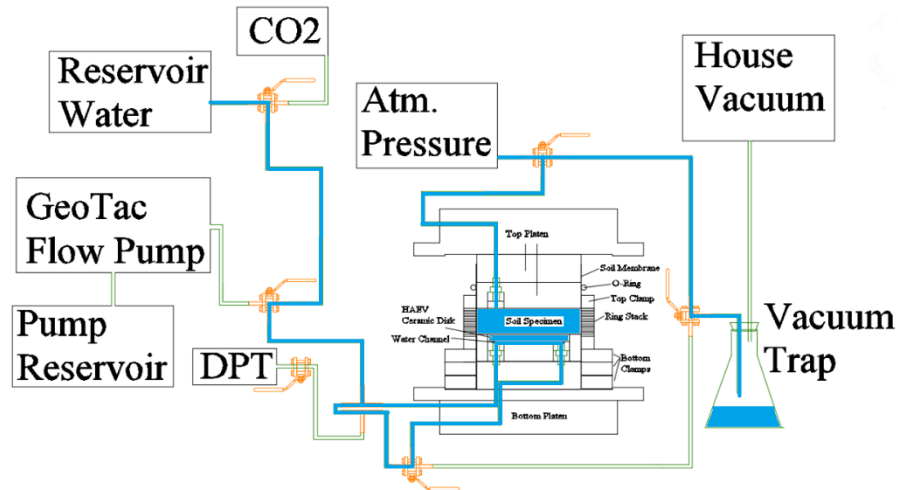


Figure E3: Water Path for Saturation Procedure

- 3) After “near saturation” states, the valve for the vacuum pump should be closed and opened to atmosphere. The GeoTac Flow Pump and DPT valves should then be opened to the following configuration and the water in the tubes should be left to equilibrate.

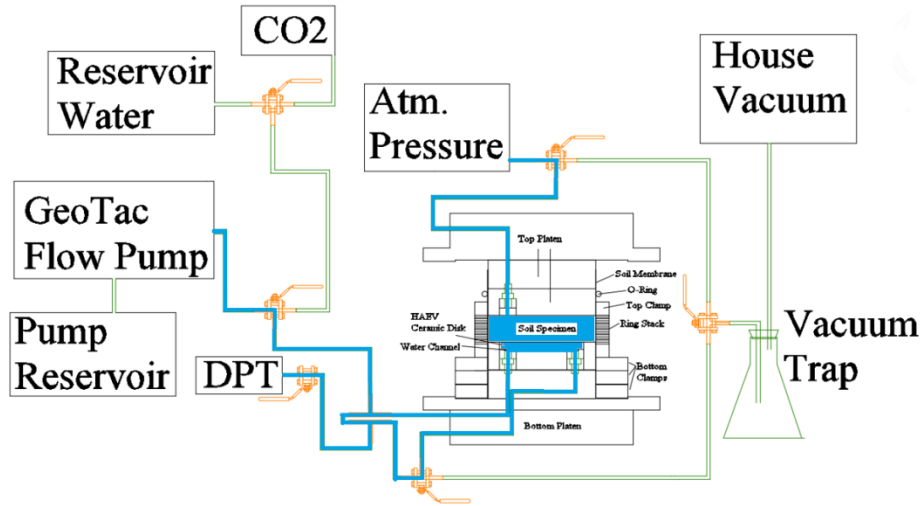


Figure E4: Water Path for Flow-Pump Control

- 4) The GeoTac software should then be opened (*Windows Desktop > DigiFlow-GP-SI*). Depending on the matric suction required by the user, the pressure in the pump can be changed by pressing the tab *Pressure Control*. The user can specify constant pressure or a ramped time selection. The *Start Pump* button then starts the desaturation of the sample. The desaturation process can take up anywhere from 1 to 3 days for a 1” tall - F75 Ottawa Sand sample to reach equilibrium (when $Flow < 0.002$ mL/min). It should be noted that the flushing procedure should be enacted if any air bubbles are visible in the DPT or pump lines.

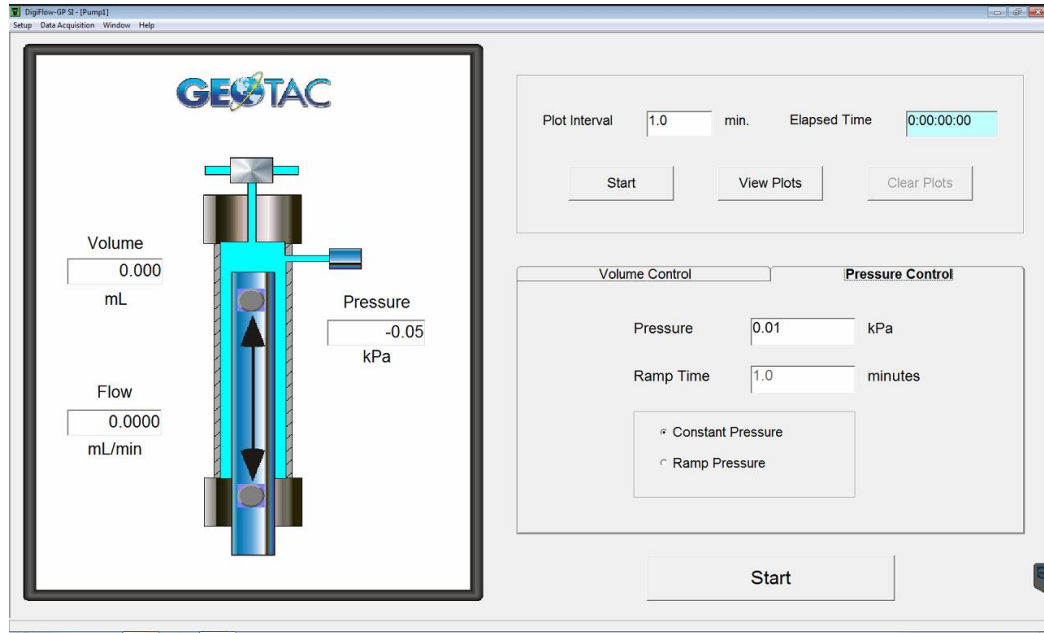


Figure E5: Initial Screen of the GeoTac Flow-Pump Software

- 5) The reservoir capacity of the Flow Pump is 75 mL, therefore if the capacity is reached (indicated by a blinking/stead red light in the program), the pump will need to be emptied into the pump reservoir. To do this, switch the valve on the pump from the sample to the reservoir and complete the following steps in the software (*GeoTac* Software > *Volume Control* > indicate the amount of water to leave pump or empty all the contents with the triangle point up with a line underneath it > *Reset Volume*) Switch the valve back to the sample specimen and proceed with the pressure control procedure.
- 6) The differential pressure transducer readings can be viewed using the following sequence (*Setup* > *Sensors* > *DPT_Nickel* > *Test*). The values of the DPT are used to ensure that the correct matric suction is achieved by taking the reading of the water pressure beneath the HAEV disk.

Cyclic Testing Procedure

- 1) Turn the hydraulic pump on. Ensure that the horizontal piston compresses the springs (the ratio changes for each spring set; for the current springs, the distance from the edge of the piston to the steel beam was found to be 0.3385 inches). This configuration is shown in the figure below. This distance can be adjusted by the *bias* screw on the Moog Servo-Amplifier. Record any changes in the Vertical LVDT. Turn on the additional sensors needed in the *LabVIEW* program (*Setup* > *Sensor Setup* > Check the following: *LVDT_CH1*, *Vertical Load*, *Top Sample LVDT*, *Bottom Sample LVDT*, *MTI Capacitance*, and *Horizontal Load* > *Save/Exit*). Note: There is an emergency stop button wired into the system. This button can be used at any time to turn off the hydraulics in the system.

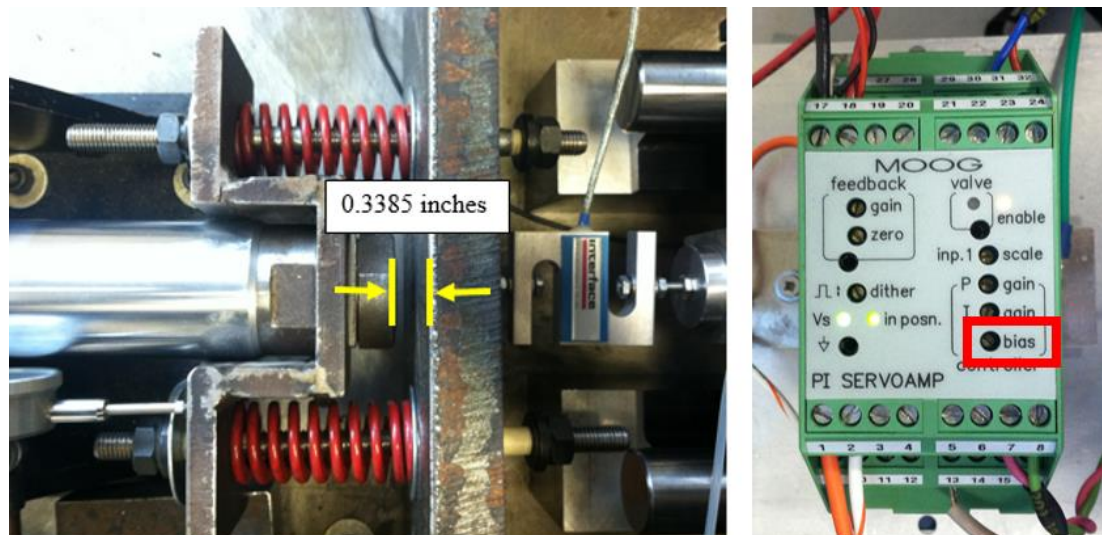


Figure E6: Actuator to Steel Beam distance (left) and PID Control (right)

- 2) Ensure that the sample is at a steady state condition (in terms of flow). The parameters of the sinusoidal motion can be inputted into the *LabVIEW* Program (Box A) and the filename and destination can be also be inputted (Box E). The sensors can displaying the live signal of the program by pressing the *Run* button (Box C). However, do NOT

press the *Trigger* button until the DAQ for the pressure readings are started in the next step.

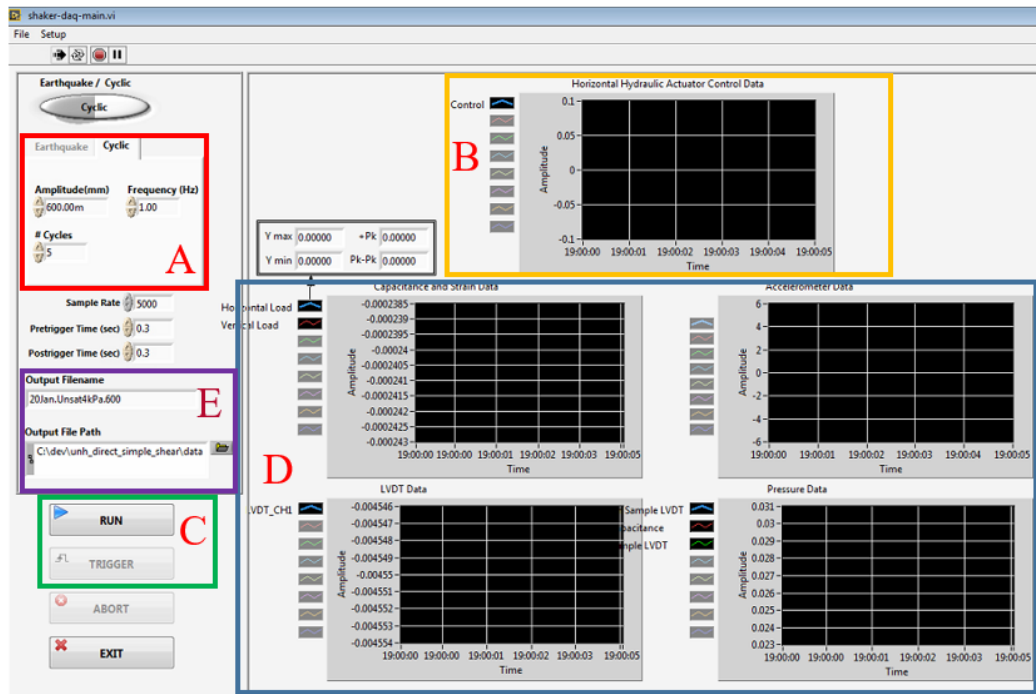


Figure E7: LabVIEW Control Panel

- 3) The data acquisition system of the flow pump and DPT readings can be initialized by the following sequence (*GeoTac Software > Data Acquisition > New Task... > input the filename > Save > Reading Schedule: Dynamic > check Run > OK*). Immediately after, switch back to the *LabVIEW* program and press the *Trigger* button.
- 4) After the test is run, switch back to the *GeoTac Software* and end the data acquisition by pressing (*Data Acquisition > Close Task > OK*). The output files from the *GeoTac* program and *LabView* program are sent to the destination folders for further analysis.
- 5) The final vertical LVDT reading should be recorded for the multistage seismic compression results using the last reading from (Box D). The hydraulic pump can then be turned off.
- 6) Depending on the type of test (either constant strain or constant suction), the test is repeated using the above procedure to either change the suction level (ie. Saturation and Desaturation Procedure) or change the imparted shear strain level (ie. Cyclic Testing Procedure).

Appendix F: MATLAB Code for post-processing analysis

The MATLAB codes are designed specifically to work with Excel Files associated with Sample Preparation and data output files from LabVIEW. The sample preparation files (designated in the following form: *SP.DATE.SaturationCondition*) and data output files from LabVIEW (designated in the following form: *DATE.SaturationCondition.Amplitude*) are stored on the desktop of the DSS Computer.

Function for Reading in Sample Dimensions

```
function[initial_sample_height,sample_weight,sample_diameter,sample_area,samp
    le_Dr,EffectiveSat,Matric_Suction] = read_sample_dimensions
sampledimensionfile = 'SP.DATE.SaturationCondition';
sheet = 1; %specifies the excel sheet of the corresponding test

initial_sample_height = xlsread(sampledimensionfile,sheet, 'F11');
sample_weight = xlsread(sampledimensionfile,sheet, 'F6');
sample_diameter = xlsread(sampledimensionfile,sheet, 'F15');
sample_area = xlsread(sampledimensionfile,sheet, 'F17');
sample_Dr = xlsread(sampledimensionfile,sheet, 'F36');
EffectiveSat =xlsread(sampledimensionfile,sheet, 'J28');
Matric_Suction =xlsread(sampledimensionfile,sheet, 'L20');
```

Function for Reading in Output File from LabVIEW

```
function[TimeInt,BottomSampleLVDT,HRead,VDistRead,HdistRead,TopSampleLVDT,VRe
    ad]= read_input

filename = 'DATE.SaturationCondition.Amplitude' ;
TimeInt = xlsread(filename,1,'A8:A30000');
BottomSampleLVDT = xlsread(filename,1,'B8:B30000');
HRead=xlsread(filename,1,'C8:C30000');
VDistRead=xlsread(filename,1,'D8:D30000');
HdistRead=xlsread(filename,1,'E8:E30000');
TopSampleLVDT = xlsread(filename,1,'F8:F30000');
VRead=xlsread(filename,1,'G8:G30000');
```

Post Processing Code for Hysteresis Loops

```
%Full Script, Plotting Data
clear all
clc

cd ('E:\Matlab')

%DSS Main Data Analysis - Converting Measurements into Loads and Strains
[TimeInt,BottomSampleLVDT,HRead,VDistRead,HdistRead,TopSampleLVDT,VRead]=
read_input;

%calibration Factors from mV to force and Distance (English Units)
Time = cumsum(TimeInt); %in seconds
BotLVDT = ((BottomSampleLVDT*-.07819860)+.00230398);%in inches
H_Load = (HRead-.0006608021)/.0000059679;
%H_Load = (HRead-.0006451051)/.0000059926; %in lbf (Tests before 2.6.16)
```

```

VDistance = (VDistRead-0.00480646)/(-0.0179222);%in inches
HDistance = (HdistRead*.0019685);%in inches
V_Load = (VRead-.0000871981)/(-0.0000035075);%in lbf
TopLVDT = (TopSampleLVDT-.003283)/(17.183411); %in inches
CorrectedTopLVDT = TopLVDT - TopLVDT(1);
CorrectedBotLVDT = BotLVDT - BotLVDT(1);

[initial_sample_height,sample_weight,sample_diameter,sample_area,sample_Dr,Ef
fectiveSat,Matric_Suction] = read_sample_dimensions;
%From Experimental Data
FrictionAngle = 40*(pi/180);
K0 = 1 - sin(FrictionAngle);
Dr = sample_Dr;

Shear_Force = H_Load/sample_area;
Shear_Strain= HDistance/ initial_sample_height;
Normal_Force = V_Load/sample_area;
Top_Strain = TopLVDT/ initial_sample_height;
%*****Delineation of Cycles*****
% cycle1start = 2000, cycle1end = 7045;
% cycle2start = 7045, cycle2end = 12085;
% cycle3start = 12085, cycle3end = 17085;
% cycle4start = 17085, cycle4end = 22100;
% cycle5start = 22100, cycle5end = 27530;

Vertmean2 = mean(Normal_Force(7045:12085));
Vertmean3 = mean(Normal_Force(12085:17085));
Vertmean4 = mean(Normal_Force(17085:22100));

%*****
%INT(erval) variable used for filtering
INT = 250;
lag = INT/5000; %SampleRate = 5000

AverageNormalPressure = (mean(Normal_Force))*6.89476

AvgHorizontalForce = mean(Shear_Force);
Non_Shifted = Shear_Force - AvgHorizontalForce;
Non_Shifted_Norm = smooth(Non_Shifted - mean(Non_Shifted(1:1500)));
% Pre-trigger time:0.35 sec @ 5000 Sample Rate = 1500
% Time_Shifting=zeros(length(Non_Shifted_Norm)+5,1);
Non_Shifted_Norm_New= Non_Shifted_Norm;
%Non_Shifted_Norm_New=zeros(length(Non_Shifted_Norm)+INT,1);
% for i=1:(length(Non_Shifted_Norm))
%     Time_Shifting(i+INT,1)=Time(i,1)+0.05;
%     Non_Shifted_Norm_New(i+INT,1)=Non_Shifted_Norm(i,1);
% end

Strain_BaseLine = mean(Shear_Strain);
Shear_Strain_Corrected = (Shear_Strain - Strain_BaseLine);
Norm_Shear_Strain = smooth(Shear_Strain_Corrected -
Shear_Strain_Corrected(1));
NegCapacitance = (Norm_Shear_Strain)*-1;

```



```

mean2 =
(max(NegCapacitance(7045:12085))+(abs(min(NegCapacitance(7045:12085)))))/2;
mean3 =
(max(NegCapacitance(12085:17085))+(abs(min(NegCapacitance(12085:17085)))))/2;
mean4 =
(max(NegCapacitance(17085:22100))+(abs(min(NegCapacitance(17085:22100)))))/2;
mean = (mean2+mean3+mean4)/3;

f= 2*pi;
timeshift = .415; %in seconds

TopMotion=(55.3623855239*(mean^2))+(0.3055884876*mean)+.000021570182;
TopMotionCurve = -1*(TopMotion * sin(f*(Time-timeshift)));
for i = 1:2129
    TopMotionCurve(i) = 0;
end
for i = 22165:28000
    TopMotionCurve(i) = 0;
end

%*****
CorrectedMotion1 = (NegCapacitance - TopMotionCurve);
for i = 1:4579
    CorrectedMotion1(i) = 0;
end
for i = 22165:28000
    TopMotionCurve(i) = 0;
end
% AvgNETSTRAIN = -1*smooth(Net_Strain);
%*****
cycle2maxstress = max(Non_Shifted_Norm_New(7045:12085));
cycle2minstress = min(Non_Shifted_Norm_New(7045:12085));

cycle3maxstress = max(Non_Shifted_Norm_New(12085:17085));
cycle3minstress = min(Non_Shifted_Norm_New(12085:17085));

cycle4maxstress = max(Non_Shifted_Norm_New(17085:22100));
cycle4minstress = min(Non_Shifted_Norm_New(17085:22100));

%*****
cycle2maxstrain =
CorrectedMotion1(find(Non_Shifted_Norm_New==cycle2maxstress,1));
cycle2minstrain =
CorrectedMotion1(find(Non_Shifted_Norm_New==cycle2minstress,1));

cycle3maxstrain =
CorrectedMotion1(find(Non_Shifted_Norm_New==cycle3maxstress,1));
cycle3minstrain =
CorrectedMotion1(find(Non_Shifted_Norm_New==cycle3minstress,1));

cycle4maxstrain =
CorrectedMotion1(find(Non_Shifted_Norm_New==cycle4maxstress,1));
cycle4minstrain =
CorrectedMotion1(find(Non_Shifted_Norm_New==cycle4minstress,1));

```

```

AvgMaxStrain = (cycle2maxstrain+cycle3maxstrain+cycle4maxstrain)/3;
AvgMinStrain = (cycle2minstrain+cycle3minstrain+cycle4minstrain)/3;
AvgNetStrain = (AvgMaxStrain +abs (AvgMinStrain))/2;

%*****Friction Correction (Horizontal Force)*****
FrictionAmp = (-46619*(AvgNetStrain^2))+(101.65*AvgNetStrain)+0.0133;
%Amp2 = AvgForce;
FrictionCorrection = -1*(FrictionAmp * sin(f*(Time-timeshift)));
% Pre-trigger time:0.3 sec @ 5000 Sample Rate = 1500 + Additional time .372
for i = 1:4579
    FrictionCorrection(i) = 0;
end
for i = 22165:28000
    FrictionCorrection(i) = 0;
end
CorrectedForceFriction = Non_Shifted_Norm - FrictionCorrection;
altcycle2maxstress = max(CorrectedForceFriction(7045:12085));
altcycle2minstress = min(CorrectedForceFriction(7045:12085));
    altmidcycle2stress = (altcycle2maxstress + altcycle2minstress)/2;
altcycle3maxstress = max(CorrectedForceFriction(12085:17085));
altcycle3minstress = min(CorrectedForceFriction(12085:17085));
    altmidcycle3stress = (altcycle3maxstress + altcycle3minstress)/2;
altcycle4maxstress = max(CorrectedForceFriction(17085:22100));
altcycle4minstress = min(CorrectedForceFriction(17085:22100));
    altmidcycle4stress = (altcycle4maxstress + altcycle4minstress)/2;

%*****G Calcs*****
G2 = (6.89475728/1000)*((cycle2maxstress) +
(abs (cycle2minstress)))/(cycle2maxstrain+(abs (cycle2minstrain)));
G3 = (6.89475728/1000)*((cycle3maxstress) +
(abs (cycle3minstress)))/(cycle3maxstrain+(abs (cycle3minstrain)));
G4 = (6.89475728/1000)*((cycle4maxstress) +
(abs (cycle4minstress)))/(cycle4maxstrain+(abs (cycle4minstrain)));

RawG234 = [G2 G3 G4];

altcycle2maxstrain =
CorrectedMotion1 (find(CorrectedForceFriction==altcycle2maxstress,1));
altcycle2minstrain =
CorrectedMotion1 (find(CorrectedForceFriction==altcycle2minstress,1));
    altmidcycle2strain = (altcycle2maxstrain+altcycle2minstrain)/2;
altcycle3maxstrain =
CorrectedMotion1 (find(CorrectedForceFriction==altcycle3maxstress,1));
altcycle3minstrain =
CorrectedMotion1 (find(CorrectedForceFriction==altcycle3minstress,1));
    altmidcycle3strain = (altcycle3maxstrain+altcycle3minstrain)/2;
altcycle4maxstrain =
CorrectedMotion1 (find(CorrectedForceFriction==altcycle4maxstress,1));
altcycle4minstrain =
CorrectedMotion1 (find(CorrectedForceFriction==altcycle4minstress,1));
    altmidcycle4strain = (altcycle4maxstrain+altcycle4minstrain)/2;

altG2 = (6.89475728/1000)*(altcycle2maxstress +
(abs (altcycle2minstress)))/(altcycle2maxstrain+(abs (altcycle2minstrain)));
altG3 = (6.89475728/1000)*(altcycle3maxstress +
(abs (altcycle3minstress)))/(altcycle3maxstrain+(abs (altcycle3minstrain)));

```

```

altG4 =(6.89475728/1000)*(altcycle4maxstress +
(abs(altcycle4minstress)))/(altcycle4maxstrain+(abs(altcycle4minstrain)));

%*****Damping Calcs*****
%Area of Loops
Area2 = abs(trapz(CorrectedForceFriction(7045:12085),
CorrectedMotion1(7045:12085)));
% format long
% a =[CorrectedForceFriction(7045) FittingCurve(7045)]
% b =[CorrectedForceFriction(12085) FittingCurve(12085)]
%,FittingCurve(7045:9565)
%,FittingCurve(9565:12085)
Area3 =
abs(trapz(CorrectedForceFriction(12085:17085),CorrectedMotion1(12085:17085)))
;
Area4 =
abs(trapz(CorrectedForceFriction(17085:22100),CorrectedMotion1(17085:22100)))
;

%Area of Triangles
OAB2 = .5*(altcycle2maxstress-altmidcycle2stress)*(altcycle2maxstrain-
altmidcycle2strain);
OABPrime2 =.5*((abs(altcycle2minstress))-
altmidcycle2stress)*(abs(altcycle2minstrain)-altmidcycle2strain);
OAB3 = .5*(altcycle3maxstress-altmidcycle3stress)*(altcycle3maxstrain-
altmidcycle3strain);
OABPrime3 =.5*((abs(altcycle3minstress))-
altmidcycle3stress)*(abs(altcycle3minstrain)-altmidcycle3strain);
OAB4 = .5*(altcycle4maxstress-altmidcycle4stress)*(altcycle4maxstrain-
altmidcycle4strain);
OABPrime4 =.5*((abs(altcycle4minstress))-
altmidcycle4stress)*(abs(altcycle4minstrain)-altmidcycle4strain);

D2=(1/f)*(Area2/(OAB2+abs(OABPrime2)));
D3=(1/f)*(Area3/(OAB3+abs(OABPrime3)));
D4=(1/f)*(Area4/(OAB4+abs(OABPrime4)));

D = [D2 D3 D4];

AltD2 = (1/(2*f))*(Area2/(OAB2));
AltD2prime = (1/(2*f))*(Area2/(OABPrime2));
AltD2mean = (AltD2 + AltD2prime)/2;

AltD3 = (1/(2*f))*(Area3/(OAB3));
AltD3prime = (1/(2*f))*(Area3/(OABPrime3));
AltD3mean = (AltD3 + AltD3prime)/2;

AltD4 = (1/(2*f))*(Area4/(OAB4));
AltD4prime = (1/(2*f))*(Area4/(OABPrime4));
AltD4mean = (AltD4 + AltD4prime)/2;

x2=altcycle2maxstrain-abs(altmidcycle2strain);
x2other= abs(altcycle2minstrain)+abs(altmidcycle2strain);
x3=altcycle3maxstrain-abs(altmidcycle3strain);
x3other= abs(altcycle3minstrain)+abs(altmidcycle3strain);

```

```

x4=altcycle4maxstrain-abs(altmidcycle4strain);
x4other= abs(altcycle4minstrain)+abs(altmidcycle4strain);

format long

avgstrain = (x2+x2other+x3+x3other+x4+x4other)/6
altG234 = [altG2 altG3 altG4]
altD = [AltD2mean AltD3mean AltD4mean]
Suction = Matric_Suction
Se =EffectiveSat
Dr = sample_Dr
%*****
figure (1)
subplot(2,1,1)
plot(Time,Non_Shifted_Norm, Time, FrictionCorrection, Time,
CorrectedForceFriction(1:28000));
%ime, ('-', (Time-(Time(INT))), Time, NetDifference, Time, Net_Difference,)
title('Horizontal Motion (Loadcell Feedback)')
xlabel('Time (seconds)')
ylabel('Horizontal Force (psi)')
legend('Non-Shifted-Norm', 'FrictionCorrection', 'CorrectedForceFriction')

subplot(2,1,2)
plot(Time,CorrectedMotion1,Time,NegCapacitance,Time,TopMotionCurve);
title('Horizontal Motion (Net Motion Feedback)')
xlabel('Time (seconds)')
ylabel('Horizontal Shear Strain')
legend('CorrectedMotion1', 'NegCapacitance', 'TopMotionCurve')

figure(2)
subplot(2,1,1)
plot(CorrectedMotion1(4579:6555), Non_Shifted_Norm(4579:6555), CorrectedMotion1
(6555:11625), Non_Shifted_Norm(6555:11625), CorrectedMotion1(11625:16675), Non_S
hifted_Norm(11625:16675), CorrectedMotion1(16675:21675), Non_Shifted_Norm(16675
:21675))
title('Soil Response with toptable consideration')
xlabel('Shear Strain')
ylabel('Shear Force (psi)')

subplot(2,1,2)
plot(NegCapacitance(4579:6555), Non_Shifted_Norm(4579:6555), NegCapacitance(655
5:11625), Non_Shifted_Norm(6555:11625), NegCapacitance(11625:16675), Non_Shifted
_Norm(11625:16675), NegCapacitance(16675:21675), Non_Shifted_Norm(16675:21675))
title('Soil Response with capacitance')
xlabel('Shear Strain')
ylabel('Shear Force (psi)')

figure(3)
subplot(2,1,2)
plot(CorrectedMotion1(4579:6555), CorrectedForceFriction(4579:6555), CorrectedM
otion1(6555:11625), CorrectedForceFriction(6555:11625), CorrectedMotion1(11625:
16675), CorrectedForceFriction(11625:16675), CorrectedMotion1(16675:21675), Corr
ectedForceFriction(16675:21675));
title('Soil Response with FrictionConsidered')
xlabel('Shear Strain')
ylabel('Shear Force (psi)')

```

```

subplot(2,1,1)
plot(CorrectedMotion1(4579:6555),Non_Shifted_Norm_New(4579:6555),CorrectedMotion1(6555:11625),Non_Shifted_Norm_New(6555:11625),CorrectedMotion1(11625:16675),Non_Shifted_Norm_New(11625:16675),CorrectedMotion1(16675:21675),Non_Shifted_Norm_New(16675:21675));
title('Soil Response with shiftedresponse')
xlabel('Shear Strain')
ylabel('Shear Force (psi)')

figure(4)
plot(Time(1:7045), Normal_Force(1:7045),Time(7045:12085), Normal_Force(7045:12085),Time(12085:17085), Normal_Force(12085:17085),Time(17085:22100), Normal_Force(17085:22100),Time(22100:28000), Normal_Force(22100:28000))
title('Vertical Pressure Response')
xlabel('Time')
ylabel('Normal Force (psi)')

```